UNIVERSITA' VITA-SALUTE SAN RAFFAELE

CORSO DI DOTTORATO DI RICERCA INTERNAZIONALE IN MEDICINA MOLECOLARE

CURRICULUM IN MEDICINA CLINICA E SPERIMENTALE

Cancer-Glia interaction in perineural invasion in pancreatic cancer: identification of FGF-BP1 as a molecular target

DoS: Dr. Carla Taveggia
Second Supervisor: Prof. Ihsan Ekin Demir

Tesi di DOTTORATO di RICERCA di Giulia Gasparini
Matr. 013828
Ciclo di dottorato XXXIV
SSD BIO/11

Anno Accademico 2020/2021

Carla Taveggia

CONSULTAZIONE TESI DI DOTTORATO DI RICERCA

La sottoscritta Giulia Gasparini
Matricola 013828
Nata a Sondrio, il 22/04/1993

autrice della tesi di Dottorato di ricerca dal titolo

Cancer-Glia interaction in perineural invasion in pancreatic cancer: identification of FGF-BP1 as a molecular target

AUTORIZZA la Consultazione della tesi

X NON AUTORIZZA la Consultazione della tesi per 12 mesi

a partire dalla data di conseguimento del titolo e precisamente dal 23/12/2021 Al / *to 23*/12/2022

Poiché /*because*:

X l'intera ricerca o parti di essa sono potenzialmente soggette a brevettabilità/ *The whole project or part of it might be subject to patentability;*

□ ci sono parti di tesi che sono già state sottoposte a un editore o sono in attesa di pubblicazione/ *Parts of the thesis have been or are being submitted to a publisher or are in press;*

□ la tesi è finanziata da enti esterni che vantano dei diritti su di esse e sulla loro pubblicazione/ *the thesis project is financed by external bodies that have rights over it and on its publication.*

Data 25/10/2021 Firma

DECLARATION

This thesis has been composed by myself and has not been used in any previous application for a degree. Throughout the text I use both 'I' and 'We' interchangeably.

All the results presented here were obtained by myself, except for:

1) Mass-Spectrometry data (Results, 1.3, pag. 60) were obtained in collaboration with the ProMiFa facility, San Raffaele Scientific Institute, Milan, Italy.

2) Electron-microscopy specimens (Results, chapter 3.1, figure 21), were processed by Dr. C. Panzeri, Alembic, Experimental Imaging Centre, San Raffaele Scientific Institute, Milan, Italy.

3) Images quantification (Results, chapter 2.1, figure 16b-c; Results, chapter 3.2, figure 22) was perfomed by Dr. V. Berno, Alembic, Experimental Imaging Centre, San Raffaele Scientific Institute, Milan, Italy.

4) Hematoxylin and eosin staining (Results, chapter 3.3, figure 23) were obtained in collaboration with the Pathology Department, San Raffaele Scientific Institute, Milan, Italy.

Figures in the introduction were used under the principle of Fair Use (D.Lgs 68, 09/04/03), i.e. the right to use copyrighted material for information, criticism or teaching purposes, without the written authorization of the person who retains the rights. All sources of information are acknowledged by means of reference.

Acknowledgements

First, I would like to thank my Director of Studies Carla Taveggia, who constantly supported me during these years with her precious help, giving me the opportunity to improve day after day.

I am also grateful to my Second Supervisor Ihsan Ekin Demir, who helped me with his useful suggestions and who constantly followed my progresses during these years.

I would like to thank all my lab mates, in particular Marta Pellegatta and Paolo Canevazzi, for the positive exchange of ideas and the technical support.

I would like to thank Prof. Massimo Falconi and the Pancreatic Surgery Department, in particular Prof. Stefano Crippa and Dr. Giulio Belfiori, for their scientific support and the close collaboration to the project.

I would like to thank Prof. Doglioni, Dr. Marco Schiavo Lena and all the Pathology Department for their scientific contribution and the support with technical aspects.

I would like to thank Dr. Renato Ostuni and Dr. Nicoletta Caronni for helping with their exceptional expertise.

Abstract

Introduction Perineural invasion (PNI) is defined as the presence of cancer cells along nerves. PNI has its highest incidence in pancreatic ductal adenocarcinoma (PDAC), where it is present in 80-100% of patients and it is also a negative factor associated with increased cancer recurrence and diminished survival. During PNI, nerves and cancer form a unique microenvironment that promotes both cancer growth and neural remodeling. Several molecules have been described to promote PNI, like neurotrophins and chemokines. Schwann Cells (SCs), the main glial cells of the peripheral nervous system, infiltrate PDAC at the early stages of disease and provide a guide to cancer cells along nerves as well as promoting neurogenesis around tumor. Despite the clear contribution of SCs to PNI, the interactions between myelinated nerves, SCs and PDAC have been poorly investigated.

Objectives Study the reciprocal interactions between PDAC and nervous cells and develop a new score to better stratify and analyze the severity of PNI in patients.

Materials and methods: We analyzed how myelinated nerves and cancer cells interact and identified the molecules governing this interaction. We used SCs-neuronal cocultures and 2D cancer cells to recreate *in vitro* PNI. In addition, to evaluate more physiologically these interactions, we developed pancreatic organoids.

Results: Our results showed that neoplastic cells can induce profound alterations in myelinated cocultures, both by direct and paracrine contact. By secretome analyses, we selected potential candidates able to induce myelin degeneration and focused on FGF-BP1, a molecule involved both in cancer progression and nerve degeneration. By treating with recombinant FGF-BP1 and inhibiting its signaling, we suggested that FGF-BP1 mediates myelin degeneration induced by cancer cells.

Moreover, we showed that myelin degeneration promotes cancer cells growth, proliferation, migration and invasion. To reproduce these results in a more physiological setting, we developed pancreatic organoids, spheroids and organoids-nerve cocultures. We also established an *in vivo* model of PNI by orthotopically transplanting cancer spheroids that we are currently validating. Finally, we applied the newly developed PNI score to a population of 507 patients who underwent surgical resection for PDAC at San Raffaele Hospital.

Conclusions: We have rigorously analyzed the interactions between PDAC and nerve and identified a candidate that could become a new therapeutic target for PDAC patients. In addition, we have detailed the role of PNI specifically in PDAC, prompting a greater attention for PNI in clinical settings.

Table of Contents

Acronyms and abbreviations

Dorsal motor nucleus of the vagus (DMV)
Central Nervous System (CNS)
Peripheral Nervous System (PNS)
Schwann Cells (SCs)
SC precursors (SCPs)
Neuregulin (NRG)-1 type III
Sterol responsive element binding protein (SREBP)
Erythroblastic leukemia viral oncogene homolog-2/3 (ErbB2-ErbB3)
Notch intra-cellular domain (NICD)
Pancreatic ductal adenocarcinoma (PDAC)
Superior mesenteric artery (SMA)
Superior mesenteric vein (SMV)
Pancreatic intraepithelial neoplasia (PanINs)
computed tomography (CT)
magnetic resonance imaging (MRI)
endoscopic ultrasonography (EUS)
neuroendocrine tumors (NETs)
Fluorouracil, leucovorin, irinotecan, and oxaliplatin (FOLFIRINOX)
genetically engineered mouse model (GEMM)
Perineural Invasion (PNI)
Dorsal root ganglia (DRG)
Conditioned Media (CM)
Myelin Basic Protein (MBP)
Neurofilament (NF)
Cytokeratin 19 (CK19)
Fibroblast Growth Factor Binding Protein 1 (FGF-BP1)

List of figures and tables

Introduction

1. The human pancreas

The pancreas is a retroperitoneal organ with both exocrine and endocrine functions. It lies in the retroperitoneum at the level of L1 and L2 vertebrae, surrounded by a not well defined fibrous capsule (Longnecker, 2021).

It is commonly divided into three parts: the head, separated from the rest of the organ by the left border of the superior mesenteric artery (SMA), the body, and the tail, which extends towards the spleen. The ventral part of the head has an embryologically different origin from the rest of the pancreas. It derives from the ventral pancreatic bud that at the 7th week of gestation rotates to fuse with the dorsal pancreatic bud. This results in smaller and stiffer lobules in the ventral pancreas and a different distribution of islets of Langerhans and vasculature (Adda et al, 1984). Islets of Langerhans density is almost two-fold higher in the body-tail as compared to the head of the pancreas. Interestingly, the head of the pancreas is more susceptible for islet cells loss, that will eventually lead to diabetes development, as well as for cancer growth.(Wang *et al*, 2013). Further studies are needed to understand why the risk to develop such pathologies is increased in this region of the pancreas.

The pancreas is vascularized by two major arteries, the coeliac artery and the superior mesenteric artery (SMA) (Villasenor & Cleaver, 2012).

These two arteries give rise to the superior and inferior pancreaticoduodenal arcades that vascularize the head of the pancreas. The superior pancreaticoduodenal arteries derive from the gastroduodenal artery, which originates from the common hepatic artery; the inferior pancreaticoduodenal arteries, instead, stem directly from the SMA. The body and tail of the pancreas are vascularized by multiple branches all deriving from the splenic artery (Kumar *et al*, 2021).

Venous drainage of the pancreas follows the arterial pattern and drains into the portal system. The portal vein is formed immediately behind the pancreas by the confluence of the splenic vein and superior mesenteric vein (SMV). The splenic vein receives blood

from the body and tail of the pancreas. The head of the pancreas is drained by two systems: the superior pancreatic veins, that end in the gastroepiploic vein or directly in the portal vein, and the inferior pancreatic veins that drain into the SMV (Mahadevan, 2019; Ibukuro, 2001) (Figure 1).

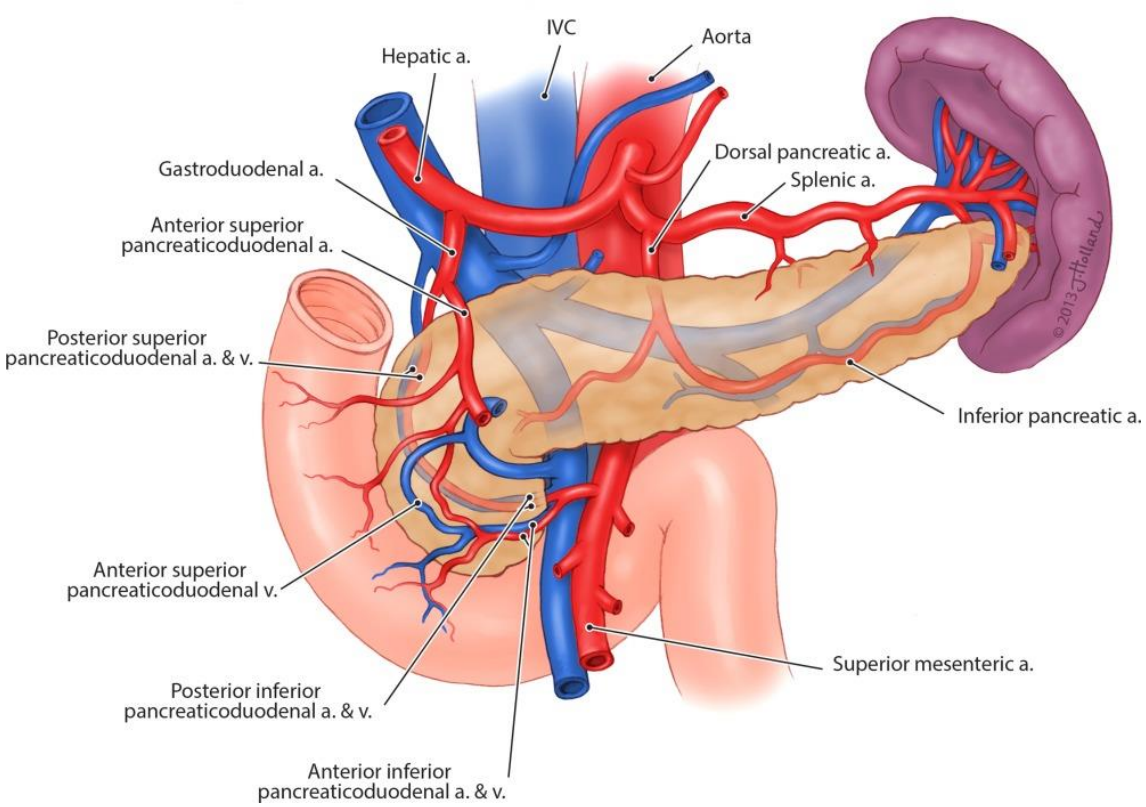

Figure 1. Vascular anatomy of the pancreas: arterial and venous drainage

Pancreatic vascularization. Arterial vessels derive from the superior mesenteric artery and from the coeliac trunk. Venous vessels follow the path of the corresponding arteries. IVC, inferior vena cava (Cesmebasi *et al*, 2015).

Functionally, the pancreas can be divided into an exocrine and an endocrine part. The exocrine pancreas is composed by acinar and ductal cells, it is responsible for the secretion of digestive enzymes. The endocrine pancreas is composed by the islets of

Langerhans, whose function is to synthetize and release different hormones in the blood stream.

The exocrine part of the pancreas accounts for most of the pancreatic volume, approximately 85%, while the endocrine part represents less than 4% of the total pancreatic volume. Approximately 90% of the pancreatic blood supply is dedicated to the exocrine pancreas (Lewis *et al*, 1998).

The remaining 20% is essentially composed of mesenchyme (Pandol, 2010). During development, mesenchymal tissue supports the proliferation of precursor cells and the normal growth of the pancreas (Landsman *et al*, 2011) (Hibsher *et al*, 2016).

The exocrine and the endocrine pancreas represent two structurally separated regions: even if the islet of Langerhans are found scattered among exocrine pancreas, these two components have very typical structures (Figure 2). The cellular composition of exocrine and endocrine pancreas is distinctive, giving rise to two different systems: the acinar-ductal one for digestive enzyme secretion and distribution, and the islet one for hormone production and homeostasis.

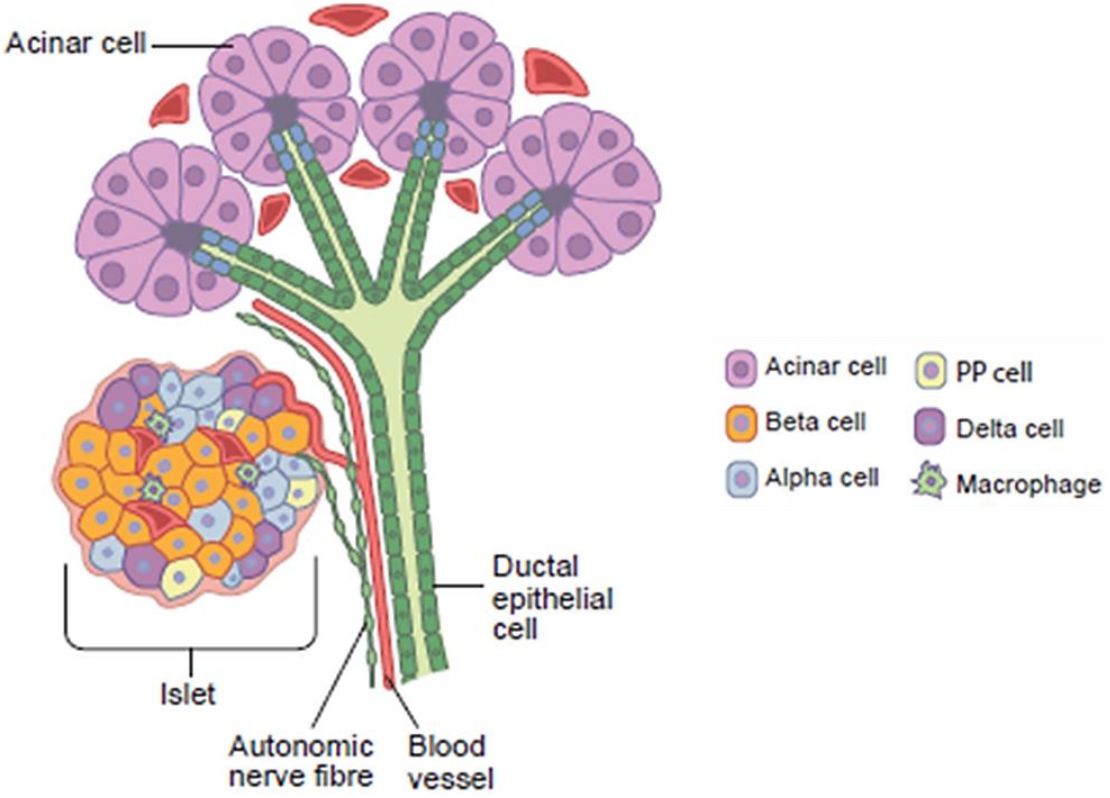

Figure 2. Normal pancreatic morphology

Normal pancreatic structure showing the proximity of acinar and ductal cells with islet of Langerhans, composed by α cells, β cells, δ cells, γ cells and resident macrophages. Blood vessels and nerves supply all pancreatic compartments (Rickels *et al*, 2020).

1.*1 Exocrine pancreas*

Exocrine pancreas relies on functional units composed of an acinus and its matching draining ducts. The small ductules from the acinus drain into interlobular (also called intercalated) ducts, which in turn drain into the main pancreatic duct (Reichert & Rustgi, 2011). Acinar cells are responsible for the secretion and storage of zymogens and digestive enzymes. The timing of production and secretion of these enzyme is highly regulated to ensure a proper supply of digestive enzymes (Williams, 2010).

From a structural point of view, both acinar and ductal cells are polarized towards the lumen of the duct where they release their content. On their basal membrane, acinar cells express receptor for hormones and neurotransmitters that drive enzymes secretion; the

nucleus and the endoplasmic reticulum are located in the basal region, while zymogen granules, that are fundamental for storing and secreting enzymes, can be found in the apical region of the cell. Tight junctions between acinar cells create a barrier against the leakage of digestive enzyme (Husain & Thrower, 2009).

Ductal cells provide the epithelial lining of the pancreatic ductal system. They contain a high number of mitochondria, as they need energy to transport ions. Ions secretion is regulated by secretin and acetylcholine. These two molecules mediate the activation of the chloride channel cystic fibrosis transmembrane conductance regulator (CFTR) on the luminal membrane and the activation of two potassium channels, the voltage- and Ca^{2+}-activated K^+, big conductance (BK, maxi-K), and the intermediate (IK, KCa3.1) Ca^{2+}-activated K^+ channels (Schnipper *et al*, 2020)on the basolateral membrane. High levels of chloride ions in the lumen determines a subsequent chloride/bicarbonate exchange (Venglovecz *et al*, 2021), resulting in an alkaline fluid, necessary to prevent intra-pancreatic activation of the acinar digestive enzymes and to neutralize the acid chyme leaving the stomach and entering the duodenum (Grapin-Botton, 2005).

Another cellular component of the pancreas is represented by centroacinar cells, which are localized between ductal and acinar cells. These cells express ductal markers, like Sex-determining region Y box 9 (SOX9), though it was also demonstrated their role as β-cell precursors in zebra fish (Delaspre *et al*, 2015). Their exact role in humans is not completely understood (Beer *et al*, 2016).

Pancreatic stellate cells are, in physiological conditions, inactive cells that encircle acinar and ductal structure. It has been proposed that they provide a basement membrane for the formation of epithelial structures (Pandol, 2010). The role of stellate cells is more intriguing during pathological states: for instance, in pancreatic cancer they differentiate into myofibroblast-like cells expressing α-smooth muscle actin (SMA) that secrete pro-inflammatory cytokines and growth factors used by the neoplastic cells to grow and proliferate (Masamune & Shimosegawa, 2013). In addition, activated stellate cells promote a desmoplastic reaction and increased extracellular matrix deposition, creating a barrier around cancer that protects it from chemotherapy (Schnittert *et al*, 2019).

1.2 Endocrine pancreas

Endocrine cells are organized in the islet of Langerhans, distributed in the exocrine tissue. In a normal pancreas, there are more than 1 million islets, which are composed of different type of cells: 60% are β cells, 30% α cells, and the final 10% includes δ-cells, γ cells and ε-cells (Da Silva Xavier, 2018).

β cells are responsible for the production and secretion of insulin in response to various stimuli, like high blood glucose concentration and incretin hormones (Marchetti *et al*, 2017). α cells produce glucagon, the counter regulator of insulin whose major function is to prevent hypoglycemia (Wendt & Eliasson, 2020). δ-cells are somatostatin secreting cells that can be found also in the hypothalamus and in the gastrointestinal tract. Somatostatin is a negative regulator of various hormones, like insulin, glucagon and pancreatic polypeptide (Arrojo e Drigo *et al*, 2019). γ cells are pancreatic polypeptide-producing cells, found in higher number at the head of the pancreas. Pancreatic polypeptide is involved in metabolism balance and it is considered a satiety hormone (Asakawa *et al*, 2003). ε-cells are responsible for ghrelin secretion, whose main function could be to act as paracrine inhibitors of insulin secretion (Wierup *et al*, 2013).

The proportion of the different types of cells constituting the islet vary according to age, size of the islet and their location, with smaller islet comprising mainly β cells (Atkinson *et al*, 2020).

Exocrine and endocrine cells are connected by a microvasculature network, the insulo-acinar portal system. Capillaries leave the islet cells of Langerhans to drain into secondary capillaries around acini and ducts, and ultimately into the portal vein. This venous system exposes exocrine cells to a high concentration of insular hormones that participate in the exocrine cells secretion (Shiratori & Shimizu, 2018).

Different pathologies can affect the pancreas, both in the endocrine and in the exocrine component, like diabetes, acute and chronic pancreatitis, neuroendocrine tumors, and cancer. Here we will specifically focus on pancreatic adenocarcinoma arising from ductal cells, an aggressive cancer with a dismal prognosis.

1.3 Innervation of the pancreas

Pancreatic innervation is supplied by sympathetic, parasympathetic and sensory fibers (Figure 3). Nervous fibers travel both in and out of the pancreas following the blood vessels and innervate the exocrine and the endocrine pancreas in a quite complex and entangled network (Bockman, 2007).

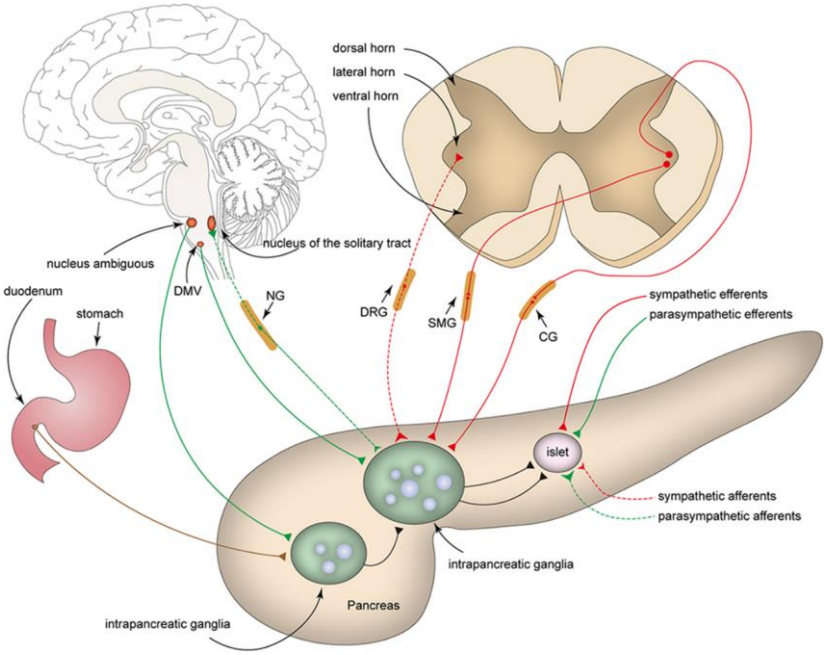

Figure 3. Pancreatic innervation

Parasympathetic fibers originate from the dorsal motor nucleus of the vagus (DMV) and the nucleus ambiguous. Sympathetic efferent fibers project from the spinal cord lateral horn to the coeliac ganglia (CG) and the superior mesenteric ganglia (SMG) (Li et al, 2019).

The coeliac plexus gives rise to the anterior and posterior hepatic plexuses and innervates the head of the pancreas. The anterior hepatic plexus runs along the common hepatic artery, the gastroduodenal artery and the pancreaticoduodenal artery. The posterior hepatic plexus runs parallel to the portal vein and its most inferior nerve fibers innervate the dorsal part of the pancreatic head (Ren *et al*, 2020).

The body and tail of the pancreas are innervated by the splenic plexus via nervous fibers that enter the pancreas following the great pancreatic artery, and also by the coeliac plexus via nervous fibers that run along the inferior pancreatic artery (Yi *et al*, 2003).

Sensory innervation of the pancreas is provided by the vagal nerve and spinal pathways. Neurons of the spinal pathway are located in T6-L2 dorsal root ganglia and travel with sympathetic fibers in splanchnic nerves and coeliac plexus. These axons include small myelinated (Aδ) and unmyelinated (C) fibers that transmit mechanoceptive and nociceptive information (Love *et al*, 2007). Vagal axons originate from the nodose ganglia and regulate glucose homeostasis via communication with pancreatic β-cells (Makhmutova *et al*, 2021). The nodose ganglia contains mainly A fibers and C fibers (Waise *et al*, 2018). Interestingly, in rats the right ganglia predominantly innervates the duodenal lobe while the left ganglia the splenic lobe, suggesting a regional distribution of the sensory innervation (Neuhuber, 1989). It would be interesting to study if this regional innervation has any influence on the different behavior of PDAC arising from the different regions of the pancreas.

Sympathetic innervation of the pancreas derives from sympathetic neurons found in the intermediolateral column of the lower thoracic and upper lumbar segments of the spinal cord. These fibers project to the sympathetic chain via white communicating rami (anatomic structures connecting the preganglionic sympathetic neurons of the spinal cord to the sympathetic chain, containing a majority of myelinated axons – hence defined white rami (Ernsberger & Rohrer, 2018)) and to coeliac and mesenteric ganglia via splanchnic nerves (Babic & Travagli, 2016). Noradrenergic fibers of the postganglionic neurons innervate intrapancreatic ganglia, endocrine islets, ducts, lymph node and vessels. Sympathetic activation induces vasoconstriction and reduces exocrine and endocrine secretion (Makhmutova & Caicedo, 2021). It has been suggested that sympathetic fibers interact with the immune pancreatic system and that a loss of islet specific sympathetic fibers might be correlated to the onset of type I diabetes in patients (Mundinger et al, 2016).

Parasympathetic innervation originates from the dorsal motor nucleus of the vagus (DMV) and directly synapses with pancreatic ganglia. Pancreas-projecting neurons are located in the left DMV area, where the hepatic and the anterior gastric branches of the

vagus are found. However, also nerve projections deriving from the coeliac branches of the vagus in the right DMV area give a small contribution to the innervation of the tail of the pancreas. Input to the DMV originates mainly from the nearby located nucleus tractus solitarius that transmits to the DMV via glutamatergic, GABAergic and catecholaminergic signals (Travagli & Anselmi, 2016). Parasympathetic stimulation increases insulin secretion and regulates the pulsatile secretion of insulin (Fontaine et al, 2021). Moreover, parasympathetic activation modulates the release of exocrine enzymes and participates in the cephalic phase of digestion (Power & Schulkin, 2008).

1.4 Pancreatic anatomy: human and murine comparison

Human pancreas has some peculiar differences from mouse pancreas that should be considered while using animal models to replicate human diseases.

During embryonic development, murine pancreas becomes visible at day E9. The pancreatic epithelial tissue can be distinguished by the expression of pancreatic duodenal homeobox 1 (*Pdx1*), which is one of the earliest transcription factors expressed that marks pluripotent epithelial cells (Gu *et al*, 2003). In the following days, the epithelium, supported by the mesenchyme, grows forming the ventral and dorsal bud that will fuse at E13 forming a single organ (Puri & Hebrok, 2007; Jørgensen *et al*, 2007). By E15, differentiation markers for all pancreatic cell types are expressed (Pan *et al*, 2013).

Macroscopically, the mouse pancreas is a rather diffuse organ as compared to the human pancreas, which is, instead, more compact. The mouse pancreas can be divided into three parts: the duodenal lobe, the splenic lobe and the gastric lobe (Dolenšek *et al*, 2015). The splenic lobe is the biggest one and can be compared to the body-tail of the human pancreas, with the gastric lobe as a small appendage of the splenic lobe. The duodenal lobe, instead, corresponds to the head of the human pancreas.

Microscopically, murine and human pancreases differ both for the exocrine and the endocrine components. In humans, the exocrine pancreas is organized in lobules, each composed of acini made by clusters of acinar cells that drain into intercalated ducts. These smaller ducts drain into various order of bigger ducts, and eventually converge into the duct of Wirsung, the main pancreatic duct, that together with the common bile duct, drains

in the duodenum via the ampulla of Vater (Horiguchi & Kamisawa, 2010). In mice, there is a large interlobular duct that drains the three lobules; the splenic and gastric duct merges early with the common bile duct, before the duodenal duct merges with them and then enter the duodenum (Higashiyama *et al*, 2016). Endocrine cells are more heterogeneously distributed in the mouse pancreas as compared to human; moreover, the islet of Langerhans are organized in a less complex structure in mice compared to humans (Dolenšek *et al*, 2015).

Nerve distribution is rather different in the human and mouse pancreas. A detailed morphological study on the distribution of nerve trunks in murine pancreas identifies nerves in two major locations: around blood vessels and intrapancreatic lymph nodes. Notably, the authors of this article did not detect nerves in the interlobular septae. The majority of nerves were observed in the head of the pancreas, where they also showed a higher number of nociceptive fibers (positive for substance P, a neuropeptide known mediator of pain) (Saricaoglu *et al*, 2020). In humans, nerves enter the pancreas following the blood vessels, similar to what happens in mice, but there is a lack of detailed information regarding the association between nerves and lymph nodes. Moreover, the distribution of different types of nerves presents some differences between mouse and human. While sympathetic fibers are in close contact with exocrine cells and vessels in humans, mediating an inhibitory effect on acinar and ductal secretion, in mice, acinar cells are only scarcely innervated by them (Dolenšek *et al*, 2015). On the contrary, sympathetic fibers provide little innervation to the islets of Langerhans in humans, while in mice these fibers directly contact α cells and encircle the adjacent arterioles, forming a neurovascular complex (Chiu *et al*, 2012).

2. Peripheral Nervous System

The nervous system is a network of specialized cells that connect and coordinate different parts of the body. The nervous system consists of two parts, the Central Nervous System (CNS) and the Peripheral Nervous System (PNS). The CNS comprises the brain and the spinal cord, while peripheral nerves and ganglia connecting the CNS to the rest

of the body are the component of the PNS. In this thesis I will specifically focus on the PNS.

The PNS can be further divided into somatic and autonomic nervous system. The somatic nervous system is responsible for the voluntary movements that are accomplished via skeletal muscles. The somatic system orchestrates inputs we receive from afferent (from the periphery to the CNS) and efferent fibers (from the CNS to the periphery), both deputed to the control of voluntary movements (Akinrodoye & Lui, 2020).

The autonomic nervous system controls involuntary actions and the physiological functioning of the organism. It is further subdivided into sympathetic and parasympathetic nervous systems. The type of response controlled by the sympathetic nervous system focuses on the "fight or flight" reaction, which supports immediate response in case of danger through the increase of cardiovascular function, subsequent higher oxygen availability to muscles, and decreased pain sensation, and relies on acetylcholine and norepinephrine as neurotransmitters. The parasympathetic nervous system, instead, is responsible for the "rest and digest" response, during which the physiological bodily functions take place, like digestion, salivation, urination and sleep, and uses acetylcholine as the only transmitter for muscarinic receptors (LeBouef & Whited, 2019).

2.1 Peripheral Nerve Structure

The PNS contains two main types of cells: neurons and glial cells. Glial cells of the PNS are SCs, enteric glial cells and satellite cells and have a fundamental role in providing metabolic support to neurons, insulating axons to increase conductance, and promoting regeneration after injury (Jessen, 2004). Other PNS components are fibroblasts, immune cells like macrophages, and pericytes; these cells have ancillary functions like structural and proliferative support to SCs (Dreesmann *et al*, 2009), myelin debris clearance after injury (Griffin *et al*, 1992; Forese *et al*, 2020), creation and maintenance of the blood-nerve-barrier (Shimizu *et al*, 2011), respectively. Neurons are responsible for the reception and transmission of electrical inputs. Neuronal cell bodies

covered by satellite cells constitute PNS ganglia, while peripheral nerves are composed by afferent and efferent axons, SCs and connective tissue + (Butler & Bronner, 2015).

Peripheral nerves are organized in bundles of nerve fibers that could be either myelinated or non-myelinated based on their size and function. Myelinated fibers usually mediate motor, proprioceptive and vibratory senses, while small unmyelinated or thinly myelinated fibers convey nociception and autonomic functions (Saporta & Shy, 2015). Peripheral nerves are structured into three compartments: 1) the epineurium: it is the outermost layer and surrounds the entire nerve fibers, including also blood vessel which provide nutrients to the nerve; 2) the perineurium: it is composed of flat perineural cells that isolate nerve fascicles composed of SCs-axons units; 3) the endoneurium: it is a permeable, thin collagenous tissue layer, which encloses single nerve bundles (Peltonen et al, 2013).

SCs are the main component of the peripheral nerve. They derive from the neural crest and become mature cells through a series of strictly regulated passages. One of the best characterized markers of SCs, expressed from the stage of neural crest precursor to mature SCs, is SRY-related HMG box 10 (*Sox-10*). In mice mutant for *Sox-10*, glial cells are lacking; neurons develop normally, but, at later stages, sensory, sympathetic and motor neurons degenerate, probably because of the lack of trophic support (Britsch *et al*, 2001; Finzsch *et al*, 2010).

SC precursors are tightly associated with emerging nerves and rely on survival signals from axons. A key neuronal factor is Neuregulin (NRG)-1 type III that binds to its receptors ErbB2-ErbB3 (erythroblastic leukemia viral oncogene homolog-2/3) on SCs and, at this stage of embryonic development, orchestrates proliferative and pro-survival signals. ErbB3 mutant mice lack SCs precursors and therefore SCs (Riethmacher *et al*, 1997). This pathway is conserved in evolution, as demonstrated by studies in zebrafish. ErbB2/3 mutants in zebrafish confirmed that this signaling is essential for SCs proliferation, migration along axons and post-migratory SCs proliferation, essential for the onset of myelination (Woldeyesus *et al*, 1999; Garratt *et al*, 2000a).

SC precursors are fundamental to provide trophic support to the developing nerves: in mice knock out for NRG-1 type III, SC precursor are initially present but then dye resulting in SCs absence in embryonic nerves. In this mice, sensory and motor neurons

degenerate and die (Wolpowitz *et al*, 2000), suggesting that neurons and glia depend on each other for survival in the early developmental phases.

Around E14, SC precursors develop into immature SCs that will subsequently become myelinating or non-myelinating SCs. Immature SCs stop migrating and start secreting their own basal lamina, as well as different factors like insulin-like growth factor-2 (IGF-2), Platelet-derived growth factor beta (PDGFβ), Neurotrophin-3 (NT3), leukemia inhibitory factor (LIF) (Meier *et al*, 1999; Dowsing *et al*, 1999). All these factors are important for sustaining SCs survival in an autocrine way.

In nerve morphogenesis, immature SCs are responsible for the separation of large caliber axons, that will become myelinated, from small axons that will instead form Remak bundles as non-myelinated fibers (Jessen & Mirsky, 2005). This process is termed radial sorting, it starts around birth and is essential for the correct maturation of nerves (Figure 4).

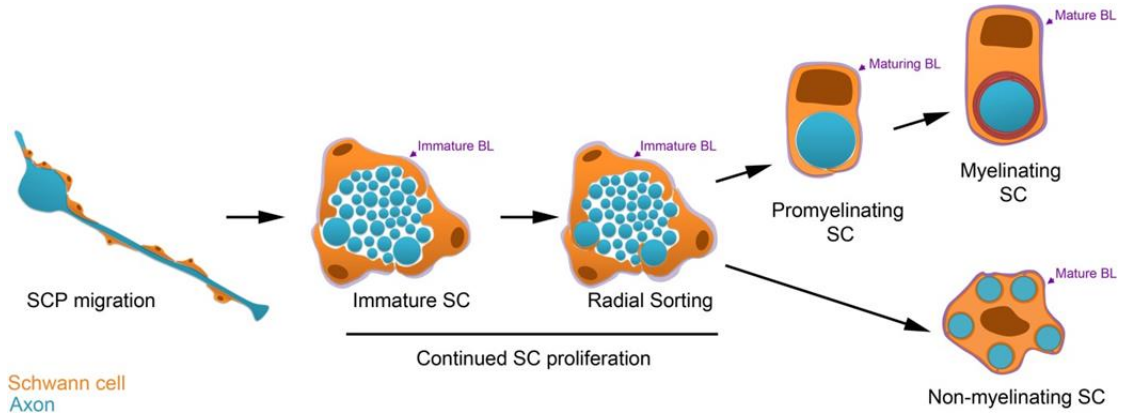

Figure 4. Myelinating and non-myelinating Schwann Cells development

SC precursors (SCPs) actively proliferate and migrate along growing axons (longitudinal section). Subsequently, SCPs become immature SCs, associate with different axons, stop migration and start secreting basal lamina (BL) – which will mature through SCs development. During radial sorting, immature SCs experience two different fates. Myelinating SCs wrap their cytoplasm around a single axonal fiber, creating the

myelin sheath. Non-myelinating SCs ensheath multiple small axons, forming a Remak bundle (Monk et al, 2015).

During radial sorting, immature SCs envelop their cytoplasm around an axon bundle and myelinating SCs associate with large caliber axons in a 1:1 ratio, segregating (defasciculating) them at the periphery of the axonal bundle. Remaining SCs will become Remak SCs, ensheathing multiple axons without producing the myelin sheath (Webster *et al*, 1973). This represents the end of the radial sorting process, which occurs around post-natal day 10 in rodents (Monk *et al*, 2015).

2.2 Myelin structure and composition

Myelin is a specialized plasma membrane that provides electrical insulation to large axons to sustain a fast conduction of action potentials (Morell & Quarles, 1959). SCs plasma membrane forms spiral layers around a single axon (Jessen et al, 2015). The apposition of these layers generates intraperiod lines, formed by the apposition of the outer faces of two consecutive wraps, and major dense lines, formed when the cytoplasm of the myelin process is extruded and the opposite plasma membrane fuse together (Horih, 1989). Myelin is not continuous along the axons but is interrupted by the nodes of Ranvier that separate one internode from the following one. Nodes of Ranvier contain a high concentration of voltage-gated sodium ion channels, responsible for a rapid saltatory conduction (Rasband & Peles, 2016) (Figure 5).

Flanking the node, paranodal junctions can be found. They are specialized sites that attach the myelin sheath to the axon and create a boundary to limit the lateral diffusion of nodal structures (Rosenbluth, 2009; Lazzarini & Nave, 2004). In addition, communication and exchanges of molecules between Schwann cells and axons across the myelin sheath is allowed by Schmidt-Lanterman incisures, specialized cytoplasmic channels crossing the myelin layer from the most outer part to the inner one (Terada *et al*, 2019).

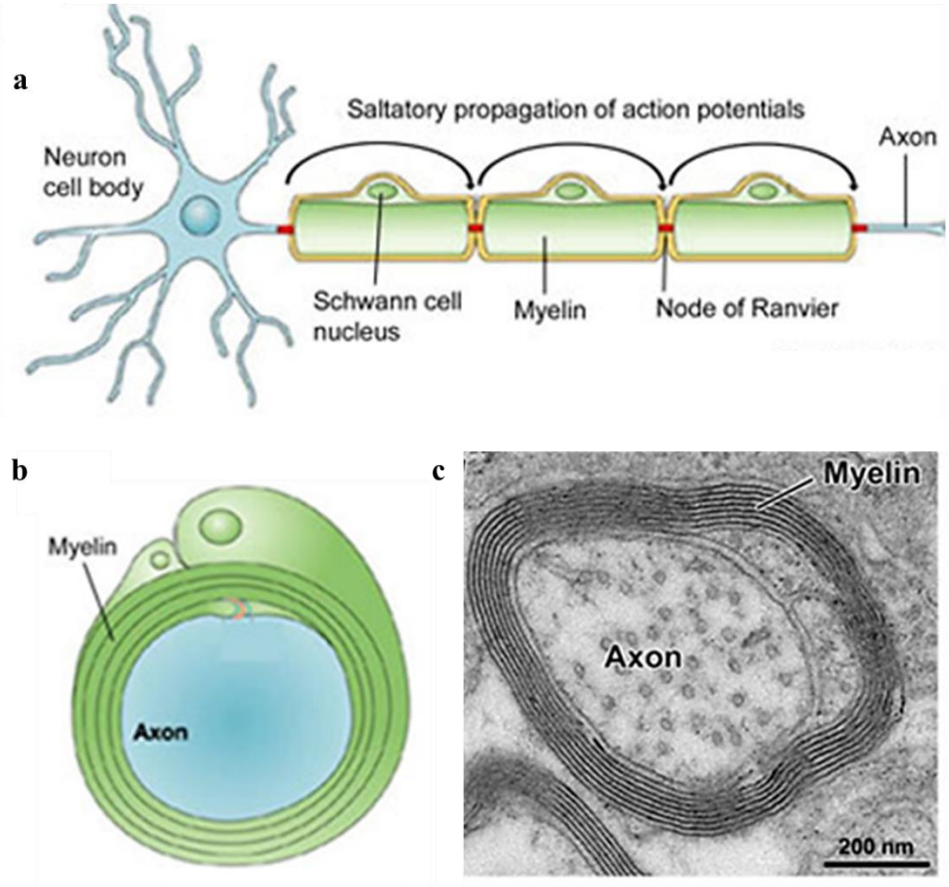

Figure 5. Myelinated nerve fiber structure

a) Cartoon illustrating a myelinated nerve fiber and the saltatory conduction of action potential. b) Illustration of transverse section of a myelinated axon. c) Electron microscopy of a myelinated axon in a murine optic nerve at high magnification, the axon is surrounded by the multilamellar structure of myelin. Modified from (Susuki, 2010).

Myelin has a unique biochemical composition. A peculiar characteristic is its high lipid content, around 70-85% of the total, as compared to a relative low protein content (20-30%). This is in contrast with the composition of most plasma membranes that typically have a 1:1 lipid to protein ratio. Myelin lipid composition is peculiar as compared to other biological membranes, since it is composed of high amounts of cholesterol and an abundant quantity of glycolipids. Lipid composition is similar between CNS and PNS, though phosphatidylcholines and sphingomyelin are more abundant in peripheral myelin (Poitelon et al, 2020).

Among lipids, cholesterol represents approximately 40% of total myelin lipids. Its relevance has been further underscored in several studies, showing that in its absence, oligodendrocytes cannot synthesize myelin (Saher *et al*, 2005). In development, SCs can uptake cholesterol from the circulation, but mainly rely on self-produced cholesterol. Indeed, mice with conditionally inactivated SCAP in SCs, a Sterol responsive element binding protein (SREBP) Cleavage Activation Protein needed for SREBP activation, are unable to produce cholesterol. SCAP inactivation therefore interferes with cholesterol synthesis and uptake, and SCs lacking SCAP result in a severe congenital hypomyelination of sciatic nerve (Verheijen *et al*, 2009). In addition, the reduced presence of cholesterol determines a down-regulation of myelin proteins (Saher *et al*, 2011).

Galactosylceramides are the major are the major glycosphingolipids of myelin. Their principal role is to increase myelin stability. They create strong hydrophobic forces between myelin membranes, thus sticking them together (Bakhti *et al*, 2014). Both Phosphatidylcholines and sphingomyelins represent classes of lipids enriched in PNS myelin. Phosphatidylcholines are structural components of the myelin membrane. They are mainly self-produced by SCs through choline uptake and represent the precursors for the synthesis of other important lipids, like sphingomyelins (Furse & De Kroon, 2015). Sphingomyelins participate in myelin membrane stability and are involved in signaling pathways regulating proteins and cholesterol trafficking to the membrane (Simons *et al*, 2000).

Lipids are fundamental for the insulating activity operated by myelin, while proteins have a role in myelin stability and in its correct functioning. Differently from lipids, myelin proteins are highly specific and differ between PNS and CNS. The major proteins in the PNS include Myelin Protein Zero (P0), Peripheral Myelin Protein 22 (PMP22), Myelin-Associated Glycoprotein (MAG), Myelin Basic Protein (MBP).

P0 is the main myelin protein, exclusively present in the PNS, and represents 50-70% of the total myelin protein content. It is expressed early in development, at E13.5, probably representing a marker of SCs lineage, and its expression levels peaks during myelination at post-natal day 21 (Lee *et al*, 1997; Stahl *et al*, 1990). P0 serves as a

structural component of myelin; it participates to maintain myelin compaction (Lemke & Axel, 1985) via homophilic interactions with other P0 proteins, as well as binding to sphingolipids and PMP22.

PMP22 represents 2-5% of total PNS myelin protein content. Though the specific functions of PMP22 have not been fully characterized, it is believed to participate in myelin stability through interactions with other proteins, like P0. Its expression is strictly regulated: indeed, alterations in PMP22 protein levels cause different neuropathies. For example, duplication of PMP22 gene causes Charcot-Marie-Tooth 1A, characterized by reduced nerve conduction velocity, distal muscle weakness, atrophy and sensory loss; instead, gene deletion causes in Hereditary Neuropathy With Pressure Palsy (Watila & Balarabe, 2015; Van Paassen *et al*, 2014).

MAG accounts for 0.1% of total PNS myelin content. Unlike the above described myelin proteins, it is expressed in both CNS and PNS myelin. It is localized in the innermost layer of myelin, in contact with the axon. MAG has adhesive properties, and it might mediate communication between SCs and axons. It is involved in a rare, autoimmune peripheral neuropathy where autoantibodies are produced specifically against MAG, resulting in sensory neuropathy with ataxia and tremor (Quarles, 2007; Pascual-Goñi *et al*, 2019).

MBP represents 5-15% of total PNS myelin proteins. Similarly to MAG, it is expressed in both CNS and PNS myelin. It is believed to participate in myelin maintenance and compaction; while it is essential only for CNS myelin structuring, MBP is not necessary for myelin lamellae formation in the PNS (Smith-Slatas & Barbarese, 2000) (Lazzarini *et al*, 2004).

2.3 The process of myelination

Numerous axonal and extracellular matrix-derived signaling pathways are activated in SCs to drive myelination.

Besides controlling important steps in pre-natal SCs proliferation and survival, NRG1 type III is the key molecule governing myelination in the PNS. It is expressed on axons

and its expression levels determines the myelinating or non-myelinating fate of SCs. Dorsal Root Ganglia (DRG) neurons, derived from mice lacking NRG1 type III, are not myelinated (Taveggia *et al*, 2005). Moreover, mice overexpressing NRG1 type III are hypermyelinated, while mice with haploinsufficient for NRG1 type III are hypomyelinated (Michailov *et al*, 2004), indicating that myelin sheath thickness is directly proportional to the levels of NRG1 type III expressed on axons.

NRG1 type III binds to ErbB-2 and ErbB-3 that are expressed on SCs, where they function as forced heterodimers (Citri *et al*, 2003). Conditional ablation of ErbB2 in myelinating SCs leads to the formation of thinner myelin sheath with a resulting widespread peripheral neuropathy. This result further underlines the important role of NRG1-ErbBs interactions in myelination (Garratt *et al*, 2000b). NRG1 type III activation of ErbB-2 and 3 results in the activation of various signaling pathways, among which the main characterized are the phosphatidylinositol 3-kinase (PI3K)-AKT 8 virus oncogene cellular homolog (AKT) pathway and the extracellular signal-regulated kinases (ERK) pathway (Newbern & Birchmeier, 2010). Several studies have shown that the concerted modulation of these pathways leads to the physiological production of myelin proteins and lipids.

Pharmacological inhibition of AKT *in vitro* reduces myelin proteins expression and impairs myelin formation in cultures, while sustained AKT activation in SCs *in vivo* resulted in nerves hypermyelination and myelin abnormalities (Domènech-Estévez *et al*, 2016). Notably, these hypermyelination and abnormalities were reversed by treating mice with rapamycin, a mammalian target of rapamycin inhibitor, suggesting the involvement of mTOR in myelination downstream of AKT (Domènech-Estévez *et al*, 2016; Heller *et al*, 2014).

Deletion of ERK1/2 in the developing neural crest determines an absence of SCs on peripheral nerves, and ERK1/2 ablation in SC precursors results in hypomyelination and reduction in the number of myelinated fibers, similarly to what observed in NRG1 and ErbBs knock out mice (Newbern *et al*, 2011). Nonetheless, ERK1/2 role in nerve development is controversial. Indeed, sustained ERK activation leads to hypermyelination (Ishii *et al*, 2013), but it has also been reported to cause demyelination in already myelinated nerves (Napoli *et al*, 2012).

At transcriptional level, positive regulators of myelination include *Sox-10*, that, in turn, can activate the transcription factor octamer-binding transcription factor 6 (*Oct-6*). Together, *Sox-10* and *Oct-6* activate *Krox-20* (Sundaram *et al*, 2021), which is considered the master regulator of myelination. Indeed, *in vivo*, SCs lacking *Krox-20* can only form one layer of myelin around a deputed axon (Topilko *et al*, 1994).

Myelination is controlled also by negative regulators, which inhibit myelin genes activation and are activated during nerve injury response. For example, *Sox-2* is downregulated in myelinating cells *in vivo*, and its overexpression in SCs suppresses myelin genes expression and inhibits myelination *in vitro* (Roberts *et al*, 2017). *c-Jun* is highly expressed in immature SCs and it is subsequently downregulated at later stages of the Schwann cells lineage, when *Krox-20* and myelination commence. Indeed, *c-Jun* overexpression in SCs inhibits myelination (Parkinson *et al*, 2008a). Interestingly, immediately after injury, *c-Jun* is upregulated as it is required for SCs de-differentiation and subsequent transformation in repair SCs; ablation of *c-Jun* in SCs impairs the regenerative abilities of nerves after injury (Parkinson *et al*, 2008b).

Notch intra-cellular domain (NICD) is a transcriptional regulator that is suppressed by *Krox-20* in vitro in myelinating SCs. Indeed, when NCID is ectopically expressed in healthy nerves *in vivo*, it induces demyelination – working as a negative regulator of myelination (Woodhoo *et al*, 2009).

3. Pancreatic ductal adenocarcinoma

Pancreatic adenocarcinoma (PDAC) is the most common malignancy of the pancreas, representing up to 85% of cases. PDAC is currently the fourth leading cause of cancer related death in Western countries and the seventh worldwide. Notably, it is expected to become the third leading cause of cancer death by 2025 in Europe (Sung et al, 2021). This increased incidence can be explained by the general ageing of our society but also by the increased prevalence of obesity and type two diabetes, both accepted risk factors for PDAC (Orth *et al,* 2019). The low survival rate is mainly due to the late stage at which PDAC is diagnosed. Only 20% of the patients arrive at clinical attention when surgical resection is feasible – and surgical resection is still the only curative treatment. The survival rate of PDAC has only slightly increased in the past years, nevertheless the cumulative rate of survival at five-years still remains around 5% (Siegel et al, 2020).

PDAC is a particularly challenging cancer to treat, not only because of the late stages at which it is usually diagnosed, but also for its tendency to form early metastasis and its

intrinsic resistance to chemo and radiotherapy treatments. This is further underscored by the fact that even recent advances in cancer treatment like immunotherapy and immune check-point inhibitors have failed in PDAC, with check-point inhibitors approved for only 2% of PDAC patients, namely those presenting high microsatellite instability (Lemery *et al*, 2017).

Among pancreatic cells, acinar cells are very sensitive to genetic and environmental stimuli as compared to other pancreatic cells (Wang et al, 2019). They are able to differentiate into ductal cells in a process called acinar to ductal metaplasia, where they lose acinar marker and express markers of ductal lineage like cytokeratin-19 (CK-19) and SOX9 (Kopp et al, 2012). During differentiation, these metaplastic acinar cells are more prone to pro-oncogenic hits like KRAS mutations and environmental stressor that may lead to a transformation into Pancreatic intraepithelial neoplasia (PanINs). Accordingly, it has been suggested that acinar to ductal metaplasia might provide an initial step for PDAC development (Chuvin et al, 2017). PanINs are recognized precursor lesions of PDAC. They are divided into three categories (PanIN 1, PanIN 2 and PanIN 3) with increasing degrees of nuclear and cellular atypia. PanIN-1 and PanIN-2 lesions can be found even in the absence of cancer, while PanIN-3 is usually associated with invasive neoplasia (Distler *et al*, 2014). The prevalence of PanINs increase with age and are most commonly found in the head of the pancreas.

PanIN stage correlates with increasing genetic mutations. KRAS is an early mutation, already found in PanIN 1 stage, while the other classical mutations of PDAC like inactivation of *p16/CDKN2A* are usually associated to PanIN 2. Finally, inactivation of *TP53* and *SMAD4* are detected in PanIN 3 (Hruban *et al*, 2008). These genetic alterations recapitulate the consequential mutations observed in most cases of human PDAC (Sakorafas & Tsiotou, 1999). The high frequency and early appearance of *KRAS* mutation in PanINs supports the role of *KRA*S as an initiating event for PDAC development (Koorstra *et al*, 2008).

Given the difficulties in treating established PDAC, it would be very important to develop methods to detect early lesions like PanINs that would allow a window for monitoring their progression towards aggressive cancer and prompt early intervention. This is

particularly true for patients with familiar PDAC, where the possible detection of PanIN3 would suggest immediate and aggressive intervention (Hruban *et al*, 2008). However, even though PanINs have provided a valid model for studying the multi-step progression of PDAC, none of the altered genes or proteins found in PanINs have been translated into early disease markers or potential therapeutic targets for PDAC.

3.*1 Clinical presentation*

PDAC clinical presentation is often aspecific, depending mainly on the size and the anatomic location of the tumor: 60-70% of PDAC arise from the head of the pancreas, whereas 20-25% from the body/tail of this organ. Tumors arising from the head of the pancreas gain earlier clinical attention than those originating in the body and tail, as in the pancreatic head runs the common bile duct which, if compressed, induces jaundice (Kamisawa et al, 2016).

Generally, the most common presenting symptoms of PDAC are malignant biliary obstruction and weight loss (Hidalgo, 2011). Jaundice is caused by the extrinsic obstruction of the bile ducts and the subsequent increase in the levels of bilirubin and alkaline phosphatase in the blood. This results in dark urine and pale stools due the absence of urobilinogen and stercobilinogen (Rodarte-Shade & Kahaleh, 2015). Around 82% of patients with PDAC of the head of the pancreas have a painless jaundice, where the only symptom is pruritus due to the high bilirubin levels (Grossberg *et al*, 2020). Jaundice is present in 80-90% of patients with pancreatic head cancer, just in 6% of patients with cancer of the body and tail. When jaundice is detected in body and tail cancer, it usually indicates the presence of hepatic metastases and/or lymph nodes compression at the porta hepatis. Weight loss is present in up to 85% of patients at diagnosis (Hendifar *et al*, 2018). Severe weight loss in cancer patients is described as cachexia, a complex metabolic disorder characterized by progressive weight loss, loss of skeletal muscle and adipose mass, and systemic inflammation (Fearon *et al*, 2011). Weight loss and cachexia represent a detrimental burden for PDAC patients: they increase post-operative complications, decrease response to chemotherapy, lower quality of life, reduce survival. In addition, around 30% of patients die because of cachexia (Hendifar *et al*, 2019). Uncommon presentation of PDAC include acute pancreatitis (caused by

obstruction of the pancreatic duct), new onset diabetes and incidental findings on abdominal imaging (Fogel et al, 2017).

Around 80% of PDAC patients experience glucose intolerance or have frank diabetes. The majority of PDAC associated diabetes is found at the same time of cancer diagnosis or within 2 years before PDAC diagnosis (Pannala *et al*, 2009; Li, 2012). The tumor usually destroys only a small portion of the endocrine mass, and the hormone secretion function is maintained even with a large loss of islets of Langerhans – the endocrine disfunction is unlikely provoked by the decreased endocrine volume. PDAC patients have altered levels of insulin and other hormones release after stimuli, suggesting that the tumor could alter the secretion of different types of islet cells (Mezza *et al*, 2020). While type I diabetes is not believed to be associated with an increased risk of PDAC, type II diabetes (non-insulin dependent) is associated with a two-fold increase in risk of cancer development (De Souza *et al*, 2016). Type II diabetes is a long disease where the prolonged hyperinsulinemia might stimulate the growth of PDAC cells via the insulin receptor present on cancer (Mutgan *et al*, 2018; Chan *et al*, 2014).

Pain appears in almost all patients, even at different disease stages, it is usually localized in the upper abdomen that radiates to the back, and it responds poorly to drugs. Pain can be present even if the tumor is small (< 2 cm) and independently on its location, even though it is more frequently reported by patients with PDAC of the body and tail (90%) as compared to those with PDAC in the head of the pancreas (70%) (Tomasello *et al*, 2019). Pancreatic pain may also result from ductal stenosis or obstruction. The origin of pain is multifactorial and comprises neuropathic, visceral and somatic causes; it could also be the result of perineural invasion. Pain can be caused also by metastases in different sites: somatic pain derives from neoplastic invasion of peritoneum and bones, while visceral pain derives from metastases to liver or ascites in the abdominal cavity (Lohse & Brothers, 2020). Pain might serve as a predictor of poor outcome in PDAC, while in other pancreatic malignancies, where neural invasion is not a key pathological phenomenon, no association between pain and survival was registered (D'Haese et al, 2014). Indeed, pain from perineural invasion might suggest the presence of metastatic disease (Ceyhan et al, 2009a).

The majority of patients have metastatic disease at presentation. Most commonly, metastasis from PDAC are found in liver, lungs, peritoneum and regional lymph nodes (Mackay et al, 2019). The number of metastatic patients at diagnosis explains the high mortality of PDAC.

Patients with PDAC of the body and tail suffer from the same symptoms, but are more likely to experience pain as presenting symptom rather than jaundice, and are usually diagnosed at more advanced stages with a higher metastasis rate (Ling et al, 2013).

3.2 Diagnosis and differential diagnosis

To date, PDAC diagnosis relies on serological markers, imaging and cytological studies.

Among serological markers, the most validated is CA 19-9. CA19-9 is a mucinous glycoprotein, normally present in glandular secretions of mucous type, that can be detected at elevated levels in patients with pancreatic cancer (Goonetilleke & Siriwardena, 2007). The commonly used CA 19-9 cut-off is 37 kU/L, which has a mean sensitivity of 80% and specificity of 90%. However, 5-10% of the population lacks the glycosyl transferase Lewis blood group antigen required for CA 19-9, expression thus reducing the diagnostic potential of CA 19-9 (Lee et al, 2020). CA 19-9 levels have been also incorporated into the definition of borderline resectable disease by the International Association of Pancreatology as a biological factor: levels of CA19-9 above 500 IU/ml indicate an inoperable tumor(Isaji et al, 2018). In addition, it is also useful for monitoring patients after surgery and during chemotherapy. Indeed, in case of an effective reduction or eradication of the cancer, CA 19-9 levels diminish under threshold level. Conversely, in case of cancer recurrence or progression, CA 19-9 levels tend to increase, offering a tool to monitor disease progression (Salleh *et al*, 2020).

Different imaging techniques are routinely used for PDAC diagnosis and staging. Abdominal ultrasound is the first-line diagnostic tool used in patients presenting with jaundice or abdominal pain, since it is a non-invasive, cost-effective modality (Lee &

Lee, 2014). Doppler ultrasound can be performed to evaluate the involvement of peripancreatic vessels (like portal vein and mesenteric vessel, aorta and inferior vena cava), and to better evaluate the margins and size of the lesion, but it is not as diffused as ultrasound (Zamboni et al, 2012).

Further investigations to confirm diagnosis are required and are usually performed with computed tomography (CT) scan. CT scan has an excellent spatial and temporal resolution and allows assessment of both local and distant disease at the same time. The CT protocol that allows the best characterization of the mass consists of four phases (unenhanced, pancreatic/late arterial phase, portal/venous phase, late phase), and it is considered the modality of choice for radiological diagnosis (Zhang et al, 2018a). In the early phase of CT, PDAC is characterized by abundant fibrous stroma and it is hypovascularized, resulting in a poor enhancement of the tumor mass compared to the surrounding healthy parenchyma. The arterial phase is the most effective for tumor detection, the tumor mass appears as a defined hypodense mass in the hyperdense pancreatic parenchyma. The venous phase is better for liver metastasis detection. Contrast-enhanced CT scan is also the gold standard for evaluating vascular involvement, one of the most important factor for predicting resectability (Lee & Lee, 2014). Nonetheless, some lesions are of difficult observations to their small size, in particular hepatic and peritoneal metastases (Miura et al, 2006).

Thanks to its great soft-tissue contrast, magnetic resonance imaging (MRI) can be useful in detecting small lesions that might be dubious at CT scan (Robertis, 2015), but there is no significant advantage of MRI over contrast-enhanced CT scan for PDAC diagnosis: usually, this radiological technique is chosen when patients present with small lesions, hypertrophied pancreas and focal fat infiltration (Takakura et al, 2011).

Positron emission tomography, in association with CT scan, is very accurate for treatment monitoring during chemo-radiotherapy given its great sensibility to detect cancer recurrence and metastases, but it is not routinely used at diagnosis (Dibble et al, 2012).

The gold standard for PDAC diagnosis is endoscopic ultrasonography (EUS) with fine needle aspiration that allows histopathological diagnosis (Puli *et al*, 2013). It has replaced endoscopic retrograde cholangiopancreatography as the endoscopic procedure for tissue

acquisition, due to its lower post-procedural risks and the high sensitivity and sensibility (Raut *et al*, 2003). The tissue acquired with fine needle aspiration allows cytological studies with a sensitivity and accuracy of diagnostic evaluation in 85- 90% of patients (Hewitt *et al*, 2012). Cytological analyses evaluate the presence of anisonucleosis, nuclear membrane irregularity or enlargement, all of which suggest malignancy. When a bigger sample of tissue is required, for example when the retrieved tissue is necrotic, EUS with a fine needle biopsy is usually performed to improve yield without higher post-procedural complications. Tissue obtained from biopsies allows the analysis of intact tissue architecture as well as the performance of immunohistochemical stainings, thus providing a more accurate diagnosis (Cheng *et al*, 2018). Both cytology and histology are required to validate the neoplastic nature of all suspicious pancreatic masses, thus supporting the definition of the appropriate therapeutic plan. While Imaging techniques, especially CT, show specific characteristic useful for differential diagnosis, cytology is usually performed to validate the diagnosis.

It is fundamental to discriminate PDAC from other solid lesions of the pancreas. Differential diagnosis should be performed mainly with high-grade neuroendocrine tumors (NETs), solid pseudopapillary tumors, metastases and inflammatory lesions like pancreatitis.

NETs are tumors derived from the islet cells of Langerhans. They are divided into functioning NETs, when they secrete endocrine hormones (insulin, glucagon, somatostatin, vasoactive intestinal peptide), or non-functioning NETs, when they do not secrete hormones. They can be further classified as low, intermediate, and high grade tumors (Klimstra *et al*, 2010). High grade NETs are rare, poorly differentiated cancers with a high proliferative rate measured with Ki67 and abundant necrosis, and among NETs only the high grade ones go in differential diagnosis with PDAC. Indeed, on CT scans, they can appear as hypovascularized mass and lymph node metastasis, thus mimicking PDAC; however, they do not present pancreatic duct dilatation (Crippa *et al*, 2016).

Solid pseudopapillary tumors are rare pancreatic tumors (1-2% of all cases), typically seen in young women. Small (<3 cm) tumors have a pure solid nature with well-defined

margin that could mimic PDAC, but younger patients' age and the presence of intratumoral hemorrhage helps in discriminating these tumors (Megibow, 2012).

Metastases to the pancreas from another primary tumor are usually found in the context of a known disease, especially renal cell and lung cancer (Adsay *et al*, 2004). Usually, metastases are solitary hypodense masses that can be differentiated by the absence of pancreatic duct dilatation and the different pattern of enhancement after contrast medium (Triantopoulou *et al*, 2012).

Among inflammatory lesions, autoimmune pancreatitis can be challenging to discriminate from PDAC because of similar imaging features. Autoimmune pancreatitis are characterized by pancreatic infiltration of IgG4 plasma cells that give rise to pancreatic fibrosis causing narrowing of the pancreatic duct and acinar atrophy. However, vascular encasement and calcification are usually absent unlike in PDAC (Takuma *et al*, 2012). Groove pancreatitis is another rare condition that can be very difficult to differentiate from PDAC, and histologic confirmation is often required for differential diagnosis (Raman *et al*, 2013).

3.3 Staging and treatment

Accurate staging of PDAC is fundamental for prognosis prediction and more importantly for correct treatment stratification and patient selection for potential clinical trials. Staging of PDAC is based on the 8th AJCC/UICC edition tumor-node-metastases (TNM) staging system (Allen et al, 2017). This system classifies cancer on the basis of its extension: T (tumor) stage refers to the size of the primary tumor, N (nodes) defines the number of nearby lymph nodes that show the presence of neoplastic cells, M (metastasis) refers to the presence of metastatic spread. TNM staging is the major determinant for prognosis and treatment. TNM 8th edition for PDAC focuses on T size, allowing an improved prognostic discrimination as well as a refined N stage based on the number of positive lymph node (Schlitter *et al*, 2017). Tumor grading is not formally part of the TNM system, but it is an autonomous prognostic factor approved by the World Health Organization (WHO - (Bosman FT et al). Grade gives information on the degree

of differentiation of tumor cells and their biological aggressiveness, and it is a validated prognostic factor for survival (Strijker et al, 2019).

PDAC Treatment aims at limiting disease progression, increasing life span and ameliorating quality of life. The National Comprehensive Cancer Network (NCCN) recognizes four categories that stratify patients according to the treatment they will receive, while the TNM system is more useful for prognostic predictions (Tempero et al, 2021).

According to imaging evidence, NCCN recognizes four categories of PDAC:

- Resectable: intrapancreatic disease only, no contact with major vessels.
- Borderline resectable: involvement of superior mesenteric vein and/or portal vein with or without impingement and narrowing of the lumen, or short segment occlusion with safe reconstruction options; tumor abutment (when the tumor is inseparable from the vessel) <180° (< or = 50% vessel circumference) of celiac artery, common hepatic artery or superior mesenteric artery
- Locally advanced: superior mesenteric vein or portal vein occlusion with no possibility of reconstruction; tumor abutment >180° of celiac artery, common hepatic artery, superior mesenteric artery.
- Metastatic: any evidence of metastatic spread.

In addition to these anatomical criteria, biological and clinical criteria should be considered (Isaji et al, 2018). Biological resectability is focused on the level of the tumor marker at diagnosis, values above 200 U/ml have been correlated with aggressiveness of the disease and the presence of micro metastasis (Ferrone et al, 2006). Further, clinical criteria consider patients' fitness for surgery to prevent possible complications.

Treatment can be schematized as follows:

Surgical resection is the only curative treatment that significantly increases patients' survival. Only 20% of patients have resectable disease at time of diagnosis, with a median overall survival (OS) of 20-22 months (Oettle et al, 2013). Currently, surgery is almost always associated with neoadjuvant and/or adjuvant therapy to increase both disease free (DFS) and overall survival (Du & Wang-Gillam, 2017).

Neoadjuvant treatment has a fundamental role in PDAC since most patients are unresectable at diagnosis. Fluorouracil, leucovorin, irinotecan, and oxaliplatin (FOLFIRINOX) or gemcitabine + nab-paclitaxel are the preferred regimens (Oba et al, 2020). FOLFIRINOX induces mainly hematological or gastrointestinal toxicities, and cumulative peripheral neuropathy by oxaliplatin (Muranaka *et al*, 2017). Gemcitabine + nab-paclitaxel regimen induces mainly hematological toxicities (Blomstrand *et al*, 2019). The aim of neoadjuvant treatment in the settings of borderline resectable and locally advanced patients is to increase the chance of radical surgical resection, both by decreasing tumor size and by excluding patients who have disease

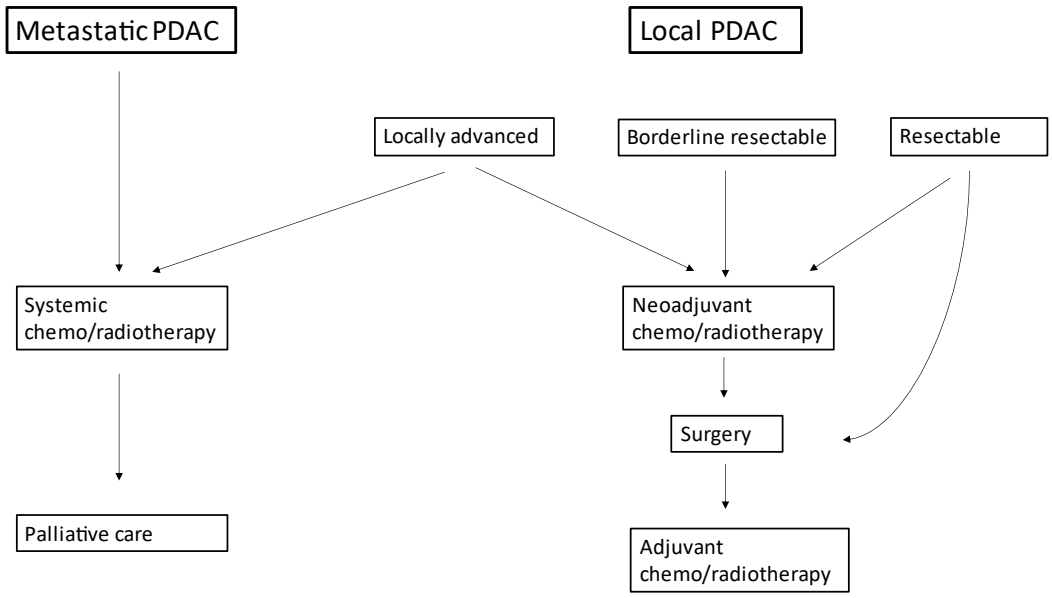

progression during treatment (i.e., with a biologically-aggressive disease) (Ferrone *et al*, 2015b). The role of neoadjuvant treatment for resectable patients is still debated, since it

could improve survival and treat undetected micro metastatic disease with the risk of delaying surgery and thus potentially favoring cancer growth ultimately limiting resection (Oba et al, 2020).

Adjuvant treatment is routinely administered to improve patients' survival after surgery. FOLFIRINOX is the best treatment option for fit patients, gemcitabine + capecitabine can be administered to the other patients, while gemcitabine alone should be reserved for very frail patients (Conroy & Ducreux, 2019).

Metastatic patients have a dramatic dismal survival rate, typically less than one year. Standard of care is FOLFIRINOX, while gemcitabine is preferred for frail patients (Conroy et al, 2011). When possible, metastatic patients should be directed to clinical trials that offer new therapeutic targeting strategies (Smithy & O'Reilly, 2021).

3.4 Prognosis

PDAC has one of the poorest prognoses among solid cancer, with a 5-year OS lower than 10%. Patients with resectable disease have a 39% 5-years OS, while patients with locally advanced disease have a 13% 5-years OS. 5-years OS drops to a grim 3% for patients with metastatic cancer at diagnosis, which are around half of newly diagnosed patients (Pancreatic Cancer: Statistics | Cancer.Net). In resected patients, the strongest predictor of survival remains lymph nodal status (Allen et al, 2017); other independent predictors of survival are perineural invasion (PNI), vascular invasion and resection margin status (Belfiori et al, 2020).

Among predictors of recurrence, lymph node ratio is the most described. (Groot *et al*, 2018). Lymph node ratio is the ratio of metastatic lymph nodes to the total number of harvested lymph nodes, it has a better prognostic performance than simply considering the number of positive lymph nodes that are more prone to be biased (You *et al*, 2019).

As mentioned, PNI is used as a predictor of disease progression. In a large metanalysis performed on 3538 patients, PNI was reported being present in 71.7% of patients and resulted as an independent negative prognostic factor for both OS and DFS (Schorn *et al*,

2017). Interestingly, a recent study indicates PNI as the only predictor of disease-free survival for early-stage pancreatic cancer. This study shows that PNI has a high prevalence even in early cancer, up to 78.7% in PDAC ≤ 20 mm and 70.6% in R0/N0 tumors, strengthening the idea that PNI is a very early phenomenon in pancreatic cancer and might represent a warning sign of a more aggressive disease (Crippa et al, 2020). In addition, another study focusing on long-term survivors (patients reaching 5 years of survival after surgery) demonstrated that the absence of PNI was the only predictor of survival (Belfiori *et al*, 2021).

Thus, recent studies indicate that PNI is a strong, negative prognostic factor for both OS and DFS; as such, it should be taken into consideration when planning adjuvant treatment for PDAC patients together with the other commonly evaluated pathological factors. Moreover, clinical trials are needed to identify and stratify PDAC patients based on PNI presence and aggressiveness of the disease; these studies might result in modification of the currently used therapies.

3.5 Pancreatic cancer: human disease, murine models and organoids

To mimic the human tumor, we can exploit genetically engineered mouse model (GEMMs) and orthotopic or heterotopic transplants in mice.

Pancreatic ductal adenocarcinoma (PDAC) GEMMs are particularly useful to study the cancer microenvironment, the immune response to cancer and the development of cancer at early stages; on the other hand, transplants are easier to perform and offer a more rapid tool for the development of pharmaceutical targets.

Both orthotopic and heterotopic transplants can be performed with neoplastic cells of murine or human origin (xenografts), derived from the primary tumor or from established bidimensional cell lines. Heterotopic transplant refers to the procedure where the organ or tissue is implanted in a different anatomical position compared to the physiological one, while orthotopic transplants maintain the same anatomical location. The use of both primary cells and established cell lines presents advantages and disadvantages. Transplanted cell lines, for example, do not faithfully recapitulate tumor biology due to the loss of heterogeneity observed in culture. On the other hand, it can be very difficult to obtain cell lines from some slowly growing tumors (Meijer *et al*, 2017).

Considering instead the use of murine vs. human cells, a disadvantage of xenografts is that they require immunodeficient mice, losing the possibility of studying the interactions between cancer cells and the immune system (Siolas & Hannon, 2013).

In addition, heterotopic models lack the cancer microenvironment that is fundamental to correctly study cancer growth and progression (Lee *et al*, 2016). Orthotopic models, instead, are widely used thanks to their lower cost compared to GEMMs, as well as to their better reproducibility. They offer the possibility to study the cancer microenvironment and, when using immunocompetent mice, characterize almost all the components of the tumor microenvironment. They are also more accurate for drug testing as compared to heterotopic models (Qiu & Su, 2013).

A recent development for orthotopic transplants is the possibility to use both murine and human organoids, to reproduce PDAC. Organoids are self-assembling, three-dimensional cultures grown into an extracellular support. They are almost identical to their organ of origin, also from a histological point of view (Kim *et al*, 2020). Organoids overcome some of the difficulties encountered with the classic bi-dimensional models used in cancer research, both for *in vivo* and *in vitro* studies. They retain tumor heterogeneity and maintain a three-dimensional architecture that enables cells to reproduce the mechanical interactions occurring *in vivo*. Moreover, organoids can be co-cultured with other cell types, like fibroblasts and immune cells, thus allowing to reach a more complex level of understanding of the tumor microenvironment (Tsai *et al*, 2018).

Organoids are relatively fast to develop and expand, features that makes them appealing for personalized medicine and drug screening (Baker *et al*, 2016). A recent study performed therapeutic profiling of patient-derived organoids and compared these results with the clinical response of a selected cohort of patients to the same drugs. Remarkably, organoids resistance to drugs, measured in terms of cell viability, turned out to be comparable to that of corresponding patients, measured in terms of progression free survival. In addition, patient-derived organoids resistant to drugs routinely used in the clinical practice were tested for sensitivity to other drug regimens, providing an interesting approach for precision medicine (Tiriac *et al*, 2018).

Another interesting application of organoids is the possibility to derive them from metastases, by means of biopsies and, more recently, from circulating tumor cells. In this

setting, organoids are a relatively fast method to perform drug screening tests - it takes around 6 weeks to establish organoids and perform drugs screening from metastases. From this perspective, they offer a prediction on treatment response, and represent an alternative treatment regimen in case of resistance to the chosen one (Frappart & Hofmann, 2020).

Organoids are not only excellent models for *in vitro* studies, but they have many advantages also for *in vivo* experiments. Transplanted organoids are a validated model to study the development of PDAC, with reproducible timing of progression from pre-invasive lesions to overt cancer and metastatic dissemination (Boj *et al*, 2015; D'Agosto *et al*, 2020a). The slow progression of neoplastic lesions occurring in organoids transplants reproduces more faithfully human PDAC growth; moreover, they recapitulate stromal deposition, molecular subtype and immunophenotype of the human disease (Filippini *et al*, 2019).

Since the characterization of the driver mutations of PDAC, many murine models have been created to reproduce the human disease. *KRAS* is activated in 95% of PDAC patients, while the tumor suppressor genes *CDKN2A*, *TP53*, and *SMAD4* are inactivated in 95%, 75% and 55% of patients, respectively (Saiki & Horii, 2014).

The precursor of the currently most used models of PDAC is the KC mouse, characterized by a heterozygous knock-in allele of (mutated) *KRAS* at the single site G12D, which is also the most commonly mutation found in patients (Kamisawa *et al*, 2016). By using this model it was possible to demonstrate that mutation in *KRAS* is sufficient to induce PDAC formation, in particular the pre-neoplastic lesions termed pancreatic intraepithelial neoplasia (PanIN). Despite the importance of this model, KC mutant mice require an extensive period do time to develop bona fide PDAC tumors. In addition the eventually formed tumors do not develop metastatic cancer (Westphalen & Olive, 2012). A rapid progression from PanIN to PDAC was obtained when the KC mutant was crossed with mice bearing additional mutations in tumor suppressor genes. Additional mutations in important tumor suppressor genes that were found to be deleted in sporadic human PDAC have generated other GEMM: deletion of *CDKN2A* (encoding the $p16^{Ink4a}$ and $p19^{Arf}$ tumor suppressors) in combination with $Kras^{G12D}$ leads to earlier

appearance of PanINs and to a rapid progression to metastatic cancer (Aguirre *et al*, 2003); *Kras*^{G12D} combined with knockout of the TGF-β2-receptor results in a well-differentiated PDAC, closely resembling the human PDAC, with a 100% penetrance – though mutation or deletion of TGF-β2-receptor are found in less than 5% of patients (Ijichi *et al*, 2006). The most used model is probably the KPC model (*PDX-1-Cre, LSL-Kras*^{G12D}*, LSL-Trp53*$^{R172H/-}$), which carries mutation in *Kras*^{G12D} and a conditionally expressed point mutant allele of *Trp53*^{R175H}. Both mutations occur in developing mouse pancreas through interbreeding with *Pdx-1-Cre* transgenic animals (Hingorani *et al*, 2005). This model resembles human histopathological alterations – like decreased vasculature and resistance to common chemotherapeutic agents. Moreover, it develops metastases resembling those observed in patients, in lung, liver and peritoneum (Ponz-Sarvise *et al*, 2015). However, it is still debated whether the KPC model develops PNI. Indeed, neural invasion has been described only when the primary pancreatic mass reached big dimension and compressed the posterior abdominal nerves, but not in terms of nerve hypertrophy and altered neural density – which are the phenomenon commonly observed in human patients. (Demir *et al*, 2015a).

4. **Perineural Invasion**

PNI is defined as the presence of cancer cells along and inside nerves. Specifically, cancer cells can be found in the epineural, perineurial and endoneural space of nerves (Liebig et al, 2009). Though the ability of neoplastic cells to exploit nerve for their growth process has been hypothesized almost 200 years ago (M Jobert, 1840), only in more recent years PNI has been accepted as a fourth route of cancer dissemination – together with the "classical" vascular, lymphatic spread and direct invasion.

PNI is an invasive phenomenon still not completely understood; it is emerging as a negative prognostic factor in different malignancies, even if the prevalence of PNI vary greatly among the various types of cancer. In gastric cancer and cholangiocarcinoma, PNI is found in 41% and 80% of cases respectively, and it is a recognized indicator of aggressive disease and poor OS (De Franco et al, 2018; Zhang et al, 2020). In colorectal cancer, PNI has a lower prevalence as compared to other gastro-intestinal malignancies, around 10-30%. Nevertheless it is a validated prognostic factors that might be related to aggressive disease (Knijn et al, 2016). In head and neck cancer, PNI is present in up to 80% of patients and it correlates with increased recurrence and diminished OS but also with pain (trigeminal neuralgia) and facial nerve paralysis (Bakst et al, 2019; Amit et al, 2016). Finally, in prostate cancer, PNI is associated to a more aggressive disease and greatly reduces OS of patients (Zareba et al, 2017).

Though PNI is getting more and more attention in different types of cancer, the understanding of its pathogenesis is still limited by inadequate or incomplete *in vivo* and

in vitro reliable models mimicking it. The most used *in vitro* model to study PNI relies on co-cultures of neoplastic cells with dorsal root ganglia (DRGs) neurons explants, obtained either from embryos or from adult mice (Huyett *et al*, 2017; Gil *et al*, 2010; Na'ara *et al*, 2016). These models exploit the radial growth of axons from the DRGs that eventually contact neoplastic cells (Ayala *et al*, 2001). When DRGs are cocultured with PDAC cells, they induce a significant neurotrophic movement of PDAC cells along the axons (Gil *et al*, 2010).

In addition to *in vitro* approaches, also *ex vivo* models have been proposed to study PNI. One particular study (Abiatari *et al*, 2009) aimed at investigating the relationships existing between PDAC cells and rat vagal nerves, in order to reveal distinct gene expression profiles typical of highly neuro-invasive cells. In this work, the authors measured the invasiveness of neoplastic cells by analyzing the time needed to move along the resected vagal nerve and divided cells into highly and minimally invasive. Through genome-wide transcriptional analyses, they were able to identify a consensus set of genes differentially regulated in the highly versus minimally invasive cells.

In vivo models are more physiologically relevant, but PNI can be difficult to detect given the small size of nerves and their anatomical location. A recent model of heterotopic transplant suggests a way to study the direct interaction of PDAC cells and nerves overcoming the problem of size and accessibility of invaded pancreatic nerves. By injecting neoplastic cells into the distal murine sciatic nerve, it was shown that neoplastic cells migrated proximally towards the spinal cord. This protocol allowed also for the collection of invaded nerves for subsequent microscopic and molecular studies (Deborde *et al*, 2018). Since this model uses the sciatic nerve that is not a site of PDAC metastatic spread, it does not allow studying the interactions between nerves and cancer and the site of the primary tumor. Moreover, the sciatic nerve has a different fiber composition from pancreatic nerves, thus influencing the overall analysis.

Therefore, the previously described animal models of PDAC, like the KPC mouse, as well as orthotopically transplanted mice, represent more reliable ways to study PNI, though further characterization is needed to find a reproducible, easy way to access invaded nerves.

4.1 Mechanisms of Perineural Invasion

Cancer cells exploit nerves like healthy tissues rely on innervation for survival. It has been well characterized that cancer can use different molecules secreted by nerve for growth and dissemination.

The first paracrine mechanism of interaction identified was supposedly mediated by tissue growth factor α (TGFα) released by nerves that promoted cancer growth via epithelial growth factor receptor (EGFR) (Bockman et al, 1994); since then, plenty of molecules have been investigated in PNI. Among the family of neurotrophins, nerve growth factor (NGF) and brain-derived neurotrophic factor (BDNF) (and their cognitive receptors TrkA/p75NTR, TrkB) have been correlated in different cancer types to increased neoplastic growth and associated to metastasis (Liebig et al, 2009). NGF is produced by PDAC cells and its receptors TrkA and p75NTR are expressed both on cancer and on nerves. Moreover, NGF released by cancer cells, enhances neural growth and its blockage reduces the migration of cancer cells towards DRG neurons in an *in vitro* model of PNI (Bapat *et al*, 2016). As a further confirmation, immunohistochemical analysis on human PDAC samples revealed that PNI was significantly correlated with high NGF levels (Ma *et al*, 2008). High NGF-TrkA expression also correlated to diminished OS, worse pain severity and more frequent PNI in human patients (Dang *et al*, 2006). Accordingly, that treatment with anti-NGF antibodies in KPC mice at 8 weeks, when PanINs start to appear, reduces metastatic abilities of neoplastic cells. However, no effect was observed on the primary tumor (Saloman *et al*, 2018). Besides, members of the glial cell line-derived neurotrophic factor (GDNF) family play a role in cancer-nerve interactions. GDNF via RET (REarranged during Transfection) signaling works as a chemoattractant for PDAC cells towards nerves, and both molecules are increased in PDAC patients (Ito *et al*, 2005). It has been proposed that GDNF secretion by nerves is one of the mediators of PNI; nerves from GDNF-deficient mice attracted less PDAC cells as compared to wild type nerves. Moreover, blocking GDNF or RET expression with specific antibodies reduced PNI *in vitro* and *in vivo* in an heterotopic model of PNI, where cancer cells where injected in the sciatic nerve and their migration was reduced (Gil *et al*, 2010). Neurturin, released by PDAC cells, promotes neuroplasticity in DRGs co-cultures, and neurite density was severely diminished when anti-NRTN antibody was added to

conditioned media of PDAC cells (Wang *et al*, 2014). Artemin, another member of the neurotrophin family of proteins, is more expressed in tumors that showed a higher incidence of lymph nodes metastasis and PNI. A recent study has suggested that Artemin promotes the migration of PDAC cells, supporting PNI and metastatization, via NF-kB-CXCR4 signaling (Wang *et al*, 2018; Gao *et al*, 2015).

Chemokines are signaling proteins involved in many physiological processes, like immune responses and wound healing; they also participate in PNI, mainly in PDAC, prostate and breast cancer. CXCR4 is highly expressed in cancer cells and mediates invasion of organs and nerves expressing CXCL12. In addition, CX3CL1/CX3CR1, which is fundamental for central nervous system homeostasis, mediates the neural tropism of PDAC already at the stage of early neoplastic lesions (Zhang et al, 2018b; Celesti et al, 2013).

To create a network of nerve fibers, cancer uses the same axon guidance molecules that organize growing axons and neurons during normal development: Slits, Semaphorins, Ephrins (Chédotal et al, 2005). PDAC cells secrete Semaphorin 3D, which interacts with Plexin D1 on nerves. The result of this interplay is the increase in cancer migration and invasiveness (Jurcak et al, 2019). Semaphorin 3A, instead, has been associated with increased metastasis and malignancy in human specimens of PDAC (Müller et al, 2007). High Semaphorin 4F expression in prostate cancer correlates with neuro-epithelial interactions and aggressive cancer (Ding et al, 2013). In addition, reduced Slit2 expression in PDAC cells might promote metastatization and reciprocal attraction between nerves and cancer; consistently, restoring the expression of this repellent molecule decreases PNI (Gohrig et al, 2014).

In the tumor microenvironment nerves grow both in size (axonogenesis) and number (neurogenesis), as compared to normal tissues. Axonogenesis and neurogenesis are present at the early stage of cancer development, already at the stage of pre-neoplastic lesions like PanINs, and probably contribute to cancer initiation and progression (Wang *et al*, 2020). Both axonogenesis and neurogenesis were described in prostate cancer (Ayala et al, 2008), in pancreatic cancer (Ceyhan *et al*, 2009c), in breast cancer (Zhao *et al*, 2014b) and in head and neck cancer (Amit et al, 2020a). Moreover, increased neural

density correlates with worse survival and pain, especially in PDAC patients (Bapat et al, 2011).

Neurogenesis relies on the proliferation and subsequent differentiation of neural stem cells. Physiologically, it takes place during embryonic and early post-natal phases in different brain areas (García-González *et al*, 2017). A study on prostate cancer found that patients had a higher number of neurons in their prostatic ganglia as compared to healthy controls, thus supporting the possibility of neurogenesis in cancer (Ayala *et al*, 2008). A recent study hypothesized that these neurons originate from neural precursors cells that migrate from the central nervous system subventricular zone to the site of the tumor, thanks to a disruption in the blood-brain-barrier during cancer development. Once neural precursors reach the tumor site, they differentiate into adrenergic neurons and sustain tumor growth (Mauffrey *et al*, 2019). However, the upstream mechanisms that contribute to neurogenesis in prostate cancer and in other types of cancer have yet to be defined.

Nerve fibers can be attracted by the tumor and grow towards the neoplastic microenvironment. Indeed, cancer cells secrete neurotrophins and axon guidance molecules that promote nerve outgrowth and hypertrophy. In PDAC, increased innervation was observed already at the stage of PanIN lesions, supporting the idea that axonogenesis and the resulting microenvironment rich in neurotrophic factors support cancer progression (Stopczynski *et al*, 2014).

Cancer cells interact with both sympathetic and parasympathetic nerve fibers. The various organs have different types of innervations, for example the stomach is mainly innervated by the parasympathetic nervous system while the pancreas has both sympathetic and parasympathetic innervation. Cancer arising in different organs will thus have a specific relationship with sympathetic and parasympathetic fibers, that can behave differently on the basis of the type of innervation of the organ (Zahalka & Frenette, 2020). In PDAC, sensory and adrenergic signals have a pro-tumorigenic effect as confirmed by the reduction of cancer progression after chemical denervation of sensory nerves (Saloman et al, 2016) and the increased response to gemcitabine after ganglionectomy of both coeliac and superior mesenteric plexus (Renz et al, 2018a). Moreover, surgical vagotomy increases PDAC progression by damaging both parasympathetic and sensory fibers. This effect was not recorded with selective denervation of the sensory fibers of the

vagal nerve (Renz et al, 2018b). Moreover, surgical vagotomy increased pancreatic inflammation and the recruitment of tumor-associated macrophages – both pro-tumorigenic events (Partecke *et al*, 2017). Interactions between cancer and nerve cells have been described also in other types of cancer, with different outcomes according to the organ of origin. In a gastric cancer model, denervation via vagotomy reduces cancer growth ((Zhao et al, 2014a). In breast cancer, sympathetic fibers via adrenergic signaling are an established pro-tumoral stimuli, promoting tumor growth, angiogenesis and metastasis (Conceição et al, 2021). In prostate cancer, increased adrenergic signaling has been associated to more aggressive tumors (Braadland et al, 2015; Magnon et al, 2013). In line with the pro-tumorigenic potential of adrenergic signaling, two recent papers have suggested that cancer is even able to create and remodel its own nervous system: during prostate cancer initiation, neural progenitors can migrate from the central nervous system to infiltrate the tumor where they are able to differentiate into adrenergic neurons, sustaining cancer growth (Mauffrey et al, 2019), while loss of *p53* in head and neck cancer leads to neurons reprogramming towards an adrenergic phenotype (therefore more cancer-promoting) via secretion of exosomes (Amit et al, 2020b).

Nerves are also exploited as metabolic source. PDAC has a particularly desmoplastic and nutrient-poor environment which is highly innervated. In this setting, it has been suggested that axons can sustain tumor growth by the release of serine. Serine deprivation, indeed, decreases neoplastic protein synthesis and tumor size (Banh et al, 2020). In prostate cancer, adrenergic neurons release noradrenaline that boosts endothelial cell metabolism and promotes an angiogenic switch, thus supporting tumor growth (Zahalka et al, 2017). The role of nerves in cancer metabolism is an emerging field, whose many aspects still need to be investigated.

4.2 Perineural Invasion in Pancreatic Cancer

PNI was first described in pancreatic cancer in 1944 and it immediately correlated to pain (Drapiewski, 1944). With time, it was noted that, among other gastrointestinal tumors, PNI has the highest prevalence in PDAC. Indeed, PNI in PDAC could reach

100% if enough histological sections are examined according to some studies (Liebl et al, 2014). It is also remarkable that PNI is present in up to 70% of early PDAC, both in R0/N0 lesions and in tumors smaller than 2 cm, where it is the only predictor of disease free survival (Crippa et al, 2020). Such an early and pervasive phenomenon supports PDAC growth with various mechanisms that are still not completely understood. From a histological perspective, nerves in PDAC are hypertrophic with increased neural density, both inside and around the tumor mass – a phenomenon defined as "neural remodeling" of PDAC (Demir *et al*, 2015a) (Figure 6).

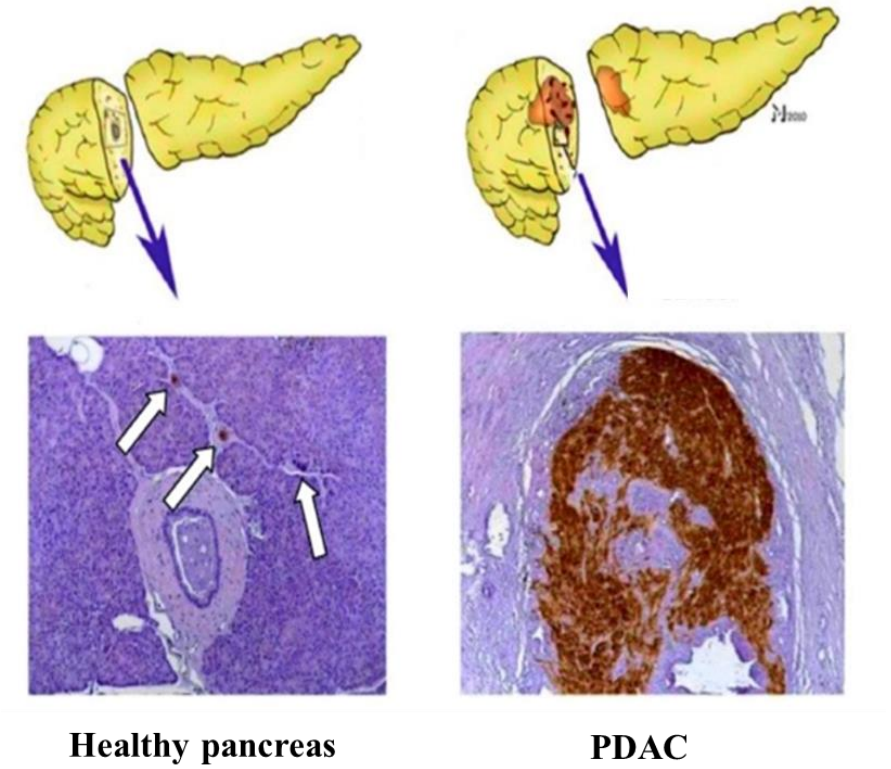

Figure 6. Nerve hypertrophy in PDAC compared to normal tissue

Representative histological section of nerves (immunohistochemically- brown labeled for the pan-neuronal marker protein gene product 9.5/PGP9.5) in normal pancreatic tissue, where nerves are limited to intra- and interlobular spaces, compared to pancreatic cancer, where nerves grow in a dysregulated fashion. Modified from (Ceyhan *et al*, 2009b).

In human PDAC, SCs are found around these enlarged nerves. Of note, most of them express glial fibrillary acidic protein (GFAP), a marker of trans-differentiated SCs. Interestingly, GFAP positive SCs are also found around PanINs, but not in normal pancreatic tissue. However, it should be noted that also pancreatic stellate cells express GFAP in physiological condition, and great attention must be given in correctly identifying the type of GFAP expressing cells (Zhou *et al*, 2019).

It has been proposed that SCs play a major role in disease progression when directly interacting with PDAC cells. *In vitro* experiments demonstrated that SCs are specifically attracted from pancreatic cancer cells. Importantly, SCs can enhance the recruitment of neoplastic cells towards DRG neurons, as depletion of SCs by irradiation decreases neoplastic invasion of DRGs. Moreover, SCs directly contact single neoplastic cells and modify their shape towards a more invasive phenotype. Specifically, pancreatic cancer cells co-cultured with isolated SCs in a three-dimensional Matrigel assay, reorganize their normally round morphology into a more elongated shape and start to migrate towards SCs. On the other hand, SCs contact cluster of cancer cells that, in turn, extend protrusion toward SCs and assume a more elongated shape. SCs can also intercalate their protrusion interrupting cell-cell contact in the cluster and facilitate single neoplastic cell dispersion. (Deborde *et al*, 2016).

The central role of SCs in sustaining neoplastic cells has been confirmed in *in vitro* models as they promote cancer cells motility and invasiveness via the secretion of TGFβ that activate TGFβ-SMAD signaling pathway in neoplastic cells, supporting PDAC aggressiveness (Roger *et al*, 2019).

It has been proposed that PNI promotes cancer metastatization via lymph node invasion. This could occur especially through the invasion of bigger axons, since large caliber fibers, differently from smaller ones, often contact lymph nodes (Cheng *et al*, 2012). The idea of PNI supporting lymph nodes metastasis is intriguing, considering the importance of the N status on patients' prognosis, but further studies are needed to characterize this interaction especially at the molecular level.

PNI has been correlated also with the often-intractable pain in patients. Pain associated to PNI and PDAC can develop in multiple ways. Invading neoplastic cells can damage nerve structure and leave it exposed, or neoplastic cells could use nerves as highways to spread and form metastasis, which are often responsible of severe pain in PDAC patients (Bapat et al, 2011).

Few studies have focused on the identification of molecules and pathways implicated in pain insurgence in PDAC patients. Among them, NGF has emerged as a central effector. Indeed, NGF released by the tumor microenvironment (especially from macrophages and fibroblasts) can act on nearby nerves, in particular CRGP positive sensory neurons, and transduce downstream signaling events upon interaction with TRKA and p75NTR receptors (Lindsay *et al*, 2005). NGF can also activate the transient receptor potential vanilloid 1 (TRPV1) on sensory neurons, enhancing pain sensitivity in PDAC patients (Zhu et al, 2011). Other factors overexpressed in PDAC, like GDNF and Artemin, can also activate TRPV1 and pain signaling (Malin *et al*, 2006). Treatment of pain in PDAC is particularly challenging for physicians. Since the main mechanism causing pain in PDAC is nerve invasion, initial treatments rely on the activity of specific pain killer drugs to ameliorate patients' quality of life. However, in unresponsive patients, physicians have tried to design pharmacological therapies aimed at blocking the coeliac plexus, by injecting neurolytic agents like alcohol or phenol to destroy nervous fibers via percutaneous or radiologically guided techniques (De Leon-Casasola, 2000). Due to the multiple side effects and to the short-term action, this treatment does not represent the best possible treatment. Approaches that specifically target PNI in PDAC are therefore needed to improve patients' quality of life.

The effectiveness of neoadjuvant chemo-radiation treatment on PNI is controversial. Some studies report that neoadjuvant chemo-radiation therapy decreases PNI frequency, from 95.4% vs. 72.5% (Ferrone *et al*, 2015a) and from 88% to 70% (Roland *et al*, 2015), while other authors reported a trend toward PNI reduction that did not reach significance (Crippa *et al*, 2020; Kurata *et al*, 2021). The different types of neoadjuvant treatment used among these studies could explain the reported difference. There is therefore a need to correlate different chemo-radiation regimens with their effectiveness on reducing PNI.

Defining the parameters required to implement a detailed classification system will facilitate the understanding of the role of PNI in PDAC. As of now, pathological reports define PNI only as present or absent, while a better stratification could give a deeper insight on PNI behavior in relationship with other pathological features. This systematic approach could also reduce the variability encountered in different studies, since it would offer a common classification method.

A similar approach was proposed for gastrointestinal malignancies: indeed, PNI has been coded into three categories, based on the depth of invasion into the nerves. In this study PDAC emerged as the type of cancer associated with the highest PNI frequency, with a direct correlation with a worse prognosis (Liebl *et al*, 2014). However, a score defining the severity of PNI specifically dedicated to PDAC is still missing.

4.3 Nerve Damage Response

SCs are incredibly plastic as they can transform into repair SCs after peripheral nerve injury. Repair SCs secret growth factors necessary to promote nerve regeneration and form tracks that serve for axon guidance. PDAC cancer cells can probably exploit these features for their own growth (Boilly et al., 2017).

Given the similarities between the processing occurring during nerve regeneration and PNI in PDAC, we will briefly describe them.

Various events can damage peripheral nerves, like traumatic or metabolic injuries or even genetic neuropathies. Unlike the CNS, in the PNS nerves can regenerate: axons regrow and remyelinate following a process called Wallerian Degeneration (Figure 7).

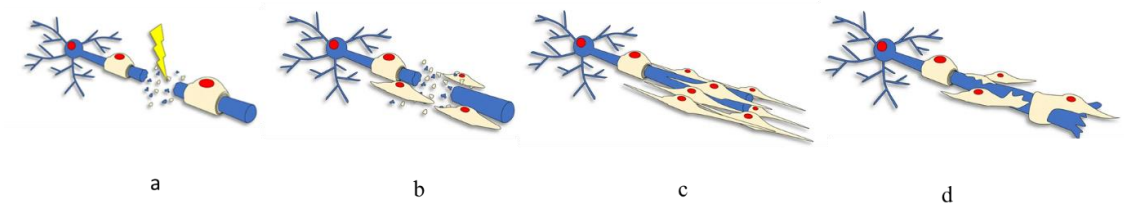

Figure 7. Progression of degeneration and axon regeneration after peripheral nerve injury.

Schematic representation of the different phases of degeneration and regeneration after peripheral nerve injury. Each step shows a single neuron (blue) interacting with SCs (light yellow). After nerve injury (a), SCs trans-differentiate into repair SCs and start clearing myelin debris (b) before the arrival of macrophages (not shown). Then, SCs proliferate and form regeneration tracks promoting axonal regrowth (c). Eventually, SCs remyelinated the regenerated axon (d). Modified from (Nocera & Jacob, 2020)

After nerve damage, SCs (both myelinating and non-myelinating) exploit their plasticity and trans-differentiate into repair cells. Repair SCs clear myelin fragments and attract macrophages from the periphery to completely remove myelin debris, otherwise detrimental to the regeneration process. In addition, they promote survival of damaged axons and guide their regrowth (Arthur-Farraj *et al*, 2012). Immediately after damage, SCs lose contact with axons. This event triggers phenotypic changes in SCs, which downregulate the expression of transcription factors and myelin-associated genes like *Krox20*, *MBP*, *MAG* and upregulate genes characteristics of the repair phenotype, like *NCAM*, *L1*, $p75^{NTR}$ and *GFAP*. Simultaneously, they activate a complex repair program, expressing genes involved in myelin degradation, trophic factors, cytokines and chemokines important to create a supportive environment for axonal repair. To facilitate correct axonal re-growth, denervated SCs proliferate and elongate up to three-fold the original cell length, forming parallel column inside the basal lamina in which they were previously enclosed and creating the so called “bands of Bungner”. The axonal growth cone elongates inside these bands and reaches the target organ (Gomez-Sanchez *et al*, 2017).

Myelin fragments clearance is essential to promote regeneration, as these fragments contain proteins that have an inhibitory effect on regeneration (McKerracher & Rosen, 2015). Myelin clearance is an early event and SCs activate autophagy programs that allow for up to 50% of myelin fragments clearance in the first week after injury, while the second phase relies mostly on recruited macrophages. Denervated SCs form ovoids of their own myelin, starting from paranodal regions adjacent to Schmidt-Lantermann incisures, where myelin is more accessible (Bolívar *et al*, 2020). Given the high percentage of lipids in myelin, it has been proposed that lipases could start myelin degradation. Already after 5 hours after sciatic nerve injury, SCs upregulate the expression of phospholipase A2, responsible for phosphatidylcholine hydrolysis in

arachidonic acid and lysophosphatidylcholine (De *et al*, 2003). This autophagy program, or, given its specificity, "myelinophagy" program, is up-regulated in SCs after crush injury and it has been suggested to rely on the JNK1/c-Jun pathway (Gomez-Sanchez *et al*, 2015). Moreover, dedifferentiated SCs secrete ECM components as well as trophic factors that are instrumental for regeneration (Chen & Strickland, 2003).

SCs also attract immune cells to complete myelin clearance. They express cytokines like tumor necrosis factor α (TNFα), leukemia inhibitory factor (LIF), interleukin-1α (Il-1α) and 1β. Recruited immune cells secrete, among other molecules, IL6 that together with LIF promotes neurons survival (Rotshenker, 2011). The majority of the inflammatory cells recruited to the nerve after damage, is represented by macrophages, which are responsible for myelin clearance in the latest phases of nerve injury (Stratton & Shah, 2016). Inflammation then returns to normal levels allowing axons to regenerate and remyelinate.

Among the regulators of the repair program, the transcription factor *c-Jun*, a negative regulator of myelination (Jessen & Mirsky, 2008), is central. *c-Jun* is upregulated in SCs a few hours after injury, it is necessary to suppress the myelination phenotype, for example by downregulating genes like *MBP* and *MPZ*, but also to activate the repair program (Parkinson et al, 2008a; Arthur-Farraj et al, 2012). If *c-Jun* is conditionally ablated in SCs, activation of the repair program fails, myelin genes are not downregulated and the genes involved in trophic support of axons are not up-regulated. In addition, mutant mice lacking *c-Jun* expression in SCs have abnormal bands of Bugner and delayed myelin clearance. These phenomena result in impaired axonal regeneration, increased neuronal death and compromised functional recovery (Arthur-Farraj et al, 2012).

Other signaling events important for the activation of the repair program are ERK and Notch pathways. Indeed, Raf/MEK/ERK induction induces SCs dedifferentiation *in vitro*, and transected nerves show a strong phosphorylation and activation of ERK1-2 (Harrisingh et al, 2004). Moreover, activation of an inducible Raf-kinase gene and the corresponding ERK pathway is sufficient to induce severe demyelination and SCs proliferation in the absence of axon damage. Raf-kinase activation, indeed, originates an inflammatory response and the breakdown of the blood-nerve-barrier, with subsequent immune cells influx. The period of demyelination and dedifferentiation is controlled by

the duration of ERK pathway activation, and by switching off ERK signaling this phenotype is reverted (Napoli et al, 2012).

The other important factor involved in nerve repair is Notch, a receptor protein that, after ligand binding, is cleaved to generate the Notch intracellular domain (NCID). NCID then moves to the nucleus where it works as a transcriptional regulator (Bray, 2006). Notch signaling is implicated in SCs dedifferentiation: indeed, NCID is upregulated in nerves after injury *in vivo*. When Notch signaling is conditionally ablated in SCs, their differentiation rate is reduced; moreover, activation of Notch signaling in normal nerves can induce demyelination (Woodhoo et al, 2009).

Once myelin fragments are cleared, SCs and macrophages secrete trophic factors to sustain axonal regrowth. Macrophages also secrete the Vascular Endothelial Growth Factor (VEGF), thus promoting neo-vascularization at the injury site. The newly formed blood vessels run parallel to the nerve bridge and can be exploited by SCs as migration substrates (Cattin et al, 2015). A prerequisite for axonal regeneration is the activation of the Regeneration-Associated program (RAG) in neurons and an increased mitochondrial density to provide energy (Girouard *et al*, 2018). Axonal regrowth starts with the creation of a growth cone that extends along the bands of Bugner and will lead to the reinnervation of the target organ. Recent evidences confirm that, without SCs, axons cannot cross the nerve gap (Rosenberg *et al*, 2014). In addition, deletion of the axon guidance molecules *Sox2*, *Slit3*, and *Robo1* leads to SCs aberrant migration after sciatic nerve injury and to disorganization of axonal regrowth (Dun *et al*, 2019).

Among the molecules involved in the process of remyelination, NRG1 surely has a central role. *In vivo* overexpression of NRG1 type III in neurons improves remyelination after nerve crush injury. Moreover, overexpression of NRG1 type I, expressed in SCs, improves remyelination as well, suggesting a positive role for NRG1 type I in the repair process (Stassart *et al*, 2013). Furthermore, conditional deletion of NRG1 in a specific subset of sensory and motor neurons caused hypomyelination and delayed regeneration after nerve injury (Fricker *et al*, 2013). In line with a role for NRG1 in regeneration, it has been proved that, after nerve damage, NRG1 receptor ErbB2 is transiently activated, and a sustained activation of the ERK pathway has been registered (Guertin *et al*, 2005).

The process of remyelination involves the seven-fold shortening of SCs, resulting in the generation of typically short myelin internodes (Sherman & Brophy, 2005). Indeed, even when the process of regeneration has been completed, myelin is thinner as compared to undamaged nerves and nerve conduction velocity is reduced.

Regeneration terminates with target organ innervation. Unfortunately, in human patients the regeneration process often fails. The main limitation is the fact that axons do not reach their target, but further studies are needed to fully understand the failure of regeneration and to identify novel mechanisms for the treatment of chronic denervation.

The paradigm of nerve damage – regeneration is instrumental to correctly study PNI: indeed, the neural remodeling induced by PDAC involves an increased axonal growth that is anticipated by the aggressive disruption of the outermost nerve layers, like the myelin sheath, that are otherwise inhibitory to axonal growth (Filbin, 2003).

Aim of the work

The aim of this work is to investigate the molecular mechanisms leading to perineural invasion in pancreatic ductal adenocarcinoma.

Previous studies demonstrated that neoplastic invasion of intrapancreatic nerves, neurogenic inflammation, and tumor metastases along extra-pancreatic nerves, are key features of pancreatic malignancies. Moreover, it is now accepted that perineural invasion is present even at very early stages in PDAC, suggesting that nerves might have an active role in promoting PDAC development and progression.

Nerves and cancer form a unique microenvironment, where Schwann cells (SCs) and axons directly interact with neoplastic cells. To fully understand the role of neural plasticity in PDAC, it is therefore important to clarify the role of both glial and neural cells. Since the role of glial cells in PDAC progression has been poorly investigated, we decided to explore whether myelinated SCs might have a role in cancer progression.

To reach this aim, we analyzed how myelinated nerves interact with pancreatic cancer cells and subsequently characterized the molecules mediating interaction with myelin. To validate the interaction between nerves and cancer in a more physiological model, we developed organoids both for *in vitro* and *in vivo* experiments.

We also established a novel *in vitro* system in which we could fully define the role of myelin. Finally, we assessed the influence of myelin on migrative and invasive abilities of pancreatic cancer cells and performed RNA seq analysis to characterize the molecular signatures at the basis of the alterations induced by myelin in pancreatic cancer cells.

Results

1. Direct and indirect contact between cancer and nerves

Nerves and PDAC can interact via two different mechanisms: directly, due to the physical proximity between cancer cells and nerves, and indirectly, via paracrine factors secreted by both cell types (Dominiak *et al*, 2020).

We therefore aimed at investigating the reciprocal effects of both direct and indirect interactions between nerves and pancreatic cancer cells. We first selected the correct model to recreate both the nervous and the neoplastic compartments. To reproduce the nervous compartment, we took advantage of a well-established co-culture system consisting of dorsal root ganglia (DRG) neurons explants from E 13.5 wild type mice. DRG explants contain sensory neurons and endogenous SCs that can migrate and proliferate along axons. In this *in vitro* physiological system it is possible to induce myelin formation upon addition of ascorbic acid (Taveggia & Bolino, 2018; Eldridge et al, 1987). To mimic PDAC, we used a cell line derived from the KPC mouse, that harbors mutations in KRAS and p53, the two mutations most commonly found in PDAC patients (Hingorani et al, 2005).

1.1 Paracrine interactions between cancer and nerves.

We initially studied whether and how factors released by cancer cells might influence nerves. Hence, we collected conditioned medium (CM) from KPC cells, and we treated myelinated SC-DRGs cocultures for up to 21 days. To obtain myelinated cocultures, SC-DRGs explants were grown in basal medium for the first week, then switched to a myelinating medium for 10 days. Once myelin was clearly visible in the cocultures, we started CM treatment. As control, we used the same media not conditioned by contact with KPC cells (CTRL). CM was obtained by adding a serum-free media to KPC cells, that was collected and filtered after 48 hours of conditioning. We performed immunofluorescence analysis for Myelin Basic Protein (MBP) and neurofilament (NF)

to assess the effects of CM treatment onto myelinated coculture. To monitor the effect of CM treatment, we performed immunofluorescence analyses at different time points upon KPC CM addition: day 0, day 3, day 7, day 10, day 15 and 21 days.

To our surprise, after 7 days of treatment, myelin started to degenerate, as observed by the reduced number of MBP positive internodes and their decreased internodal length (Figure 8).

To test if the effect was specific to CM from KPC cells, we repeated the experiment using CM from a colon cancer cell line (MC38), as colon cancer is normally characterized by a limited PNI (Cienfuegos *et al*, 2017). Notably, treatment with CM prepared from murine MC38 cells did not induce myelin degeneration nor altered the internodes length (Figure 8). This result suggests that the effect of myelin degeneration is distinctive of KPC cells.

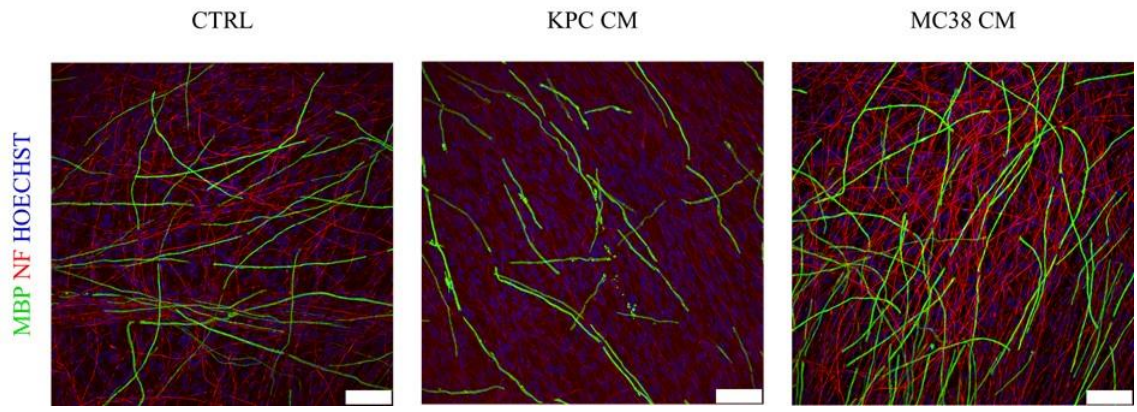

Figure 8. Myelinated cocultures treated with control CM (CTRL), KPC CM (KPC CM) and MC38 CM (MC38 CM).

Representative immunofluorescence images of myelinated cocultures treated for 7 days with control CM (CTRL), KPC cells CM (KPC CM), and MC38 CM (MC38 CM). Myelinated cocultures have been stained for MBP (fluorescein) and NF (rhodamine), nuclei have been marked with Hoechst. Scale bar = 50 um

To better characterize the alterations occurring to myelinating cells after treatment with KPC CM, we performed Western Blotting (WB) analyses on myelinated SC-DRGs cocultures treated with KPC CM or control CM at different time points. In these analyses we determined the expression level of c-Jun, a key transcription factor that labels trans-differentiating SCs (Jessen & Mirsky, 2016), using the quantitative Odyssey Imaging System (LI-COR). All results were normalized to the expression level of the protein Vinculin that we used as loading control (Figure 9a). We observed a significant increase in c-Jun protein expression in cocultures treated with KPC CM as compared to controls after 7 and 10 days of treatment (Figure 9b). This suggests that KPC CM triggers a damage-related response with activation of c-Jun, which is physiologically upregulated immediately after injury and is required for SCs trans-differentiation in repair SCs. Our result suggests that KPC CM might trigger a nerve-damage response in treated cocultures.

a)

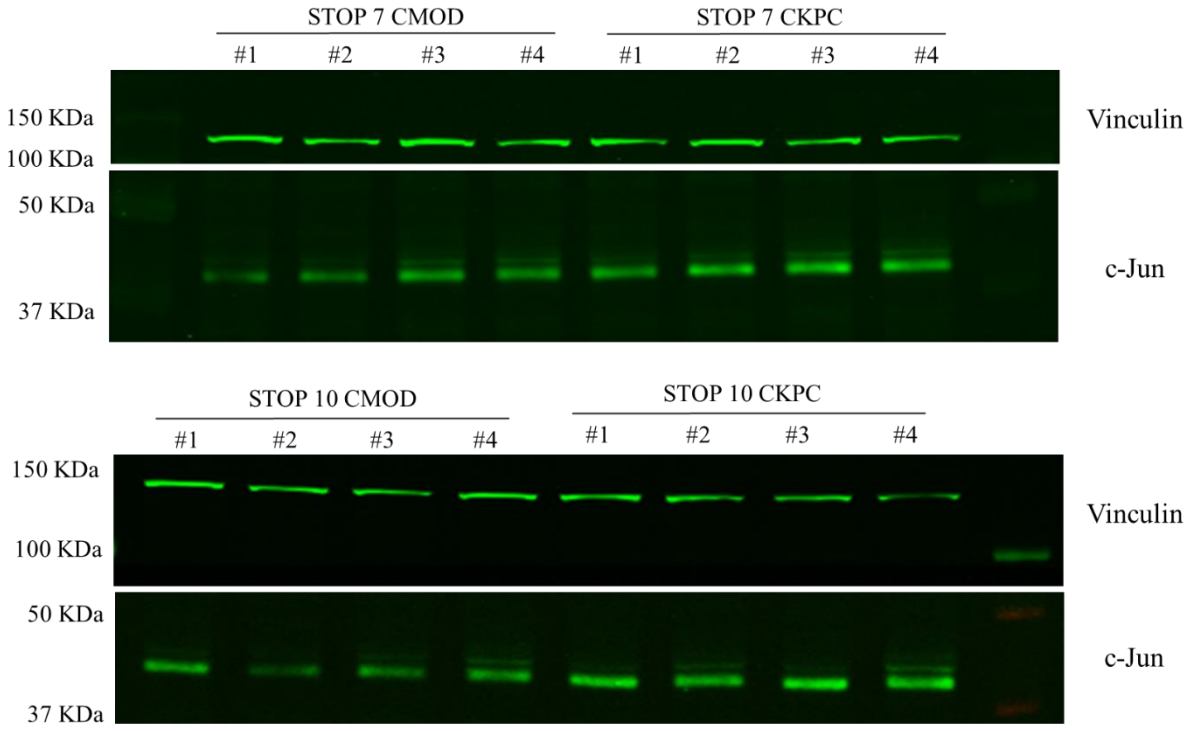

b)

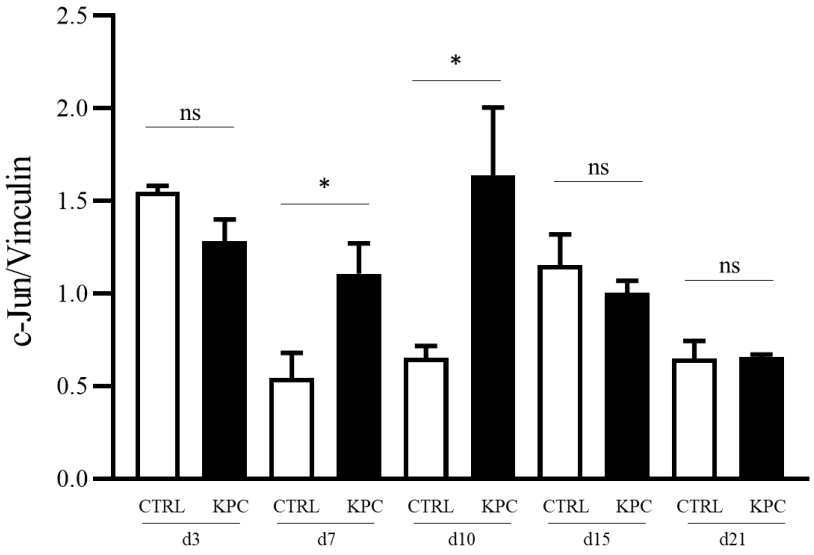

Figure 9. Time course analysis of c-Jun expression in control (CTRL) and KPC CM (KPC) treated myelinated cocultures.

a) Western Blot analysis of lysates from myelinated cocultures treated with control CM and KPC CM at day 0, 3, 7, 10, 15 and 21 of treatment. Lysates were tested for c-Jun and Vinculin as loading control.

*b) Quantification of c-Jun levels normalized to Vinculin levels. Day 3: CTRL 1.551 ± 0.0308; KPC 1.282 ± 0.1184. Day 7: CTRL 0.5455 ± 0.1351; KPC ± 1.108 ± 0.1638. Day 10: CTRL 0.6549 ± 0.0637; KPC 1.638 ± 0.366. Day 15: CTRL 1.155 ± 0.1645; KPC 1.004 ± 0.0660. Day 21: CTRL 0.6516 ± 0.0934; KPC 0.6580 ± 0.01284. Error bars represent mean ± s.e.m. (Student-t test, unpaired, * P=0.0380 at day 7, * P=0.0384 at day 10. n.s.= not significant. N= 4 biological replicates per group).*

1.2 Direct contact between cancer cells and nerves induces myelin degeneration

To determine whether KPC cells might mediate also a juxtracrine effect, we seeded cancer cells on top of myelinated SCs-DRG cocultures. Also in this set of experiments

we performed immunofluorescence analysis for MBP and NF at different time points. Just after 3 days upon contact, we observed myelin degeneration, whose integrity was severely compromised after 7 days of treatment (Figure 10). Also in this case, direct contact of myelinated cocultures with MC38 cells did not result in damaged myelin internodes.

Thus, KPC cells have a specific effect on myelinated cocultures that culminates in a faster degeneration compared to CM treatment.

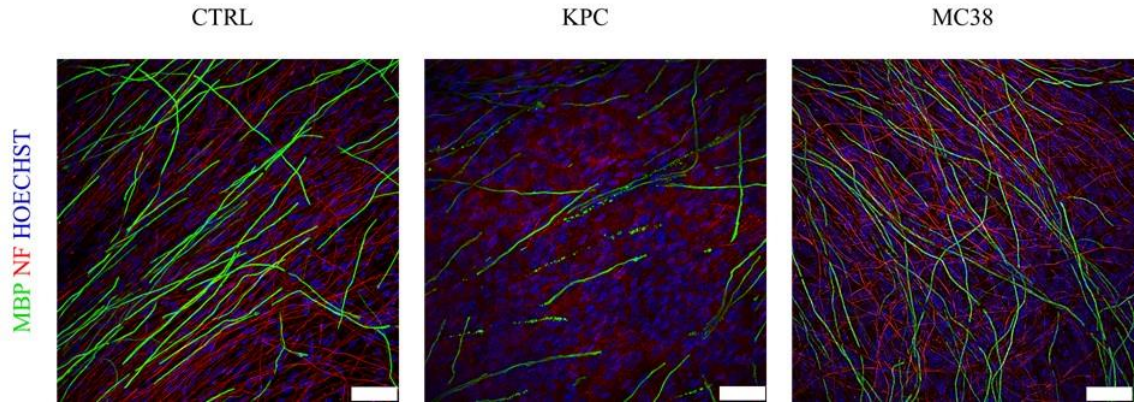

Figure 10. Direct contact of KPC cells (KPC) and MC38 cells (MC38) on top of myelinated cocultures.

Representative immunofluorescence images of myelinated cocultures after 7 days in contact with KPC cells (KPC), MC38 (MC38) or empty control condition (CTRL). Myelinated cocultures have been stained for MBP (fluorescein) and NF (rhodamine), nuclei have been marked with Hoechst. Scale bar = 50 um

1.3 Secretome analysis and choice of candidate

To characterize at molecular level the identity of the factor(s) released by KPC cells that might influence myelin integrity, we performed secretome analyses on KPC CM, using as control CM prepared from MC38 cells and from a murine primary cell line established from wild type pancreatic ducts. We collected CM after 48 hours in a serum

free media and analyzed by mass spectrometry at the San Raffaele Protein Microsequencing Facility.

Globally, we found 1180 differentially expressed proteins. Among all proteins, we focused on 23 proteins specifically upregulated only in KPC CM compared to the other two groups (ANOVA, p value <0.001, adjusted Bonferroni correction). After performing a literature review to examine the relevance of these proteins in our context of interest, i.e., pancreatic cancer and nerve-myelin damage - as suggested by the previous experiments that showed a morphological and molecular phenotype resembling those observed in the nerve damage response-, 5 molecules emerged as interesting candidates. Among the 5 selected molecules, we decided to focus on Fibroblast Growth Factor Binding Protein 1 (FGF-BP1). FGF-BP1 is the best characterized among the three known FGFBPs (Tassi et al, 2011). It is a 17 kDa protein derived from proteolytic processing in the carboxy-terminal half of a larger protein, FGF-BP (Wu et al, 1991). FGF-BP1 is an extracellular chaperon that binds in a reversable manner FGF 1, 2, 7, 10, 22, enhancing their biological and biochemical activities (Beer *et al*, 2005). FGFs are normally released and immobilized in the extracellular matrix and bound to heparan sulfate proteoglycans protecting FGFs against degradation (Häcker et al, 2005). Though FGFBPs mechanisms of action are not completely understood, three models have been proposed to explain when and how FGF-BPs interacts with FGFs *in vivo*. In the first model, FGF-BPs release FGFs from heparan sulfate proteoglycans in the extracellular matrix and conveys FGFs to their receptors. In a second hypothesis, FGF-BPs bind to FGFs after their release from heparan sulfate proteoglycans by heparanase and proteinases; in this case, FGF-BPs probably protect FGFs from degradation before they reach their receptor. Alternatively, it has been proposed that FGF-BPs bind to FGFs right after being secreted from cells. (Tassi *et al*, 2001; Sarrazin *et al*, 2011; Taetzsch *et al*, 2018).

We first determined the expression of FGF-BP1 and its signaling complex in our system. Hence, we extracted mRNA from KPC cells and MC38 cells to analyze mRNA expression levels by quantitative Real Time Polymerase Chain Reaction (qRT-PCR). We normalized all results to the expression levels of the housekeeping gene hypoxanthine guanine phosphoribosyl transferase (HPRT). Data are shown as fold changes calculated with the ΔΔCT method. This experiment proved that FGF-BP1 expression is significantly

upregulated in KPC cells compared to MC38 cells (KPC cells: 1.003 ± 0.05672; MC38 cells: 0.0227 ± 0.000318, P<0.001), confirming secretome analysis results.

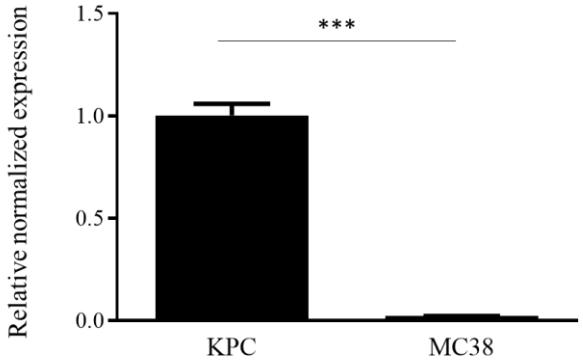

Figure 11. FGF-BP1 expression in KPC cells (KPC) and MC38 cells (MC38)

*qRT-PCR analyses of mRNA extracted from KPC cells (KPC) and MC38 cells (MC38). Error bars represent mean ± s.e.m. (Student-t test, unpaired, ***P<0.001. N=3 biological replicates per group).*

Next, we tested FGFBP1 expression on our in vitro myelinating cocultures system. Consequently, we induced myelination in SC-DRG explants for 10 days and, once myelin was clearly visible, we started the treatment with control CM and KPC CM for maximum 21 days. We then extracted RNA at different time points: day 0, day 3, day 7, day 10, day 15 and day 21. Interestingly, already 3 days after the addition of KPC CM, expression levels of FGF-BP1 were significantly lower compared to control and remained at lower levels for all the 21 days of treatment (Figure 12). This marked downregulation of FGF-BP1 suggests its involvement in the observed myelin degeneration, possibly because cocultures sense the excessive FGF-BP1 released by KPC cells in the CM and reduce the endogenous expression of the molecule as a protective mechanism (Taetzsch *et al*, 2017b; Williams *et al*, 2009).

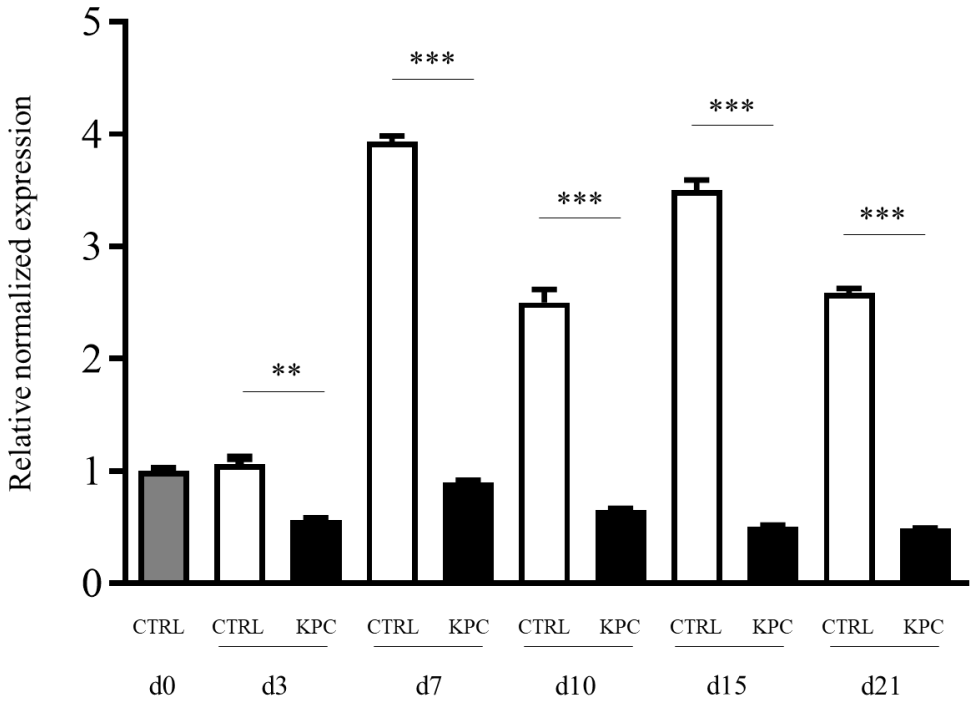

Figure 12. FGF-BP1 expression in myelinated cocultures treated with control CM (CTRL) or KPC CM (KPC).

*qRT-PCR analyses of mRNA extracted from myelinated cocultures treated with control CM (CTRL) or KPC CM (KPC). Day 3: CTRL 1.061 ± 0.0601; KPC 0.5658 ± 0.01861. Day 7: CTRL 3.936 ± 0.05093; KPC 0.9016 ± 0.01839. Day 10: CTRL 2.502 ± 0.1185; KPC 0.6540 ± 0.01528. Day 15: CTRL 3.501 ± 0.0925; KPC 0.5050 ± 0.01273. Day 21: CTRL 2.591 ± 0.03757; KPC 0.4887 ± 0.006881. Error bars represent mean ± s.e.m. (Student-t test, unpaired, **P=0.0014; ***P<0.001. N=3 biological replicates per group).*

1.4 Role of FGF-BP1 in inducing myelin degeneration

Next, we characterized the role of FGF-BP1 in our system. To mimic the activation of FGF-BP1 signaling, we treated myelinated SCs-DRGs cocultures with recombinant FGF-BP1. Instead, to block FGF-BP1 signaling, we tested the effect of an inhibitor for FGF receptors on SC-DRGs cocultures either treated with KPC CM or in direct contact with KPC cells.

Since FGF-BP1 levels are upregulated in CM from KPC cells, we treated myelinated cocultures with recombinant FGF-BP1 protein to assess whether the addition of this

protein is sufficient to induce myelin degeneration. We treated myelinated co-culture with different concentrations of recombinant rat FGF-BP1 (resuspended in PBS as vehicle) to define the treatment window that does not result in SCs-DRG coculture toxicity: we used 200 ng/ml, 500 ng/ml, 1 ug/ml, 5 ug/ml of recombinant FGF-BP1. Again, we induced myelinization in SCs-DRGs explants and after 10 days in myelinating conditions we obtained myelinated cocultures. We then added the selected concentration of FGF-BP1 and performed immunofluorescence analysis for MBP and NF to assess the effects of the recombinant protein onto myelinated coculture. We performed immunofluorescence analyses at different time points upon KPC CM addition: day 10, day 20, day 30, day 35. Preliminary results showed a small effect of degeneration obtained after 30 days of treatment with 5 ug/ml FGF-BP1, however further experiments are needed to confirm this result (Figure 13). To better assess the role of FGFBP1 we also plan to increase the period of treatment with this molecule.

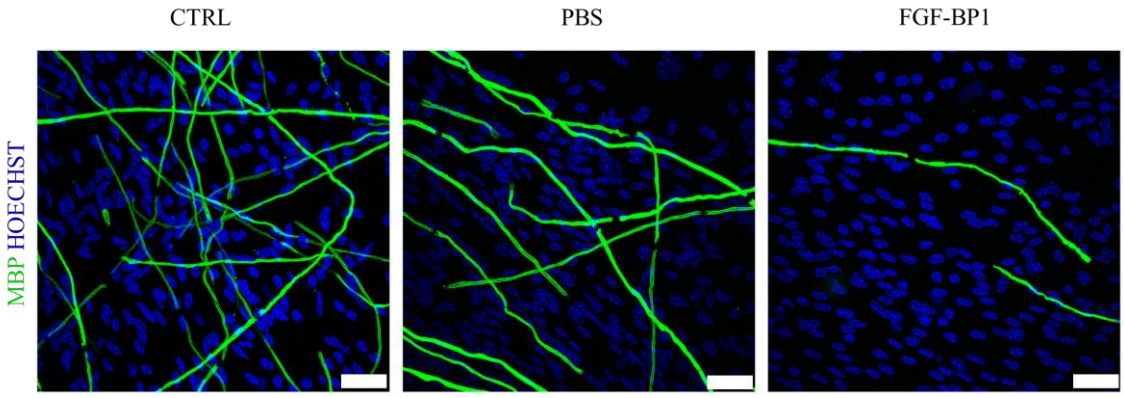

Figure 13. FGF-BP1 treatment reduces myelination in SCs-DRG cocultures

Representative immunofluorescence images of myelinated cocultures treated for 30 days with control medium (CTRL), control medium supplemented with PBS (PBS), control medium supplemented with 5 ug/ml of recombinant FGF-BP1. Myelinated cocultures have been stained for MBP (green), nuclei have been marked with Hoechst. Scale bar = 50 um.

Since there are no specific molecules targeting FGF-BP1, the most appropriate method we found to interfere with its signaling was to inhibit its receptors (the FGFRs).

Specifically, we chose FIIN 1 hydrochloride, which is an irreversible inhibitor of FGFR 1, 2, 3 and 4. Firstly, we performed titration experiments on myelinated cocultures to find the minimum inhibitor dose to avoid toxicity: we tested decreasing concentrations of 1000 nM, 500 nM, 250 nM, 100 nM, 50 nM and 10 nM. After dose adjustment experiments, we found that 100 nM of FIIN 1 hydrochloride was the ideal concentration.

To interfere with the signaling induced by the high expression of FGF-BP1 present in the KPC CM, we treated myelinated cocultures with KPC CM supplemented with the FGF-BP1 inhibitor. Specifically, we induced myelination in our cocultures as above described and, after 10 days, myelin internodes were clearly visible. Thus, we started treatment with KPC CM supplemented with 100 nM FIIN hydrochloride. As control, we used KPC CM and KPC CM supplemented with DMSO, which is the vehicle for FIIN hydrochloride. To monitor the effect of FIIN hydrochloride treatment on myelinated cocultures, we repeated the same experiment using control CM instead of KPC CM.

Interestingly, we observed that addition of 100 nM FIIN hydrochloride reduced myelin degeneration after 7 days of treatment. To consolidate this result, we performed immunofluorescence analysis for MBP and NF. As shown in Figure 14a, we observed reduced myelin degeneration, longer and more abundant internodes compared to cocultures treated with only KPC CM. Of note, addition of 100 nM FIIN 1 hydrochloride to co-culture treated with control CM did not hamper myelination.

To quantify the observed effect, we counted the number of internodes present after 7 days of treatment in the different conditions and performed ANOVA test to compare the different groups (Figure 14b). Strikingly, FIIN hydrochloride treatment improved the mean number of internodes. We observed a statistically significant increase in the number of internodes in the KPC CM + FIIN hydrochloride condition compared to the other conditions, KPC CM only or KPC CM + DMSO (KPC CM: 242.5 ± 33.39; KPC CM + DMSO: 261.7 ± 32.60; KPC CM + FIIN 100 nM: 638.9 ± 47.64; $P < 0.001$ for KPC CM

+ FIIN 100 nM against the other two groups; P = 0.934 for KPC CM vs KPC CM + DMSO). Interestingly, the mean number of internodes was comparable among control conditions and treatment with KPC + FIIN 100 nM (P value not significant). These results suggest that inhibition of FGFRs markedly decreases the detrimental role of KPC CM onto myelin status.

a)

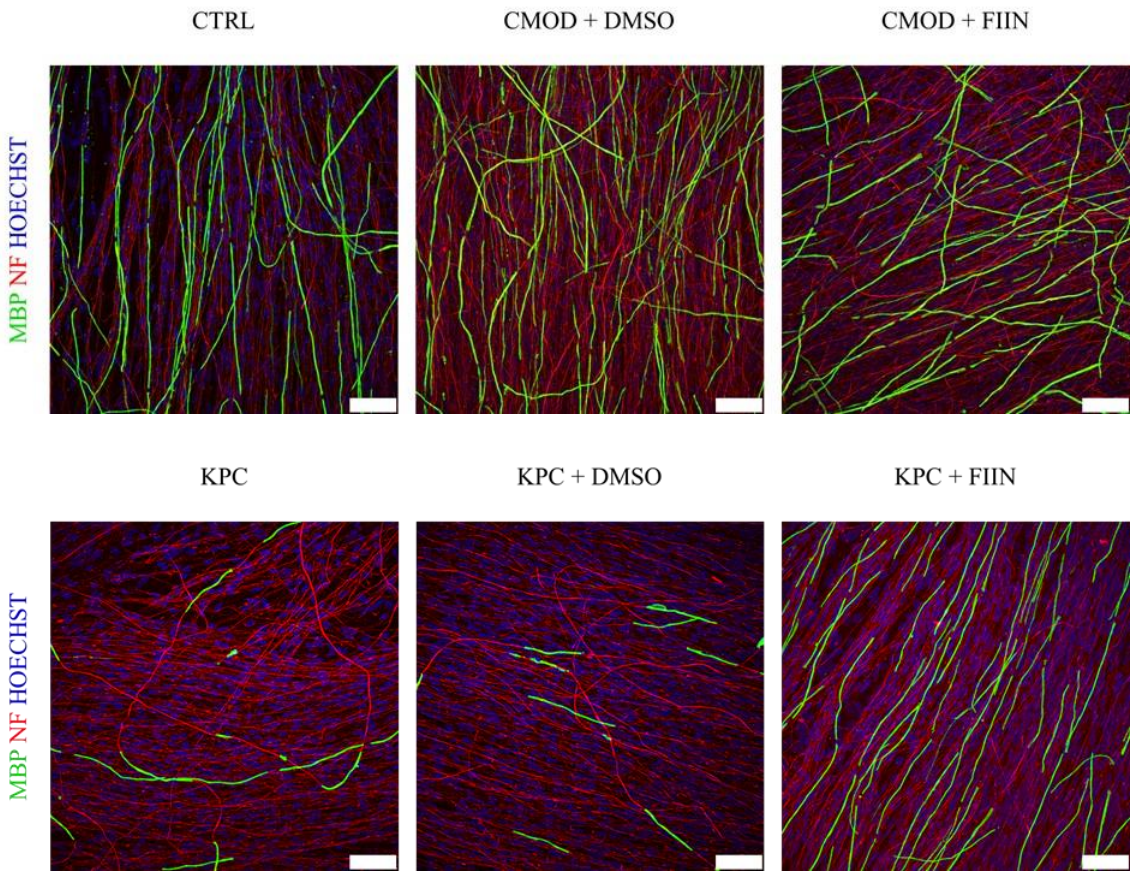

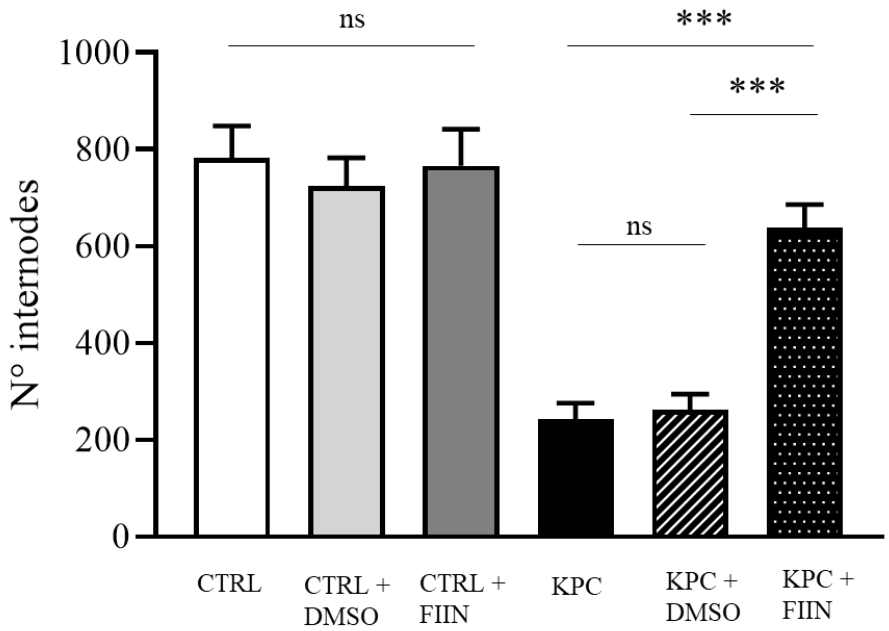

b)

Figure 14. FIIN 1 hydrochloride inhibitor reduces myelin degeneration induced by KPC CM

a) Representative immunofluorescence images of myelinated cocultures treated for 8 days with control CM (CTRL), control CM and DMSO (CTRL + DMSO), CTRL + FIIN (CTRL +FIIN) compared to myelinated cocultures treated with KPC CM alone (KPC), KPC CM and DMSO (KPC+DMSO), KPC CM and FIIN 1 inhibitor (KCP+FIIN). Myelinated cocultures have been stained for MBP (fluorescein) and Neurofilament (rhodamine), nuclei have been marked with Hoechst. Scale bar = 50 um.

*b) Quantification of the number of myelin internodes in the different conditions 8 days after treatment. Error bars represent mean ± s.e.m. (Student-t test, *** P<0.001. N=3 replicates per group).*

To further investigate the role of FGF-BP1 signaling in cancer-nerve interaction, we tested if FIIN 1 could reduce myelin degeneration induced by KPC cells directly contacting SCs-DRG myelinated cocultures. Thus, we added 100 nM FIIN to cocultures myelinated for 10 days and seeded with 10.000 KPC cells. After 8 days of treatment, we

performed immunofluorescence analysis for MBP, NF and CK19 a marker of pancreatic cancer cells (Bouwens, 1998). Remarkably, treatment with FIIN 100 nM reduced the degeneration observed in control cocultures (Figure 15). This observation confirms the implication of FGFs signaling in the myelin degeneration phenotype induced by KPC cells with both paracrine and juxtracrine signaling.

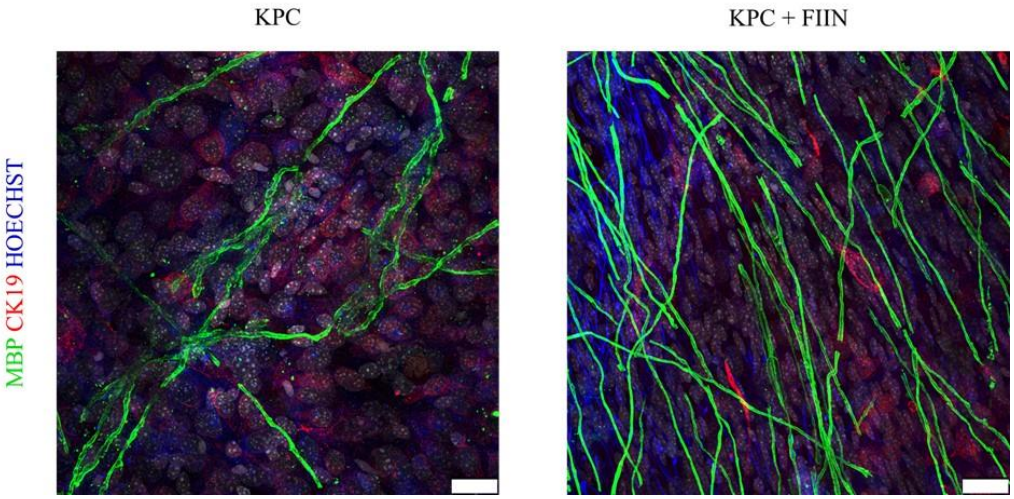

Figure 15. FIIN 1 hydrochloride inhibitor reduces myelin degeneration induced by KPC cells direct contact

Representative immunofluorescence images of myelinated cocultures after 8 days in direct contact with KPC cells (KPC) or with KPC cells and FIIN treatment (KPC + FIIN). Myelinated cocultures have been stained for MBP (fluorescein) and CK-19 (rhodamine), nuclei have been marked with Hoechst. Scale bar = 25 um

To test whether FIIN might have a primary role on KPC cells survival and/or proliferation, we treated isolate KPC cells with 100 nM of FIIN and performed immunofluorescence analysis with Phospho-histone 3 and Tunel assay kit, respectively. No difference was observed for proliferation nor survival (data not shown), suggesting that the observed myelin rescue is not due to less vital KPC cells.

2. The role of myelin in supporting cancer growth

The above-described results show that KPC cells induce myelin degeneration both by paracrine mechanisms and direct contact, possibly via FGFs signaling. To define the possible advantage(s) of KPC cells in inducing myelin degeneration, we next investigated the effects myelin has on KPC cells.

2.1 Myelin supports cancer proliferation and morphologically alters cancer cells

To analyze how myelin influences KPC cells, we assessed if direct contact with non-myelinated or myelinated SCs-DRG cocultures might alter KPC cells morphology and/or proliferation. To better monitor potential KPC cells changes, we tracked them with a fluorescent live cell tracker that is stable for up to 72 hours and is retained in living cells in multiple generations. We seeded 30.000 KPC cells per single DRGs, either myelinated or not, and fixed the cells after 16, 20, 24 and 28 hours of co-culture. In collaboration with the Advanced Light and Electron Microscopy BioImaging Center (ALEMBIC) at San Raffaele Institute, we analyzed the area, the sphericity, and the length of the major axis of KPC cells seeded on top of myelinated or non-myelinated DRGs. We measured both single and clustered KPC cells.

KPC seeded on top of myelinated DRGs showed a statistically significant increase in area surface and cell length, while the sphericity was significantly reduced (Figure 16a-b). These results suggest that KPC cells in contact with myelinated cocultures undergo morphological alterations, are more elongated and less compact, and form bigger clusters of cells. In addition, we performed immunofluorescence analyses for phospho-Histone 3 as marker of proliferation and we digitally counted the number of signal-positive cells in both conditions. Proliferation was statistically significantly higher in KPC cells seeded on top of myelinated cocultures compared to KPC cells on top of non-myelinated cocultures (Figure 16c).

a)

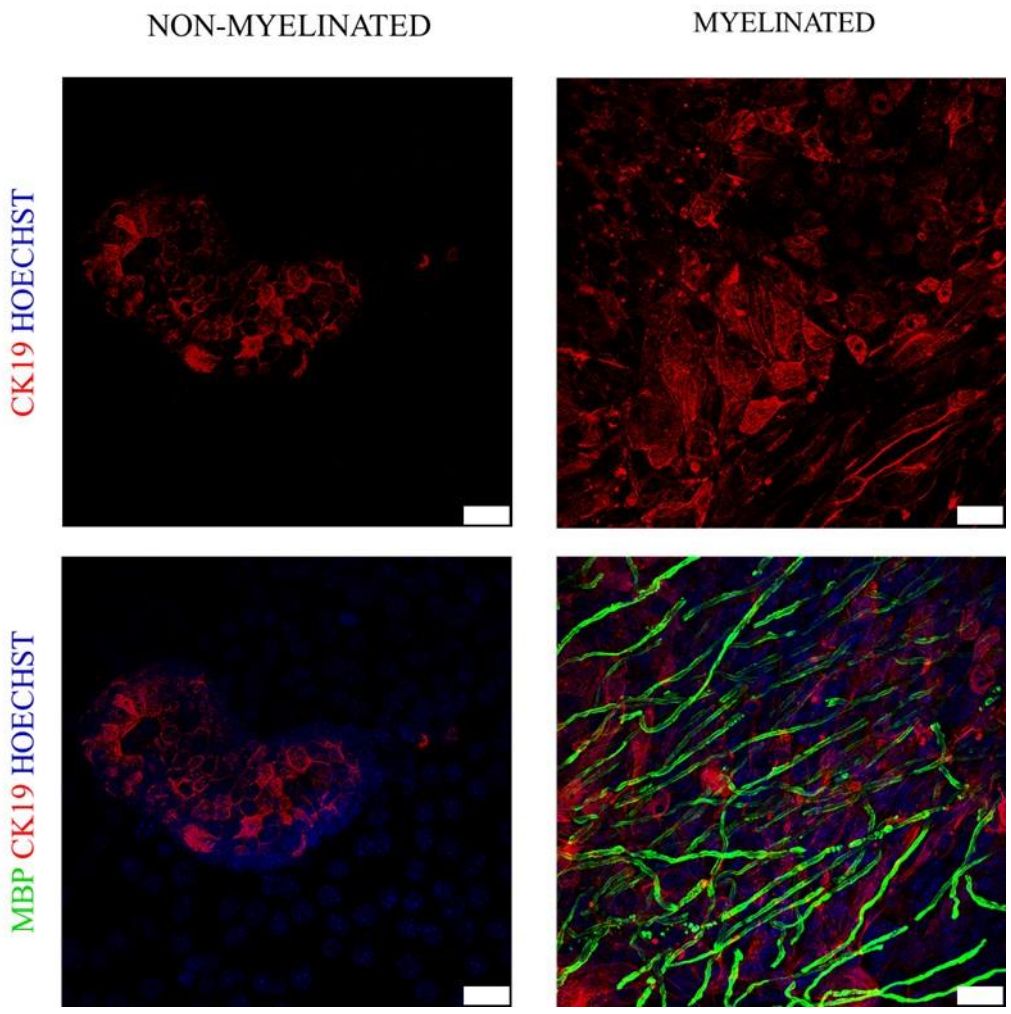

b)

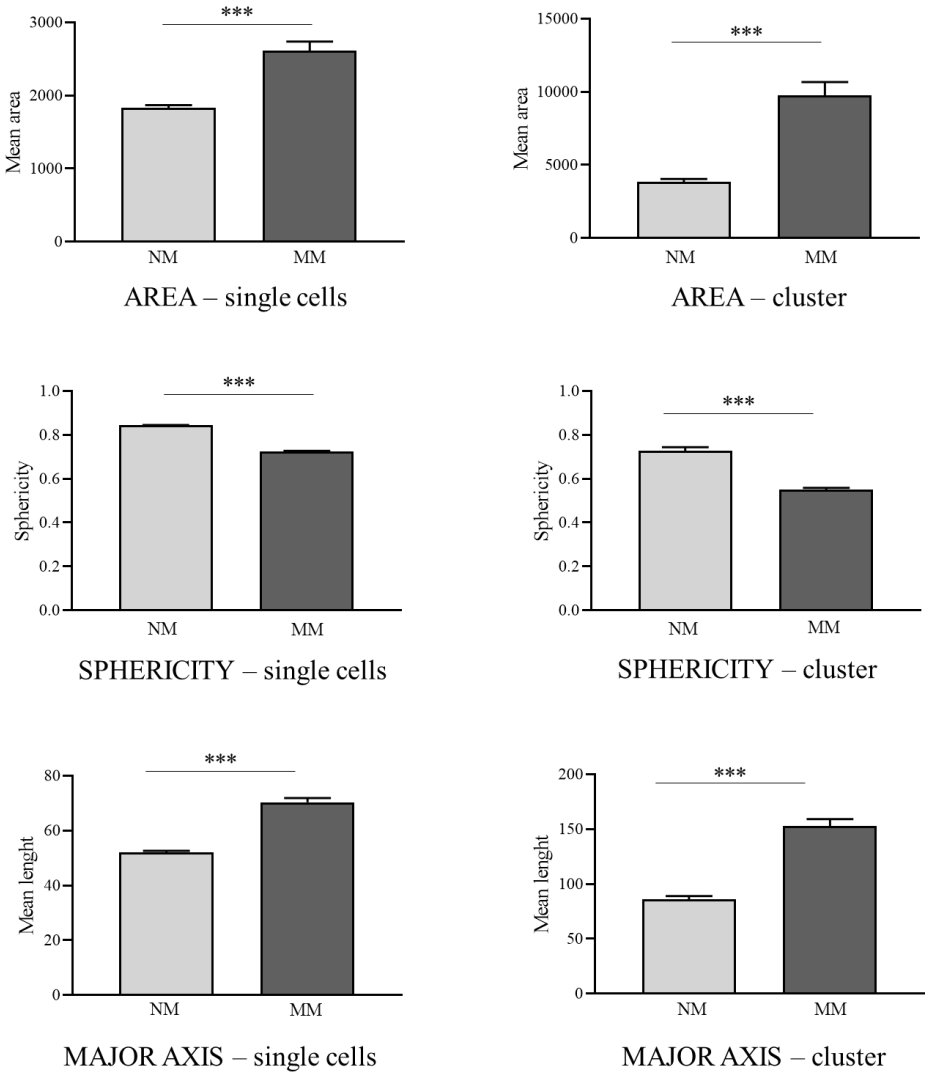
***
Mean area
3000
2000
1000
0
NM
MM
AREA – single cells
***
Mean area
15000
10000
5000
0
NM
MM
AREA – cluster
***
Sphericity
1.0
0.8
0.6
0.4
0.2
0.0
NM
MM
SPHERICITY – single cells
***
Sphericity
1.0
0.8
0.6
0.4
0.2
0.0
NM
MM
SPHERICITY – cluster
***
Mean lenght
80
60
40
20
0
NM
MM
MAJOR AXIS – single cells
***
Mean lenght
200
150
100
50
0
NM
MM
MAJOR AXIS – cluster

c)

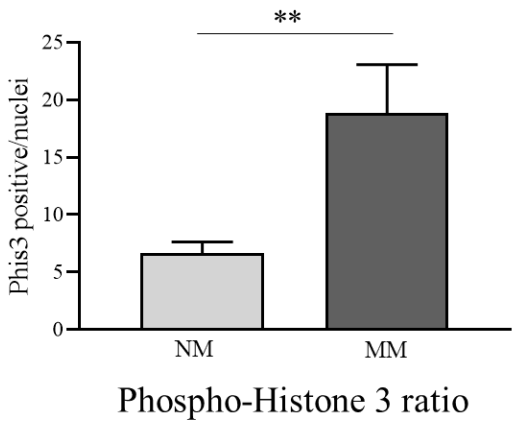
**
Phis3 positive/nuclei
25
20
15
10
5
0
NM
MM
Phospho-Histone 3 ratio

Figure 16. KPC cells undergo morphological alterations when in contact with non-myelinated (NM) or myelinated (MM) cocultures.

a) *Representative immunofluorescence images of KPC cell marked with CK-19 (rhodamine) seeded on top of non-myelinated (NM) or myelinated (MM) cocultures. Myelin is stained for MBP (fluorescein), nuclei have been marked with Hoechst. Scale bar = 25 um*

*b) Graphs summarizing the quantifications of area, length, and sphericity of KPC cells seeded on top of non-myelinated (NM) or myelinated (MM) cocultures. Single cells mean area NM 1829 ± 40.33; MM 2615± 124.9; cluster mean area NM 3857 ± 186.7; MM 9767 ± 899.1. Single cells sphericity NM 0.8434 ± 0.0018, MM 0.7231 ± 0.0037; cluster sphericity NM 0.7261 ± 0.01796, MM 0.5511 ± 0.00792. Single cells mean major axis length NM 51.98 ± 0.6262, MM 70.39 ±1.544; cluster mean major axis length NM 85.91 ± 3.016, MM 153.0 ± 6.105. Error bars represent mean ± s.e.m. (Student-t test, *** P < 0.001. N= 4 biological replicates per group).*

*c) Quantification of the number of phospho-histone 3 positive KPC cells seeded on top of non-myelinated (NM) or myelinated cocultures. Mean phospho-Histone 3 positive nuclei NM 6.642 ± 0.9904, MM 18.85 ± 4.215. Error bars represent mean ± s.e.m. (Student-t test, ** P = 0.0304. N= 4 biological replicates per group).*

2.2 Myelin supports cancer migration and invasion

Our results indicate that myelinated cocultures are able to influence KPC cells morphology and proliferation. To define whether they could also influence cancer cells migration and invasive abilities we set up experiments using a Transwell system.

We used a 24 well plate with polycarbonate inserts of 6.5 mm in diameter with 8 um pores. To assess the influence produced by cocultures on KPC cells, we seeded in the bottom chamber of the Transwell one single SC-DRGs explant either non myelinated, myelinated or myelinated degenerated. 3 insert for each condition were used. The cocultures were moved in the bottom chamber of the 24 well, washed with PBS once and left overnight in a basal medium before performing the experiment.

For the migration assay, we seeded 30.000 KPC cells on the top membrane of the insert in the same medium used in the bottom chamber. After 24 hours, we aspirated the medium and removed the cells that did not migrate by wiping with a cotton swab. Migrated cells on the bottom membrane were then fixed with paraformaldehyde and stained with Crystal Violet to visualize and count them. We observed that migrating KPC cells followed a trend, with the least cell migrated in the empty control and increasing migration from non-myelinated, myelinated to degenerated cocultures treated with CM. As shown in Figure 17, a statistical ANOVA test confirmed our observations.

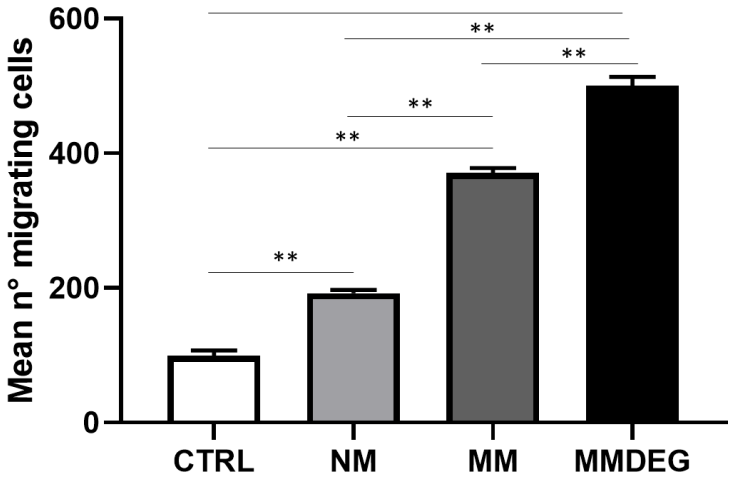

Figure 17. KPC cells migrate towards degenerated cocultures.

Quantification of the migrated KPC cells in the different conditions: control condition is represented by an empty bottom chamber (CTRL). Non myelinated cocultures were obtained by growing SC-DRGs explants in basal medium for 1 week (NM). Myelinated cocultures were obtained by inducing myelination in SC-DRGs explants for 10 days after 1 week of growth in basal medium (MM). Degenerated myelin was obtained by treating for 14 days with KPC CM already myelinated cocultures (MMDEG).

*Mean CTRL 99,14 ± 8,108; NM 192,1 ± 5,024; MM 370,8 ± 7,624; MMDEG 500,7 ± 13,28. Error bars represent mean ± s.e.m. (ANOVA test, ** P < 0.001. N=9 insert per group).*

To assess if myelin also influences the invasiveness of KPC cells, we performed a similar experiment with the addition of a Matrigel film on the top membrane of the insert,

to mimic the presence of an extracellular matrix that cancer cells need to degrade to reach their target. Similarly to the above described experiment, we grew in the bottom chamber non myelinated cocultures, myelinated cocultures and myelinated cocultures treated with KPC CM for 14 days. To assess KPC invasion, we seeded 70.000 KPC cells on top of the Matrigel film.

After 24 hours, we stained with Crystal Violet the bottom side of the insert membrane to visualize and count migrated KPC cells. In general, we observed that KPC cells are significantly attracted by the cocultures in the bottom chamber compared to the empty control. Interestingly, also in this case KPC cells invade more towards degenerated myelin cocultures, while we did not observe any difference in the number of invading cells towards the other two conditions (Figure 18), as confirmed also by statistical analyses (ANOVA). This result might indicate that KPC cells are more prone to undergo the modifications required for obtaining an invading phenotype when myelin is damaged and therefore less compact and more readily available.

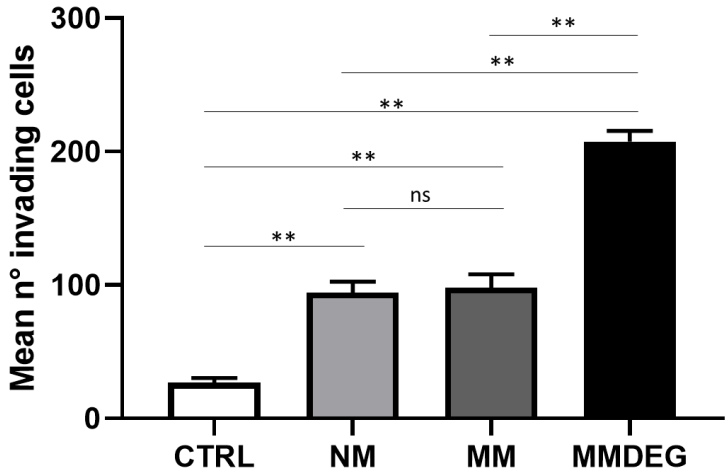

Figure 18. KPC cells invasion increases towards degenerated cocultures.

Quantification of the invaded KPC cells in the different conditions: control condition is represented by an empty bottom chamber (CTRL). Non myelinated cocultures were obtained by growing SC-DRGs explants in basal medium for 1 week (NM). Myelinated cocultures were obtained by inducing myelination in SC-DRGs explants for 10 days after

1 week of growth in basal medium (MM). Degenerated myelin was obtained by treating for 14 days with KPC CM already myelinated cocultures (MMDEG).

*Mean CTRL 26.75 ± 3.567; NM 94.47 ± 8.260; MM 98.14 ± 9.889; degenerated cocultures 207.6 ± 8.016. Error bars represent mean ± s.e.m. (ANOVA test, ** P < 0.001. N=9 inserts per group).*

To further characterize KPC cells migration and invasion abilities, we performed RNA-seq analysis on migration and invasion experiments. We are interested in comparing the differentially expressed genes of KPC cells that have migrated or invaded to those KPC cells who have remained on the top part of the membrane. Briefly, we repeated the migration and invasion experiments as above described. After 24 hours, we removed the medium and selected 18 inserts for each of the four conditions (CTRL, NM, MM and MMDEG) for both the migration and invasion experiments. Of these, 9 inserts were used to collect RNA from the top side of the membrane, the other 9 to collect RNA from the bottom part of the membrane. To avoid interference, cells were removed with cotton swab on the side of the membrane that was not used to collect RNA. Lysates were shipped to an external facility (GeneWiz) for RNA seq analysis. The results of these analyses will serve as future development of my studies to identify the molecules mediating the above-described mechanisms.

2.3 Cancer cells uptake myelin and exploit it to proliferate

Recent studies focusing on the role of lipids in PDAC have suggested that lipid droplets are used as sources of energy during cell migration via oxidative metabolism (Rozeveld et al, 2020). Since myelin is mainly composed of lipids, we decided to investigate if KPC cells could uptake myelin droplets.

Thus, we isolated and purified myelin in form of a lipidic suspension from murine brain. We collected four brains from wild type mice and mechanically minced them into small pieces. We then homogenized the tissue with a pre-chilled Dounce homogenizer in 2.5 mL of a 0.85 M sucrose solution. Then, we transferred the homogenate to

ultracentrifuge tubes and added 0.25 M sucrose solution to create a gradient. Tubes were spun overnight at 67.000 g. We then collected the myelin fraction, visible as a defined interface between the two layers of sucrose 0.25 and 0.85 M. We osmotically shocked myelin and centrifuged for 30 minutes at 9000 rpm. Thus, we obtained a clear myelin pellet that was tested with Western Blot for the MBP protein. We determined myelin concentration with BCA assay and stored 1 mg/ml aliquots at -80 °C until use.

Next, we determined whether KPC cells could uptake myelin. Therefore, we seeded 20.000 KPC cells on glass coverslips and, after 8 hours, we starved the cells for 16 hours. Next, we switched the cultures to a serum free media condition with or without myelin. 24 hours after myelin addition, we performed immunofluorescence analysis for Phalloidin to stain cancer cells and MBP for myelin. Remarkably, we were able to visualize KPC cells reaching for myelin lipid droplets (Figure 19a).

We next wondered if and how KPC cells use the ingested myelin. To assess if myelin could be used as a proliferative stimulus, we repeated the myelin feeding experiment and performed immunofluorescence analysis for CK-19 and phospho-Histone 3 24 hours after treatment. Interestingly, the number of phospho-Histone 3 positive cells was significantly increased among KPC cells treated with myelin (P=0.0445, Figure 19b).

a)

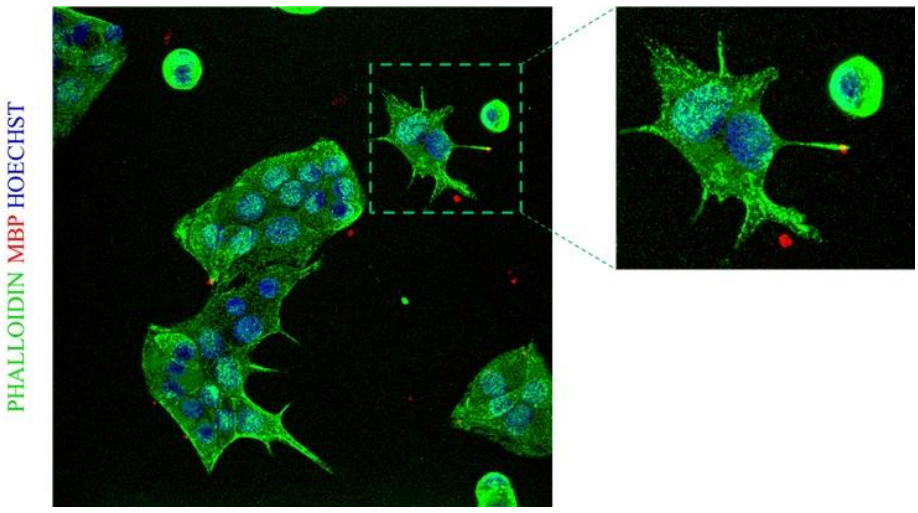

b)

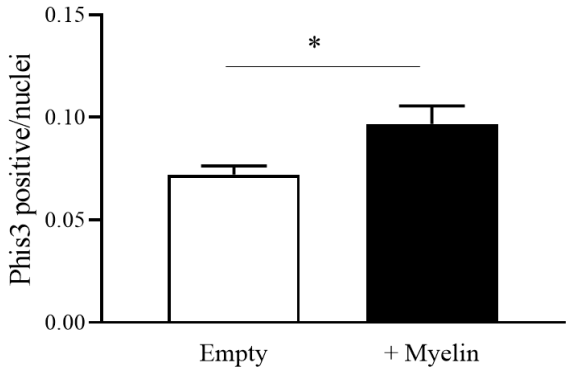

Figure 19. KPC cells uptake myelin lipid droplets and use it to proliferate

a) Representative immunofluorescence images of KPC cells incorporating myelin droplets. KPC cells are stained with Phalloidin (fluorescein) and myelin droplets with MBP (rhodamine). Nuclei are marked with Hoechst.

*b) Quantification of phospho-Histone 3 positive KPC cells in control condition (CTRL) or upon myelin addition to medium (+Myelin). Mean empty condition 0.072 ± 0.004; mean KPC + myelin 0.097 ± 0.008. Error bars represent mean ± s.e.m. (Student-t test, * P=0.0445. N=4 biological replicates per group).*

3. PDAC organoids to study PNI

To validate the above-described results in a more physiological setting, we established organoid cultures from primary KPC cell line, murine healthy pancreas, surgically resected PDAC patients and healthy human controls. Organoids recapitulate the epithelial architecture of their organ of origin, and the three-dimensional structure reproduces the environmental signals present in both normal tissue or cancer while retaining the original genetic mutations (Lau et al, 2020), offering a fair more valid model to mimic different normal and pathological conditions.

3.1 Organoids establishment

We prepared human organoids only from patients whose diagnosis of ductal adenocarcinoma of the head of the pancreas was confirmed both clinically and radiologically. In parallel, as a control, we established organoid cultures from healthy pancreatic tissue from the leftovers of pancreas digestion from the islet transplant program, kindly provided by Prof. Piemonti (OSR, Diabetes Research Institute).

All patients, after signing an informative agreement, underwent surgical pancreaticoduodenectomy and the resected specimens were collected in sterile towels, placed on ice and immediately transferred to the Pathology Unit for a preliminary histological characterization. After isolating the tumor, the pathologist provided us a small part of it that we collected in a 50 mL sterile Falcon tube containing basal medium. The tissue was stored at 4°C for 16 hours to eliminate fat and blood cells from the specimen. Next, we separated the cells from the surrounding fibrous tissue by mechanical dissection followed by enzymatic digestion with 0.125 mg/ml collagenase, 0.125 mg/ml dispase and 0.125 mg/ml DNAase for 1 hour. Finally, to remove the undigested material we passed it through a 40 μM cell strainer. The collected material was then centrifuged at 300 g for 5 minutes at 8 °C to obtain the cells. Collected cells were then resuspended in cold Matrigel and plated in pre-warmed 4 well culture plates. All organoids formed and developed in cell culture incubator at 37°C, 5% CO2 in regular organoid growth medium in 6-7 days.

To maximize human organoid preparation, we tried to establish organoids from patients who underwent neoadjuvant therapy before surgery, since more and more patients are candidates for preoperative chemotherapy treatment. However, and in agreement with previous studies, we were not able to establish them (Boj et al, 2015).

To establish spheroids from murine pancreatic cancer, we used primary pancreatic cancer cells derived from the tumor bulk of KPC mice established in Dr. Tuveson's lab. These cells were a kind gift of Dr. Piemonti (San Raffaele Scientific Institute). In particular, we resuspended 10000 KPC cells (K8484) in cold Matrigel and after a week in mouse organoid medium, we obtained a confluent spheroid culture. In parallel, we also

developed organoids directly from frozen tumor-derived material, but we mainly worked with spheroids since we did not have KPC mice available.

To establish healthy murine organoids, we collected pancreases from wild type mice in a 50 mL sterile Falcon tube containing cold basal medium. We then transferred the pancreas in a sterile 10 mm Petri dish and mechanically digested the organ. The minced material was transferred to a 15 ml tube containing 10 ml of warmed Digestion solution. We incubated at 37°C for 5 minutes on a shaker. After enzymatic digestion, we performed mechanical digestion by pipetting with P200 and we filtered with a 40 μM cell strainer, then we pelleted the material at 200 x g for 5 minutes at 8 °C, discarded the supernatant and washed twice with 10 mL of Basal Medium by repeating the pelleting method above described. We resuspended the pellet in an appropriate volume of cold Matrigel (Corning) and plated the organoids following the same procedure used to establish human organoids. Regardless of the species and of the health status, we were able to successfully grow pancreatic organoid cultures and expand and maintain organoids in culture up to 8 months. To characterize the established organoids, we performed both immunofluorescence and electron microscopy analyses.

Since CK-19 and SOX-9 genes have been specifically associated to pancreatic ductal lineage (Cleveland et al, 2012), we used these markers to further characterize our developed organoids in immunofluorescence analyses (Figure 20). CK-19 is mainly expressed in ductal epithelial (bile and pancreatic duct, renal collecting ducts) and gastrointestinal epithelia. In the pancreas, CK-19 is normally expressed in the exocrine ducts but not in the exocrine acinar and endocrine islet cells (Bouwens, 1998). The transcription factor SOX-9, instead, belongs to a family of transcription factors that plays a critical role in the development and differentiation of multiple tissues during embryogenesis, among which the pancreas (Wegner & Stolt, 2005). Indeed, SOX-9 is expressed from the early stages of pancreatic development and is required to maintain the pancreatic progenitor pools and to establish the pancreatic endocrine and exocrine cell fates (Lynn et al, 2007; Seymour et al, 2007). In addition, SOX-9 is expressed in centroacinar and ductal epithelial cells of the pancreas and it is considered a marker for pancreatic ductal lineage of pancreatic neoplasms (Shroff et al, 2014).

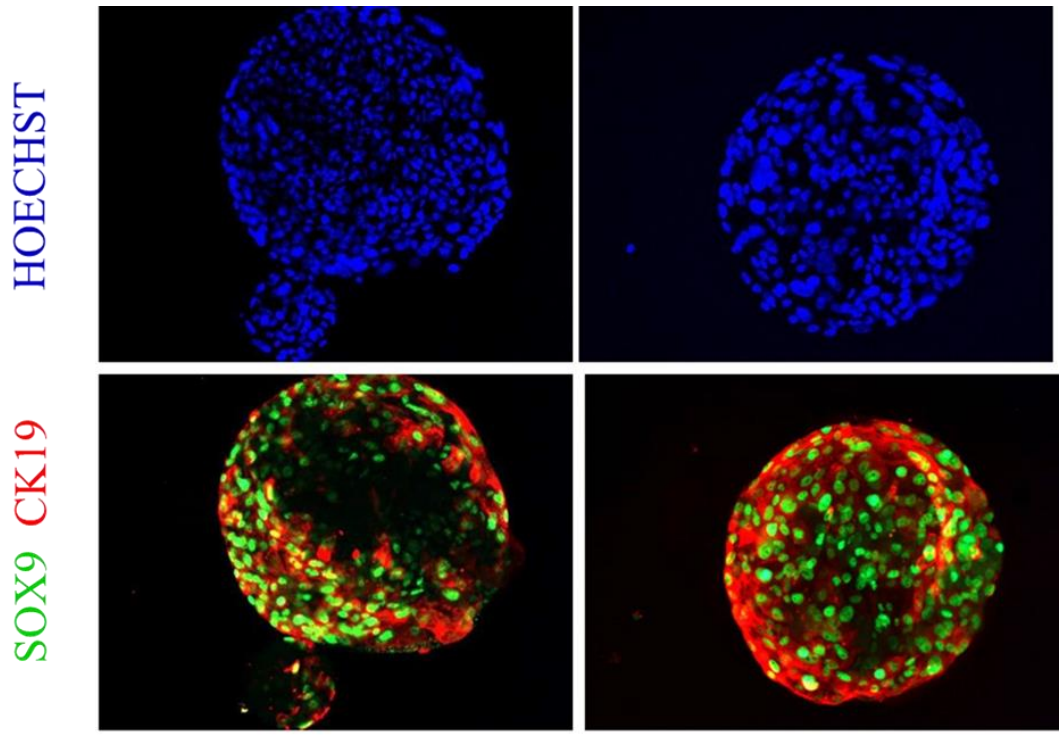

Figure 20. Healthy and KPC spheroids immunofluorescence

Representative immunofluorescence images of healthy and KPC spheroids grown for 7 days and immunostained for Cytokeratin-19 (rhodamine) and Sox-9 (fluorescein). Cultures were also stained with Hoechst to identify nuclei.

Recent studies have shown that in addition to immunofluorescence analyses, scanning electron microscopy studies as well as pH measurement analyses and ion sensitive fluorescent indicators could provide a precise assessment of pancreatic organoids physiological characteristics, including secretion (Molnár et al, 2019).

Hence, to further characterize our spheroids, we performed morphological analyses using scanning electron microscopy on KPC and healthy murine organoids. In collaboration with Dr. Carla Panzeri at the OSR imaging facility (ALEMBIC), we obtained detailed images of sectioned spheroids. We observed that both healthy and KPC spheroids form a cellular monolayer that is polarized towards the inner part of the sphere (Figure 21). On the apical membrane, we also observed a brush border as well as secreted

vesicles being extruded by the spheroids (Figure 21, bottom panels). Collectively, these studies confirmed that we obtained bona fide spheroids, validating our system.

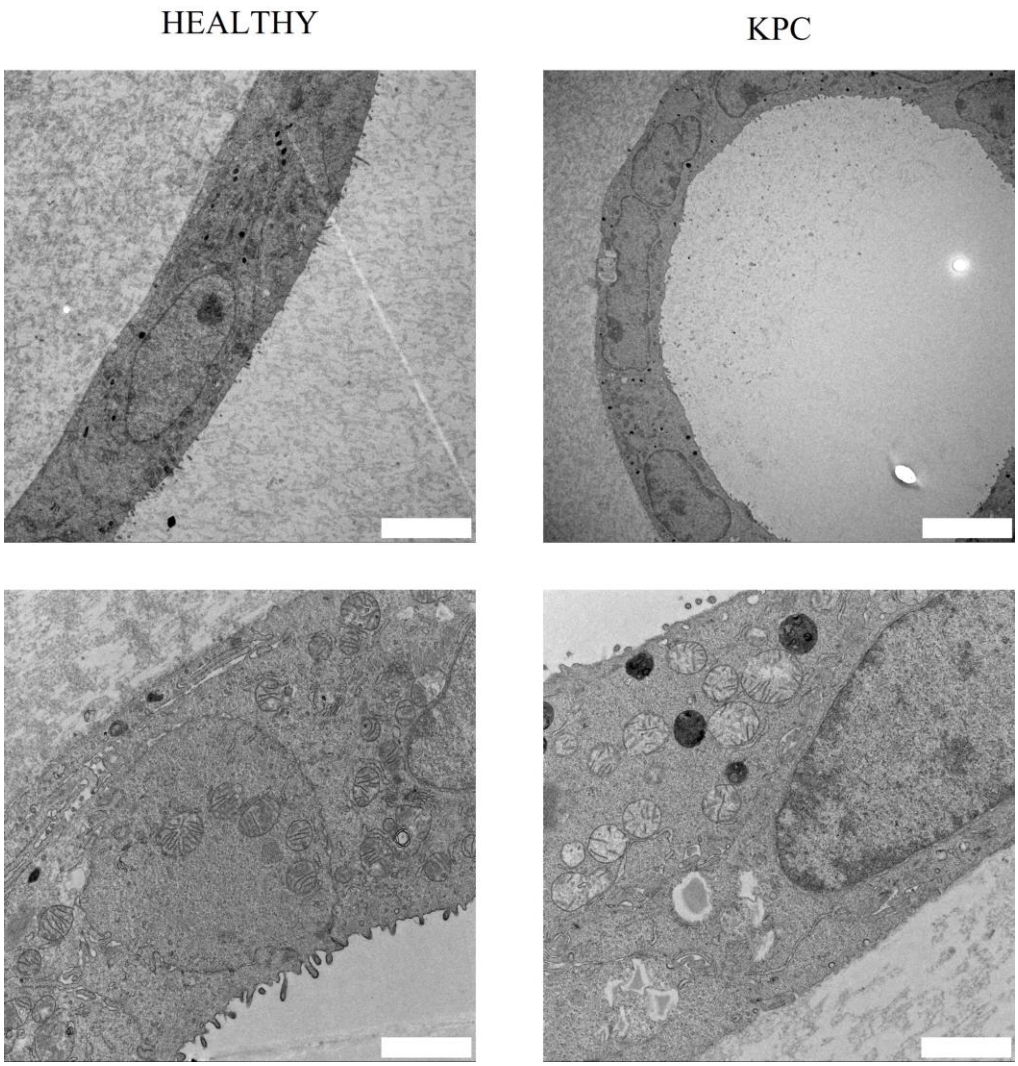

Figure 21. Morphological analysis of healthy and KPC spheroids.

Representative electron micrographs of healthy and neoplastic spheroids after 7 days

3.2 Spheroids – DRGs cocultures

Next, we applied the organoids system to study PNI. Thus, we grew established coculture SCs-DRGs neurons together with murine spheroids, both healthy and neoplastic.

We first tested different combinations of growth factors to ensure that both cell types could survive and grow, thus establishing compatible culture conditions for these groups of cells. To obtain the cocultures, we resuspended a confluent dome of spheroids in 150 ul of cold Matrigel in a 15 mL falcon. In parallel, we dissected E13.5 DRGs from wild type mice. Importantly, we dissected DRGs from the same level of the spinal cord that were grown either with KPC organoids or with healthy controls. We could successfully grow spheroids and SCs-DRGs cocultures in a Matrigel drop for up to 1 week. All cultures were set up in chambered coverslip with 15 micro-wells placed on a glass bottom that provided the optimal support for visualization and whole-mount immunofluorescence analysis. To perform whole-mount immunofluorescence we adapted a protocol originally developed in Tuveson Lab (Tuveson Lab). Particular care was put in maintaining the integrity of the Matrigel dome to preserve the three-dimensional structure. All immunofluorescence images were performed and analyzed in collaboration with Dr. Valeria Berno (OSR ALEMBIC).

Previous studies have reported that PDAC alters nerve fibers diameter and increases their growth in pancreatic cancer (Demir *et al*, 2015b). To assess if KPC spheroids affected also SCs-DRGs cocultures, we determined whether SCs-DRGs cocultures grew differently when in contact with healthy or neoplastic spheroids.

Remarkably, KPC spheroids induced a statistically significant increase as mean length of the neurites ($P = 0.0103$, Figure 22). This result is consistent with observation made on human neoplastic specimen and confirms that spheroids – SCs-DRGs cocultures is a reliable model to reproduce PNI *in vitro*.

a)

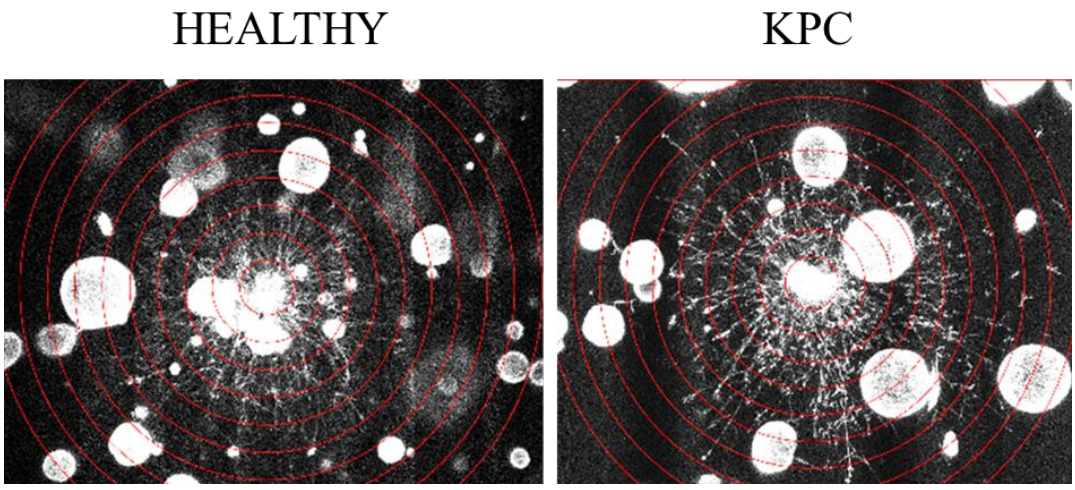

b)

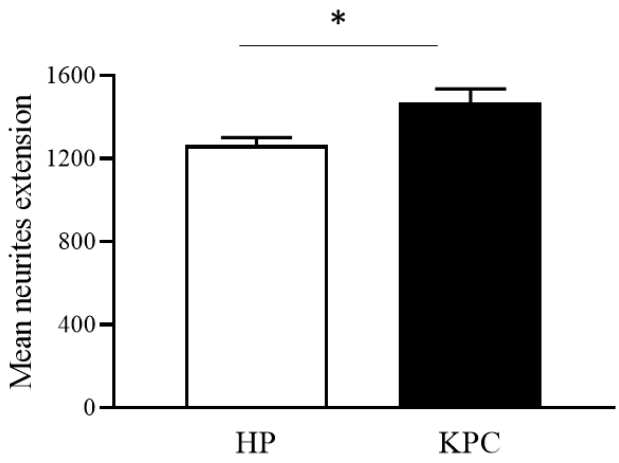

Figure 22. Morphological analysis of healthy organoids (HP) and KPC (KPC) spheroids.

a) Representative reconstructed immunofluorescence images of healthy and neoplastic spheroids after 7 days of co-culture with SCs-DRG neurons. Cocultures were stained for Phalloidin.

b) *Quantification of mean neurite extension: healthy pancreas (HP) organoids 1264 ± 36.18; KPC organoids 1469 ± 65.49. Error bars represent mean ± s.e.m. (Student t test, * P=0.0103. N=3 replicates per group). Neurite extension was measured using pixels (783,8 pixel/mm).*

3.3 Orthotopic spheroids transplants

Orthotopic organoids transplant is a valid model to study PDAC. When transplanted, they can recreate a cancer microenvironment better reproducing the original PDAC specimen, as compared to *in vitro* culture conditions. In addition, organoids can recapitulate all the stages of PDAC development, slowly progressing from pre-invasive lesion to a metastatic disease (Boj *et al*, 2015). It is controversial whether PNI can be observed in the commonly used mouse models of PDAC, as it has only been described at very late tumor stage where the cancerous mass compressed nerves ab extrinsic (Stopczynski *et al*, 2014) . Orthotopically transplanted organoids, instead, show a slow neoplastic growth, and we hypothesized that this gradual growth may allow for PNI to develop.

Thus, in collaboration with Dr. Caronni from Dr. Ostuni's lab (OSR), we orthotopically transplanted KPC spheroids as previously described (Boj *et al*, 2015; D'Agosto *et al*, 2020b). Briefly, we injected 1 million cells from a spheroids suspension in the pancreas of anesthetized wild type mice. We monitored tumor growth by ultrasound performed at the OSR Preclinical Imaging Facility every two weeks. After 75 days, at mice sacrifice, we collected the organs of interest in formalin to be analyzed by the Pathology Department of our Institute. Specifically, we collected the pancreas to verify the histological aspect of the primary tumor. To assess the presence of metastasis, spleen, duodenum, stomach, liver, kidneys, lungs, peritoneum and diaphragm were retrieved. Pathologists' evaluation confirmed the presence of a primary pancreatic tumor mass, which at histology closed resembled human PDAC as characterized by presence of glandular atypia and high stromal infiltrate (Haeberle & Esposito, 2019). Moreover, they also observed metastatic dissemination in the abdominal cavity and on the liver capsule. Interestingly, metastatic disease was found also in the lungs of these mice, strongly resembling metastatic disease of human patients from a histological perspective (Figure 23a-b). Thus, orthotopic spheroids transplants successfully gave rise to a primary

pancreatic cancer that resembles human PDAC, and we were also able to obtain metastases to the same organs commonly involved in human patients.

Once assessed that orthotopically transplanted KPC spheroids are very faithful to human PDAC, we tested whether we could observe the presence of PNI in this system. To this aim, we monitored the development of the tumor mass with ultrasound and sacrificed mice after tumor development, but we used a different technique to collect abdominal organ. The largest and more readily available nerve trunks and ganglia are the nerves running along the vertebral column and the respective coeliac and mesenteric ganglia, and these are also the locations where PNI is found in human patients. To harvest these nerves, we collected en bloc the region of interest of the mouse abdomen: starting from the pancreas with duodenum and spleen, we dissected posteriorly collecting the kidney and the posterior muscular layer and the fascia above the vertebral column. In this way, we could maintain at least in part the anatomical orientation of the specimen to try and localize PNI. We then included the abdomen in OCT and are currently retrieving tissue sections to perform immunofluorescence for PDAC and nerve markers. Preliminary results show a strong innervation of the neoplastic pancreas, with the presence of numerous nerve fibers positive for NF. In addition, we observed the presence of neoplastic cells budding from the primary tumor that are attracted by nearby nerves, as shown in Figure 23c.

We are currently working on validating these results in a wider cohort of cases and we also plan to compare our findings with healthy pancreas specimens.

a)

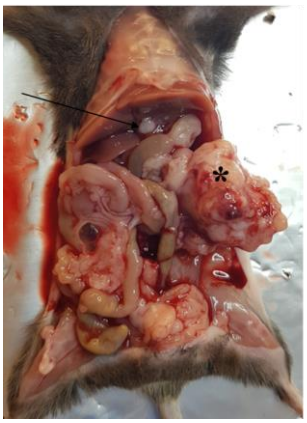

b)

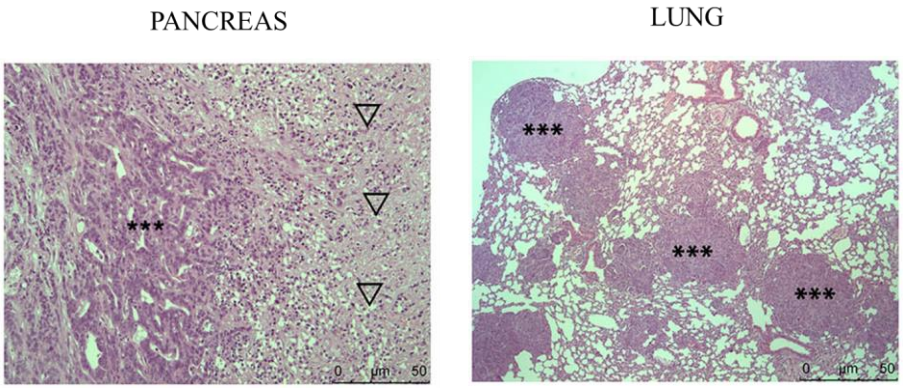

c)

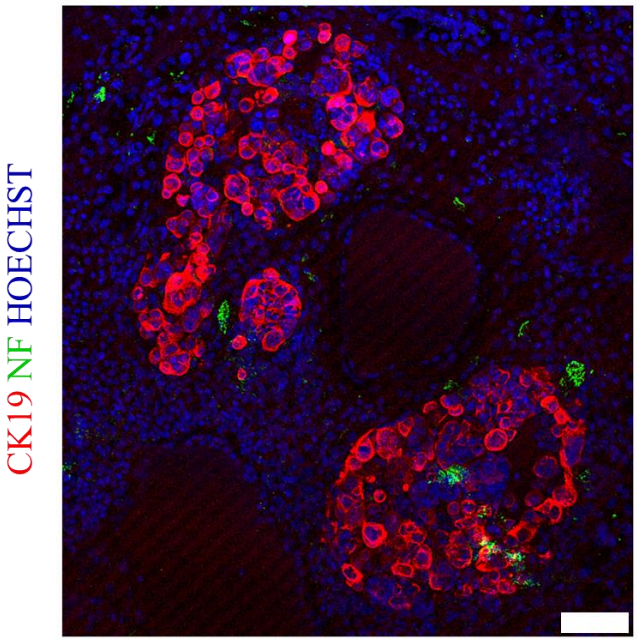

Figure 23. Orthotopic transplants of neoplastic spheroids

a) *Representative images of the primary pancreatic tumor (*) developed after 75 days of transplants. Arrow indicates metastases to the liver.*

b) *Hematoxylin and eosin staining of pancreas showing the primary tumor (***) and the extensive necrosis (▽). Hematoxylin and eosin staining of metastases to the lung (***).*

c) *Representative immunofluorescence image of tumor originated from transplanted* spheroids *marked with CK19 (rhodamine) that surrounds nerve, stained for NF (fluorescein). Nuclei are marked with Hoechst. Scale bar = 50 um.*

4. VANISSh Protocol: Vascular And Neural Invasion Severity Score

In collaboration with the Pathology Unit and the Pancreatic Surgery Unit, we have developed a new score to better stratify the severity of perineural and perivascular invasion. The primary aim of the Vascular And Neural Invasion Severity Score

(VANISSh) is to evaluate both retrospectively and prospectively the newly proposed scoring systems and correlate them with disease free survival (DFS). Secondary aims are to correlate these scores with other clinical variables such as early recurrence, site of recurrence, disease specific survival (DSS) and neoadjuvant treatment. The VANISSh protocol is an observational study that was approved by the OSR internal Ethical Committee (protocol n.165/INT/2018) and it is a registered Clinical Trial (NCT04024358).

Dr. Schiavo Lena and Prof. Doglioni, from the OSR Pathology Unit based on their experience with pancreatic pathologies, proposed the following PNI stratification:

0: Not identified/Absent

1: Invasion of scarce nervous trunk of small diameter (<1 mm)

2: Diffuse invasion in small nervous trunk or medium nervous trunk (>1 mm but <3 mm) or intraneural invasion

3: Massive invasion or big nervous trunk (>3 mm) or necrosis of the invaded nerve

For retrospective analyses we enrolled 507 patients, with a histologically confirmed PDAC, who underwent surgical resection at our institute from January 2015 to December 2019. Since there were no significant differences in terms of pathological features between tumors of the head or the body and tail, we did stratify for regional differences. We separately analyzed patients who underwent upfront surgery (n=278) from those who received neoadjuvant treatment (n=229). Neoadjuvant treatment significantly reduced PNI: indeed, while PNI was present in 79.9% of the upfront surgery patients, it was reduced to 70.7% in patients who received neoadjuvant treatment (p=0.022). The chemotherapeutic regimen did not influence PNI incidence, as PNI was absent in 24.6% of patients receiving a non-platinum based therapy compared to a 33.9% of patients who received a platinum based therapy (p=0.146).

4.1 The impact of PNI on disease free survival and disease specific survival

To establish whether PNI might affect DFS, we first performed univariate Kaplan-Meier analyses with the most known clinical and pathological features. Among these, we selected statistically significant factors to perform Cox survival analysis.

On univariate analysis on patients who underwent upfront surgery, only pathological factors emerged as indicators of recurrence, like tumor grade and dimension, lymph node involvement, margin status, grading, perineural and perivascular invasion. Remarkably, more severe PNI correlated with a higher probability of recurrence: patients who did not have PNI had a median of 36 months of DFS, patients with PNI 1 had 24 months, patients with PNI 2 had 22 months and patients with PNI 3 had only 15 months of DFS (p=0.000; Figure 24a).

Univariate analyses for neoadjuvant treated patients confirmed the same pathological features observed in the above described group of patients except for grading. This can be explained by the fact that neoadjuvant treatment destroys cancer cells resulting in a less aggressive grading score. Also in this group, PNI severity significantly correlated to the median time of DFS: PNI 0 patients had 28 months of DFS, PNI 1 22 months, PNI 2 18 months, PNI 3 had only 13 months of DFS (p=0.004; figure 24b).

At multivariate analyses, PNI did not emerge as an independent prognostic factor neither for the upfront group (p=0.811, CI 95% 0.598-1.929) nor the neoadjuvant one (p=0.761, CI 95% 0.485-1.698). In the upfront group, T stage and N status were the only significant predictors of survival (p=0.004, CI 95% 1.299-3,718 and p=0.003, CI 95% 0.798-19.50 respectively). In the neoadjuvant group, only T stage emerged as independent predictor of recurrence (p=0.046, CI 95% 1.007-2.233).

a)

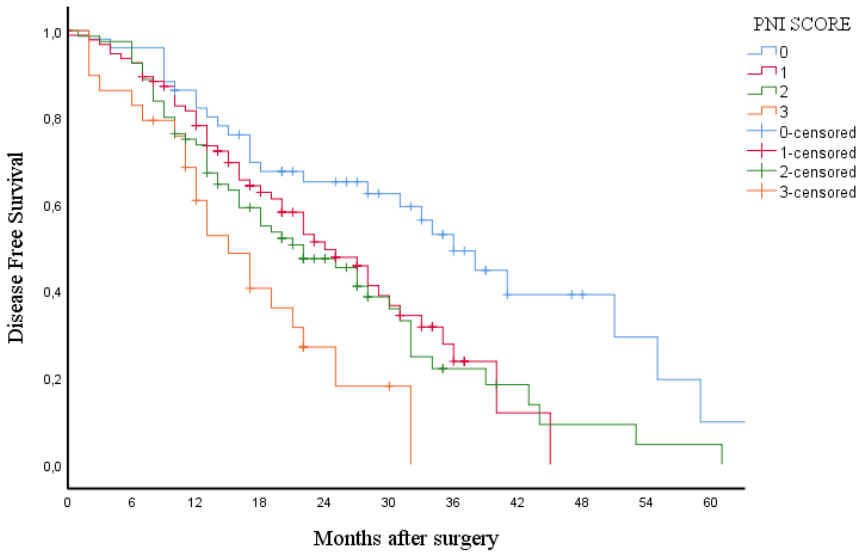

b)

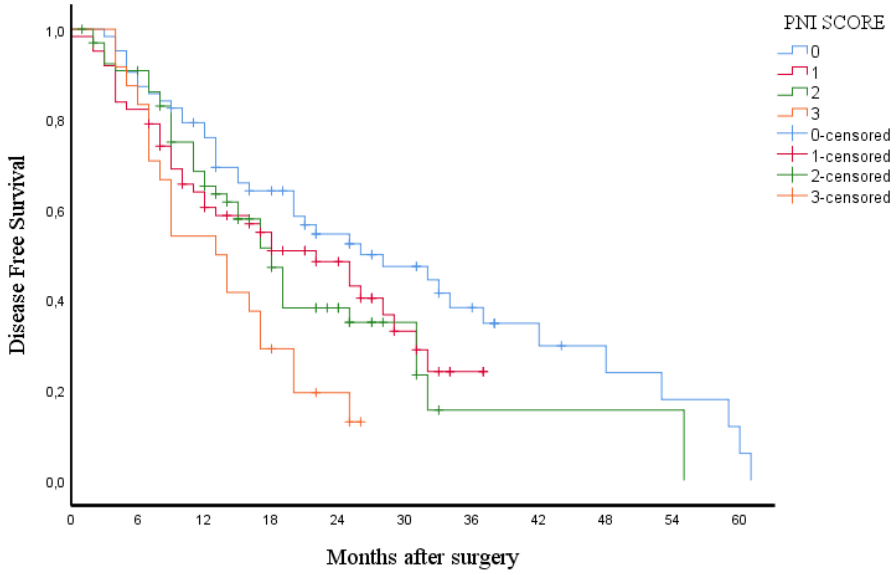

Figure 24. PNI impact on DFS in the upfront (a) and the neoadjuvant (b) group

a) DFS stratified by PNI score calculated with Kaplan-Meier method. DFS was 36 months for patients without PNI, 24 months for patients with PNI score 1, 22 months for patients with PNI score 2, 15 months for patients with PNI score 3 ($p<0.001$)

b) DFS stratified by PNI score calculated with Kaplan-Meier method. DFS was 28 months for patients without PNI, 22 months for patients with PNI score 1, 18

months for patients with PNI score 2, 13 months for patients with PNI score 3 (p=0.004)

To analyze the impact of PNI on Disease Specific Survival (DSS), we performed uni- and multivariate analysis. PNI emerged as a significant factor at univariate analyses only in the neoadjuvant group (P = 0.009, figure 25), while it did not reach significance in the upfront group.

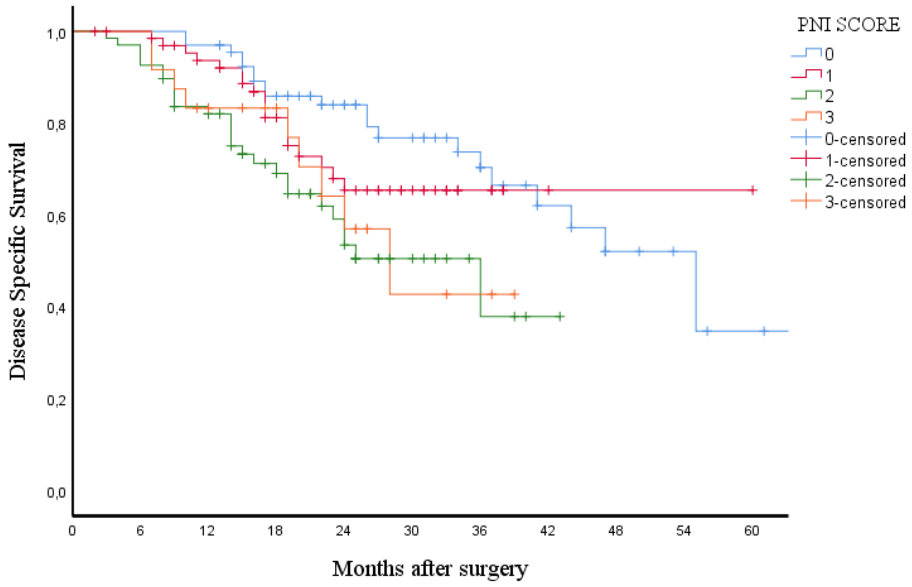

Figure 25. PNI impact on DSS in the neoadjuvant group

DSS stratified by PNI score calculated with Kaplan-Meier method. DSS at 1 year was 95% for patients without PNI, 92% for patients with PNI score 1, 82% months for patients with PNI score 2, 77% months for patients with PNI score 3 (p=0.009).

4.2 PNI correlates with other pathological features

Next, we analyzed if more aggressive pathological features correlate with a more severe PNI score. We focused on T status, N status, grading, and margin status (R), as these are the most important pathological factors for PDAC patients. Interestingly, worsening of all the selected factors significantly correlated with a more severe PNI, suggesting the validity of the proposed score (Figure 26-27).

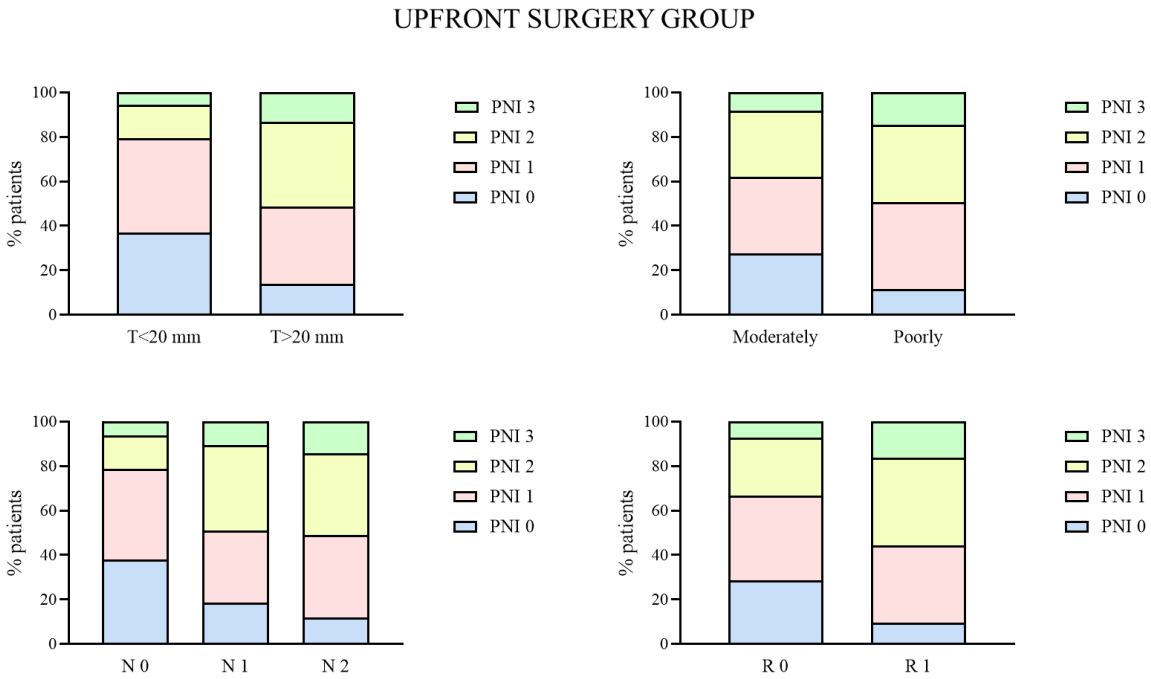

PNI severity score (upfront group)						
	0 **N (%)**	**1** **N (%)**	**2** **N (%)**	**3** **N (%)**	**P**	**Kendall's Tau-B**
Tumor size					< 0.001	0.270**
≤20	27 (48.2)	31 (30.4)	11 (12.4)	4 (12.9)		
>20	29 (51.8)	71 (69.6)	78 (87.6)	27 (87.1)		
N status					< 0.001	0.219**
0	25 (44.6)	27 (26.5)	10 (11.2)	4 (12.9)		
1	16 (28.6)	28 (27.5)	33 (37.1)	9 (29)		
2	15 (26.8)	47 (46.1)	46 (51.7)	18 (58.1)		
Grading					0.006	0.162**
Moderately	41 (73.2)	51 (50)	44 (49.4)	12 (38.7)		
Poorly	15 (26.8)	51 (50)	45 (50.6)	19 (61.3)		
Margin status					< 0.001	0.248**
R 0	44 (78.6)	59 (57.8)	40 (44.9)	11 (35.5)		
R 1	12 (21.4)	43 (42.2)	49 (55.1)	20 (64.5)		

Figure 26. PNI correlates with other pathological features in the upfront surgery group.

*Increasing PNI severity correlates with increasing T size, higher number of positive lymph nodes, poorer differentiation grade and higher risk of positive margin status. Graphs represent the percentage of patients in each group of PNI for the corresponding pathological feature. Contingency tables were used to calculate p-values. Kendall's Tau-B was used to obtain the correlation coefficient of strength and direction of the association. **significant at level p<0.001 (two-tailed).*

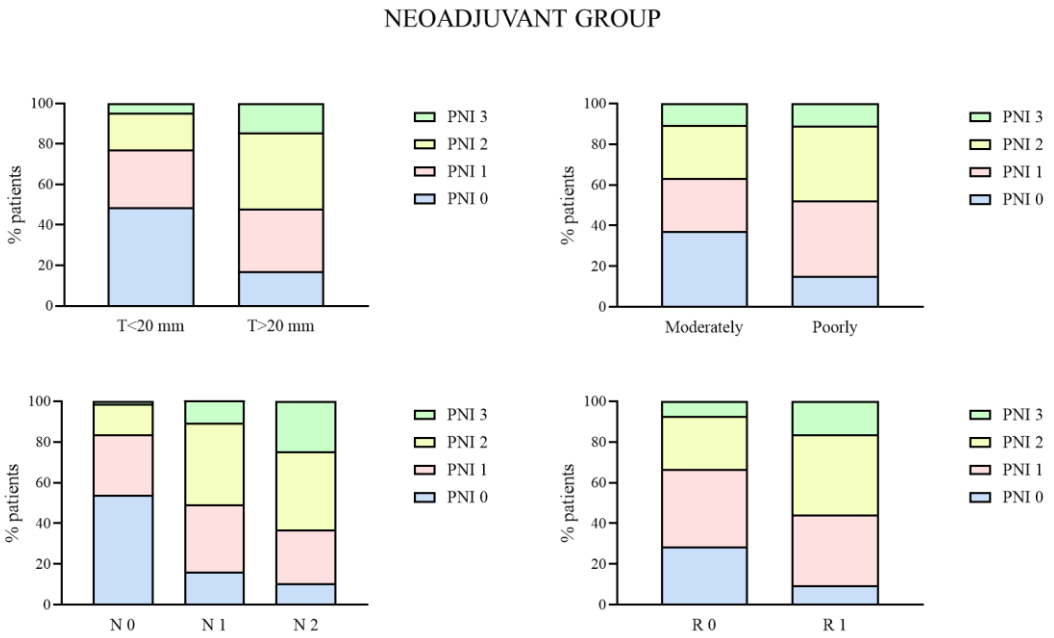

PNI severity score (neoadjuvant group)						
	0 **N (%)**	**1** **N (%)**	**2** **N (%)**	**3** **N (%)**	**P**	**Kendall's Tau-B**
Tumor size					< 0.001	0.331**
≤20	43 (64.2)	25 (36.2)	16 (23.2)	4 (16.7)		
>20	24 (35.8)	44 (63.8)	53 (76.8)	20 (83.3)		
N status					< 0.001	0.416**
0	47 (70.1)	26 (37.1)	13 (18.8)	1 (4.2)		
1	14 (20.9)	28 (40.6)	34 (49.3)	9 (37.5)		
2	6 (9)	15 (21.7)	22 (31.9)	14 (58.3)		
Grading					0.005	0.162**
Moderately	54 (80.6)	38 (55.1)	38 (55.1)	15 (62.5)		
Poorly	13 (19.4)	31 (44.9)	31 (44.9)	9 (37.5)		
Margin status					< 0.001	0.417**
R 0	58 (86.6)	45 (65.2)	26 (37.7)	6 (25)		
R 1	9 (13.4)	24 (34.8)	43 (62.3)	18 (75)		

Figure 27. PNI correlates with other pathological features in the neoadjuvant group

Increasing PNI severity correlates with increasing T size, higher number of positive lymph nodes, poorer differentiation grade and higher risk of positive margin status. Graphs represent the percentage of patients in each group of PNI for the corresponding pathological feature. Contingency tables were used to calculate p-values. Kendall's Tau-

*B was used to obtain the correlation coefficient of strength and direction of the association. **significant at level p<0.001 (two-tailed).*

These results suggest that the newly developed score is accurate in dividing PNI in the different proposed categories. Indeed, increasing PNI severity correlates with the worsening of important pathological features like T, N, grading and margin status. In addition, the score stratified well with worsening DFS in both groups, but a longer time of follow up is mandatory to draw conclusion on the correlation of PNI score and DSS.

Data collection and analyses from the prospective cohort will increase the population dimension as well as the length of follow up, offering a more thorough analysis of this phenomenon.

Discussion

In this work, we focused on the interactions between cancer cells with myelinated or non-myelinated axons. We showed that paracrine factors released by neoplastic cells are sufficient to induce profound alterations in myelinated cocultures, which is specific to pancreatic cancer. We also observed that direct contact between cancer cells and nerves reproduces more aggressively myelin degeneration, a phenotype that activates the classical pathways of nerve damage, as confirmed by the upregulation of c-Jun, the key master factor regulating Schwann cells dedifferentiation to prompt nerve regeneration (Parkinson et al, 2008b; Arthur-Farraj et al, 2012).

Among the factors identified in our secretome analyses, we focused on those specifically upregulated in KPC CM as compared to controls based on the following criteria: involvement in cancer growth and progression, involvement in myelin and nerve damage. Thus, we selected five candidates. After literature review, we narrowed our studies on investigating the role of FGF-BP1, since it is relevant for both PDAC and nerve regeneration. The reliability of our analyses was confirmed by our results, showing that in vitro, FGFBP1 is necessary and likely sufficient to cause myelin degeneration of already myelinated SC neuronal cocultures. Indeed, FGF-BP1 is upregulated in PDAC, increasing availability and signaling of FGFs, therefore promoting tumor growth. Moreover, FGF-BP1 binding and releasing of FGF2, mediates a pro-angiogenic switch leading to an increased growth of endothelial cells (Czubayko et al, 1997). FGF-BP1 also correlates to invasion and metastases in PDAC, as it might modulate FGF22 activation in cancer associated fibroblasts, that in turn promote cancer cells migration and invasion (Zhang et al, 2019). Several FGFs are involved in promoting PDAC (Ndlovu et al, 2018; Kang et al, 2019), thus it is likely that FGF-BP1 interacts also with other ligands to promote cancer.

In the PNS, FGFs have a protective role after nerve injury (Maddaluno et al, 2017); for example, activation of FGFs signaling prevents degeneration of unmyelinated sensory axons (Furusho et al, 2009). Specifically, FGF-BP1 has a role in the development and maintenance of the neuromuscular junction (Taetzsch et al, 2018).

Next, given the striking phenotype observed with myelin degeneration, we wondered what advantage KPC cells could gain from inducing myelin degeneration. We hypothesized that myelin degeneration and its subsequent removal are necessary for cancer cells to alter nerve structure and induce axonal growth, thus initiating PNI, since myelin is otherwise inhibitory to axonal regrowth (Brosius Lutz & Barres, 2014). This represents a completely new area of investigation, as no data are available on the interaction between cancer and myelinated nerves.

KPC cells are affected by the presence of nerves as well. Indeed, our results showed enhanced growth and proliferation rate when KPC cells are in contact with myelinated nerves, and myelin increases also the migrative and invasive abilities of KPC cells. Moreover, KPC cells can uptake purified myelin droplets and use them to proliferate.

These data offer a new insight on the ability of cancer cells to exploit nerves for their sustainment, in particular we could speculate that myelin is an energetic source for KPC cells. Accordingly, it has been suggested that pancreatic cancer cells have an altered lipid metabolism that supports both increased uptake and storage of lipids as well as de novo synthesis of cholesterol and other lipoproteins, therefore providing a key resource to fuel proliferation and metastatization (Rozeveld et al, 2020; Guillaumond et al, 2015). Remarkably, a meta-analysis on 4513 PDAC patients revealed that a high-cholesterol diet might increase the risk of developing PDAC, suggesting a possible contribution of exogenous cholesterol presence to PDAC development (Chen et al, 2015).

To use a more physiological system than bidimensional KPC cells, we developed pancreatic organoids and spheroids. We were able to coculture spheroids and SC-DRG explants, and we demonstrated that KPC spheroids induce a significant growth in SC-DRGs compared to healthy organoids. This result validates our coculture system as it recapitulates the nerve hypertrophy observed in PDAC patients (Tan et al, 2021) and offers a reliable model to study PNI. Moreover, to study PNI in an in vivo model, we set up orthotopic spheroids transplants and plan to characterize the presence of nerve invasion, thus establishing a system that will allow to test how to interfere with the development of PNI.

Finally, we decided to investigate in detail the pathological definition of PNI by developing a novel score that stratifies PNI on the basis of the different severity of nerve

invasion. This score will help understand the clinical significance of the different types of PNI in PDAC, as so far it has only been considered a present or absent phenomenon (Crippa et al, 2020).

KPC cells influence on myelinated cocultures

It is widely accepted that PDAC and nerves have strong interactions from the very early phases of cancer development, with a growing literature supporting this observation (Crippa et al, 2020). However, there are no studies focusing on the interactions between myelinated nerves and PDAC, most likely because of the difficulty in obtaining reproducible in vitro myelinated cocultures. Our expertise in the research of myelination and the extensive use of in vitro neuronal cultures allowed us to address the foundation of these interactions.

Remarkably, we found that factors released by KPC cancer cells could induce myelin degeneration already after 7 days (Figure 8). Not surprisingly, direct contact with KPC cells exerts a stronger effect, inducing myelin degeneration in only 3 days (Figure 10). Interestingly, myelin degeneration was specifically induced by PDAC, as CM from colon cancer cells did not have any effect. This result is in line with previous studies that have reported that PDAC is the gastrointestinal cancer with the highest prevalence of PNI (Liebl et al, 2014).

More importantly, the observed myelin degeneration correlates with a significant upregulation of the master regulator of nerve-damage, c-Jun. c-Jun, which is upregulated in SCs early after damage (Gomez-Sanchez et al, 2017), promotes reprogramming of SCs into repair cells, a necessary prerequisite to induce the entire nerve degeneration and regeneration program. During this process, repair SCs express trophic factors that support nerve regrowth, like GDNF, BDNF, artemin, p75NTR and N-cadherin (Arthur-Farraj et al, 2012). Accordingly, it has been proposed that nerve-cancer interaction recapitulate the same molecular processes occurring during regeneration (Boilly et al, 2017). Remarkably, all these molecules are also implicated in supporting PNI in PDAC, promoting cancer growth or nerve-cancer interactions. Therefore, we posit that PDAC could hijack the trophic factors used by nerve to regenerate for its own advantage.

Among the secreted molecules that participate in the early events of PNI and thus induce myelin damage, we investigated FGF-BP1. FGF-BP1 is normally expressed in skin, eye, stomach, ileum, and colon (Aigner et al, 2002), and it is upregulated in some types of cancer. In hepatocarcinoma upregulated FGF-BP1 expression correlates to a more aggressive tumor stage and diminished overall survival. Indeed, it associates with increased migration and metastatic potential in an in vitro model of hepatocarcinoma (Huang et al, 2015). FGF-BP1 expression is also markedly increased at early neoplastic stages in PDAC and in colon cancer, and high levels of FGF-BP1 were also reported in metastatic colorectal cancer and advanced PDAC (Tassi et al, 2006). Moreover, FGF-BP1 is overexpressed in human PDAC compared to normal adjacent pancreatic tissue as emerged by immunohistochemical analysis and confirmed by tissue micro array analysis on 176 patients (Expression of FGFBP1 in pancreatic cancer - The Human Protein Atlas, 2016). Interestingly, in a study on 109 PDAC patients, FGF-BP1 emerged as an independent predictor of survival at Cox regression analysis, surpassing other established prognostic factors like lymph node status (Zhang et al, 2019).

In the PNS, FGF-BP1 has been described in the developing neuromuscular junction (NMJ) to promote the formation and maintenance of the structural integrity of the NMJ (Taetzsch et al, 2017a), and it interacts with the FGFs that have a neuroprotective effect in the PNS (Maddaluno et al, 2017).

We now report that FGF-BP1 expressed in myelinated cocultures is reduced after treatment with KPC CM (Figure 12). This might represents an attempt of myelinated nerves to reduce the influence of a cancer-secreted molecule that might induce nerve damage if overexpressed, thus supporting the notion that PDAC actively participates to nerve remodeling. More importantly, we showed that FGF-BP1 could mediate myelin degeneration, suggesting a specific role for FGF-BP1 released by cancer cells in inducing PNI. In future studies it will therefore be important to define how FGF-BP1 could sustain PDAC growth and nerve-cancer interactions, and to explore whether FGF-BP1 and its downstream signaling are involved in the process of myelin damage. We have already started to address these issues by developing KPC cells knocked out for FGF-BP1 by Crispr-Cas9 technology. Thus, we will use these cells to confirm the results reported in

these studies on the effects of FGF-BP1. More importantly, we plan to perform orthotopic transplant of knocked down KPC cells and organoids and monitor tumor growth and neural invasion in vivo. These studies will confirm the role of FGF-BP1 in mediating PNI and reveal if interference with its signaling might become a novel therapeutic strategy for PDAC patients.

If successful, we might consider inhibiting FGF signaling in animal models of PDAC, characterized by enhanced PNI, and monitor tumor growth, metastatic spread and PNI.

Myelin influence on KPC cells: a lipidic fuel for cancer?

In our studies we also addressed this fundamental question: What advantage would obtain KPC cells in inducing myelin damage? Myelin is mainly composed of lipids and, based on very recent evidences suggesting a central role for lipids in promoting PDAC metastases (Rozeveld et al, 2020), we hypothesized that myelin could indeed represent an attractive energetic source for KPC cells.

Accordingly, our results confirmed that in KPC cells contacting myelinated cocultures, the size of single cancer cells as well as the size of clustered cells is increased, with cells being enlarged and more outstretched. This results into increased proliferation, indicating that KPC cells are prone to grow and expand when myelin is available. This is in line with previous studies where neoplastic cells take advantage of different factors secreted by nerves, which are upregulated in PDAC tissue samples, like NGF (Saloman et al, 2018), artemin (Ceyhan et al, 2007), GDNF (He et al, 2014) and many others. Thus, myelin lipids might represent a novel, pro-tumoral factors that underlies once more the importance of nerves for cancer growth.

Our data also indicate that myelin represents a strong, attractive factor for KPC cells, supporting both migration and invasion (Figures 16 and 17). Based on the results of our studies, we could speculate that myelin is used as an energetic source to promote growth. Additional studies are required to corroborate this hypothesis. Thus, we are planning to perform metabolomics and lipidomic analyses on KPC cells fed with myelin to define which metabolic pathways are activated upon myelin uptake. Hopefully, this will also lead to the identification of metabolic alterations that could represent novel therapeutic

targets for PDAC patients, as it is already known that high-fat diet and obesity are both risk factors for PDAC (Xu et al, 2018; Chen et al, 2015).

We also intend to understand which receptor(s) is responsible for myelin uptake in KPC cells. It is known that Low Density Lipoprotein Receptor (LDLR) is upregulated in PDAC and mediates the uptake of cholesterol lipoproteins (Guillaumond et al, 2015), thus, in future studies, we will perform quantitative RT-PCR analyses to investigate the expression level for LDLR mRNA on RNA collected from KPC cells after myelin uptake to begin with.

Our results are in agreement with recent studies showing that pancreatic cancer cells pre-exposed to lipids enhance their migration and invasion (Rozeveld et al, 2020). With reference to this, we plan to investigate how myelin promotes migration and invasion starting from the lipidomic and metabolomics data.

Organoids as a valuable tool to study PNI

One of the main results of this study was to develop a 3D culture model using organoids and spheroids, which represent a valuable tool to study PDAC and to investigate PNI. We successfully embedded DRG explants into spheroids and established reliable methods to validate neurons growth. To our knowledge, no other attempts to co-culture pancreatic organoids and nerves have been thus far obtained. Though this system might need additional adjustments, it represents a new, more physiological system to mimic in vitro PNI in PDAC compared to the currently used models with bidimensional cancer cells.

Using this novel culture technique, we observed that DRG neurons grow more substantially when embedded in neoplastic spheroids. This is in agreement with what observed in human patients, in whom nerves show hypertrophy and increased density in PDAC compared to normal pancreas (Demir et al, 2015a), further corroborating the faithfulness of our newly created model to the human disease. To assess if direct contact with KPC organoids will induce myelin degeneration, further work is needed to find the suitable growth conditions.

Organoids represent a valuable tool also for in vivo studies. Orthotopically transplanted spheroids faithfully model PDAC progression as they can reconstruct the proper microenvironment (Baker et al, 2016). Interestingly, using our derived spheroids, we visualized metastatic spread of PDAC cells to lung and liver, in line with recent studies (Filippini et al, 2019). Lung metastases were particularly intriguing, since they involve KPC migration along blood or lymphatic vessels, or even nerves. The possibility that our transplanted spheroids exploit nerves to spread tumor cells is supported by the fact that we observed neoplastic cells in the nervous trunks that run parallel to the aorta and the coeliac and mesenteric ganglia. In conclusion, we propose that spheroids transplant could represent a valid model not only to investigate tumor formation and metastasis, but also PNI.

Thus, in future studies, we could take advantage of this model to develop therapeutic strategies to target PNI, cancer metastatization and pain.

PNI is a phenomenon with different degrees of severity

To correlate our in vitro and in vivo preclinical studies to human PDAC and to facilitate possible translational results of our research, we have developed a new scoring system for PNI that takes into account the different size of involved nerve fibers, the depth of invasion of cancer cells and the possible presence of necrosis. All these three aspects correlate with a more aggressive cancer. We observed a significant correlation between worsening of PNI and more severe pathological features like tumor stage, lymph node involvement, grading and positive resection margins (figures 26 and 27). These results prove that greatest attention should be given to the severity of PNI, as it becomes more and more serious in association with the worsening of the other analyzed pathological features. Thus, combining PNI to all these factors might become a very useful tool to stratify disease aggressiveness in patients. The interaction of neoadjuvant chemo/radiotherapy with PNI is still controversial. Our results suggest that neoadjuvant treatment reduces PNI, in agreement with recent studies showing that the extent of PNI is significantly lower upon neoadjuvant treatment compared to patients who underwent upfront surgical resection (Roland et al, 2015; Barnes et al, 2019). Nevertheless, other studies referring to older chemotherapeutic schemes did not report a positive impact of

neoadjuvant treatment in reducing PNI (Crippa et al, 2020). To correctly understand the impact of neoadjuvant treatment on PNI, a meta-analyses that compares the different therapeutic schemes is needed.

Interestingly, our PNI score showed a good stratification of DFS, with a progressive reduction of the median months of survival with increasing PNI. At multivariate analyses, PNI failed to reach statistical significance, and probably a longer follow up time is needed. Indeed, a recent study suggested that PNI could become the only independent predictor of survival for long term survivor patients (Belfiori et al, 2021).

In conclusion, we have rigorously analyzed the interactions between PDAC and nerve, specifically focusing on the role of myelinated nerves in promoting cancer by applying the most innovative techniques, like SCc-DRGs cocultures and pancreatic organoids, as well as detailing the role of PNI in the clinical setting.

Hopefully, our results will provide a strong premise for the further development of therapeutic strategies targeting pancreatic cancer, helping to improve the outcomes of such an aggressive disease.

Methods

1. In vitro cell culture systems

1.1 Mouse dorsal root ganglion (DRG) explants

Explants were obtained from wild type C57/BL6 females pregnant from wild type C57/BL6 males. Embryos were separated from the mother at E13.5 and spinal cords were isolated. Dorsal root ganglia (DRG) were then taken from each spinal cord and plated onto rat collagen-I (Cultrex) coated glass coverslips. Schwann cells-DRG neuron cocultures were maintained in growing conditions for one week in NB medium (B27 supplement, D-glucose 4g/l, L-glutamine 2mM, Nerve Growth Factor (NGF) 50 ng/ml in Neurobasal medium (Invitrogen)); myelination was then induced for ten days by switching growing media into differentiating media (Fetal bovine serum 10%, L-glutamine 2 mM, D-glucose 4 g/l, Nerve Growth Factor (NGF) 50 ng/ml in MEM medium (Invitrogen), 50ug/ml ascorbic acid).

1.2 Neoplastic cells

KPC cells were kindly gifted by Dr. Lorenzo Piemonti. They were primarily derived from the KPC mice from the Tuveson Laboratories. KPC cells were grown in 100 mm Petri dish in a medium composed of IMDM (Sigma-Aldrich), Fetal bovine serum 10% and Penicillin/Streptomycin 5% (Gibco). We thawed cells at 37° C and we transferred them immediately to a 15 ml tube containing warmed KPC medium. We centrifuged the cells at 1200 rpm for 5 minutes and plated them in 100 mm Petri cell culture dish containing 10 ml of medium. We splitted cells 1:10 when they reached confluency. We grew KPC cells in 37°C incubator with 5% CO2.

MC38 cells were kindly gifted by Dr. Giovanni Sitia. They are a commercial cell line of colon carcinoma. MC38 cells were grown in 100 mm Petri dish in a medium composed of DMEM (Sigma-Aldrich), Fetal bovine serum 10% and Penicillin/Streptomycin 5% (Gibco). Culturing conditions were the same as for KPC cells.

1.3 Primary murine pancreatic ductal cells

Healthy pancreatic ductal cells were derived as described in (Reichert et al, 2013). Briefly, the pancreas was collected from an adult wild type mouse and mechanically minced under sterile conditions, followed by chemical digestion with Collagenase type V (Sigma-Aldrich) at 37 °C for 20 min on a shaker. The digestion reaction was stopped by the addition of 10 ml of G solution (HBSS, glucose 0.9 g/L, 47.6 μM CaCl2). We pelleted the homogenate at 300 x g for 5 minutes at 4 °C. Then we collected the supernatant and added 1 ml of trypsin-EDTA, followed by an incubation at RT for 5 min. We then added 2 ml of trypsin inhibitor to the mixture and resuspended thoroughly. We added fresh G solution, then we filtered with a 40-μm cell strainer (Falcon) and centrifuged the digestion mix at 300g for 5 min at 4 °C. Then we removed the supernatant and plated the cell pellet on a collagen-coated 60 mm Petri dish in PDC medium (DMEM/F12 (Gibco), 5% Nu-Serum IV (BioSciences), 1% Penicillin-streptomycin (Gibco), 25 μg/ml Bovine pituitary extract Biosciences), 20 ng/ml Epidermal growth factor (Biosciences), 100 ng/ml Cholera toxin (Sigma-Aldrich), 5 nM 3,3,5-Triiodo-L-thyronine, 50 μM (Biosciences), 1 μM Dexamethasone (Sigma-Aldrich), 5 mg/ml Glucose (Sigma-Aldrich), 1.22 mg/ml Nicotinamide (Sigma-Aldrich)). When confluent, cells were passaged and then maintained in culture.

1.4 Conditioned media preparation

Conditioned media (CM) was obtained following the same procedure for KPC, MC38 and primary murine pancreatic ductal cells. Cell were cultured for 48/72 hours until they reached 90% confluence, then were rinsed twice with PBS and a serum-free conditioning medium was added (MEM (Gibco), glucose 4g/L, Glutamine 2mM). After 48 hours, CM

was collected, centrifuged at 1200 rpm for 5 minutes at room temperature and filtered with 0.45 um filter (Millex-HV, Millipore) to remove any possible residual cells. CM for secretome analysis was collected in triplicate and analyzed by Mass-spectrometry by the ProMiFa facility in HSR.

After collection, CM for treatment of neuronal explants was additioned with 5% FBS, 50ug/ml ascorbic acid and 2mM Glutamine. Aliquots were stored at -80°C until usage no longer than two months.

1.5 Immunofluorescence on in vitro cultures

Cells were fixed with 4% paraformaldehyde (PFA) for 20', rinsed twice in PBS and permeabilized with cold methanol for 5'; after washing, explants were incubated in blocking (5% Bovine Serum Albumine (BSA) (Sigma-Aldrich), 1% Donkey Serum (Jackson Immunoresearch), 0.2% Triton X100 (Sigma-Aldrich) in phosphate buffered saline (PBS)) for at least one hour and then incubated overnight at 4°C with appropriate primary antibodies in blocking solution. The following day we washed cells twice with PBS 1x for 2 minutes before incubation with the appropriate secondary antibodies (diluted in blocking solution) for 1 hour at room temperature. We performed nuclei staining with Hoechst (0.7 ng/ml) for 10 minutes before coverslip mounting with Vectashield (Vector Laboratories).

We acquired Epifluorescent images with a Leica DFC 7000 T and Leica SP5 confocal microscopes.

1.6 Western Blotting

DRG explants and KPC or MC38 cells were lysed with lysis buffer (2% SDS, 95 mM NaCl, 10 mM EDTA, phosphatase inhibitors (PhoSTOP, Roche) and protease inhibitors (complete Mini EDTA free, Roche)), boiled for 5 min and spinned at 14,000 rpm for 10 min at 16°C to eliminate insoluble material. Total protein concentration was determined

by BCA protein assay (Thermo Fisher Scientific) according to the manufacturer's instructions. The same amount of homogenates were loaded with standard reducing sample buffer, samples were denaturated, resolved on SDS-polyacrilamide gel and electroblotted onto a nitrocellulose membrane (Protan Biosciences). To verify the equal loading of samples, membranes were stained with Ponceau red (Sigma-Aldrich), and then blocked with 4% dry milk in TBS 1x 0.05% Tween 20 (Sigma-Aldrich). The appropriate regions of the nitrocellulose membrane were cut and incubated with specific primary antibodies diluted in a solution made of 5% BSA (Sigma-Aldrich), 0.05% NaN3 (Sigma-Aldrich) in 1x PBS (Dulbecco's phosphate buffered saline, Gibco) at 4° overnight. The following antibodies were used: rabbit anti Vinculin (1:1000, Sigma-Aldrich), rabbit anti cJun (1:1000). IRDye infrared secondary antibodies were used (IRDye 800 CW and 680LT, Li-Cor Biosciences). To quantify the results, Odyssey Infrared Imaging system (Li-Cor Biosciences) was used according to the manufacturer's instructions. Integrated intensity of the fluorescent signal was used to quantify protein expression of each sample. All samples were normalized for the housekeeping protein Vinculin. Results were then analyzed with the Prism Software package (GraphPad) for statistical evaluation.

1.7 RNA extraction and reverse transcription

DRG explants as well as cell homogenates were prepared with Trizol (Roche Diagnostic GmbH, Germany). RNA was then prepare by mean of chloroform extraction and isopropanol precipitation. 300 ng of RNA was reverse transcribed to cDNA using SuperScriptIV Reverse Transcriptase (Invitrogen, U.S.A.) as per manufacturer's instructions. Each pool was composed of at least 8 coverslip of the same experiment. The cDNA was then stored at -80°C in aliquots until use.

1.8 qRT-PCR

To analyze the expression of FGF-BP1, we used the following primers pairs: Fw 5' – GTG ACC CAA CTG ACT GCC TT – 3' and Rev 3' – GGA CCT TGT TGT GCT CCC

TT – 5'. Samples were normalized for the housekeeping gene Hprt using the following primers pairs: Hprt (Fw 5' – CAG ACT GAA GAG CTA CTG TAA TG – 3' and Rev5' – GGG CTG TAC TGC TTA ACC AGG – 3'). Standard curves were performed to check the right amount of cDNA template and the optimal cycling conditions to use for each gene. qRT-PCR for FGF-BP1 and Hprt were performed using Sso Fast TM EvaGreen Supermix (Biorad). Cycling conditions for all the genes were: 95 °C for 5 minutes, 95 °C for 30 seconds, 60 °C for 30 seconds and 72 °C for 1 minute (40 cycles). Quantitative PCR was performed on the C1000 Termal Cycler with CFX96 Real-Time system (Biorad). Real-time PCR results were analyzed with Bio-Rad CFX Manager 3.1. All data were analyzed using the comparative Ct method (ΔΔCT): data where first corrected for the endogenous housekeeping gene (ΔCT) and results were then expressed relative to the reference sample (ΔΔCT). Statistical analyses were performed using the Prism Software package (GraphPad).

1.9 Transwell invasion and migration assays

KPC cells were seeded onto transwell inserts with a polycarbonate membrane pore size of 8 μm (Corning, cat# 3422) in 24 well plates. For migration assays, 30.000 KPC cells were seeded in each insert, while for invasion 70.000 KPC cells were used. For invasion assays, a Matrigel film was prepared before KPC cells seeding: 100 ul of Matrigel diluted 1:10 in PBS was added to each insert and placed at 37°C to solidify. After two hours, the excessive unsolidified Matrigel was removed and KPC cells were seeded. The selected explants on the respective coverslips were moved in the 24 well and left overnight in fresh C medium before performing the experiment. C medium was also used to seed KPC cells on the top insert. After 24 hours, medium within the transwell inserts was removed. Cells that did not migrate across the transwell membrane were removed by gently wiping with a cotton swab. Migrated and invaded cells were fixed with 4% paraformaldehyde and stained with crystal violet (Sigma-Aldrich). Migrated and invaded cells were visualized with a phase-contrast microscope, imaged with Axiocam 105 Color (Zeiss) camera and processed using ImageJ software. At least 8 fields for each

insert were counted. Statistical analyses were performed using the Prism Software package (GraphPad).

1.10 Myelin preparation

We isolated and purified myelin in form of a lipidic suspension from murine brain. We collected four brains from wild type mice and mechanically minced them into small pieces. We then homogenized the tissue with a pre-chilled Dounce homogenizer in 2.5 mL of a 0.85 M sucrose solution. Then, we transferred the homogenate to ultracentrifuge tubes and added 0.25 M sucrose solution to create a gradient. Tubes were spun overnight at 67.000 g. We then collected the myelin fraction, visible as a defined white interface between the two layers of sucrose 0.25 and 0.85 M. We resuspended the myelin fraction in the osmotic shock buffer, and we myelin and centrifuged for 30 minutes at 9000 rpm. We thus obtained a clear myelin pellet that was tested by Western Blot for the presence of MBP protein. We determined myelin concentration with BCA assay and stored 1 mg/ml aliquots at -80 °C until use.

2. Human and murine pancreatic organoids cultures

For the generation of human organoids, surgical specimens were transferred from the operating room to the Pathology Unit in ice as rapidly as possible (always in less than 30 minutes of devascularization). The pathologists provided us with neoplastic tissue that was not needed for clinical diagnosis.

The tissue was immediately placed in Basal Medium (Advanced DMEM/F-12 (Gibco) with 1% P/S, 1% GlutaMAX (Gibco) and 10 mM HEPES (Sigma-Aldrich)), and left overnight at 4° C to remove red blood cells and fat.

We minced the specimens into 1 mm3 pieces in a sterile culture dish containing Basal medium. Next, minced specimens were transferred to a 15 ml tube containing 10 ml of warmed Digestion solution (Basal medium, 0.125 mg/ml Collagenase type I (Gibco),0.125 mg/ml Dispase II (Sigma-Aldrich), 0.1 mg/ml DNase I). We incubated at 37°C for 1-2 h on a shaker. After enzymatic digestion, we performed mechanical

digestion by vigorously pipetting with a Gilson P200 pipette to isolate ductal cells. When the tissue was sufficiently disgregated, we filtered with a 40 μM cell strainer (Falcon) and transferred the digestion solution to a fresh 50 mL conical tube containing 10 mL cold Wash Medium (DMEM high glucose (Gibco), GlutaMAX 100x and pyruvate 1x (Gibco), 1% FBS and P/S). We pelleted the cell suspension at 200 g for 5 minutes at 8 °C, then we discarded the supernatant and washed the pellet twice with 10 mL of Wash Medium, repeating the pelleting method above described.

We resuspended the pellet in an appropriate volume of cold Matrigel (Corning). We seeded 50 μL of matrix-resuspended cells per each well of a pre-warmed 4-well culture plate. Then we incubated Matrigel domes containing PDAC cells at 37°C for 5-10 minutes until the basement matrix solidified and we overlaid the matrix droplets with 500 μL of human organoid growth medium:

Human organoid growth medium	
B 27 w/o Vitamin A	1x
Nicotinamide	10 mM
N-AcetylCysteine	1.25 mM
rH R-Spondin 1	10 ng/ml
FGF 10	100 ng/ml
rh Noggin	100 ng/ml
A83 -01	500 nM
rh EGF	50 ng/ml
h Gastrin	10 nM
PGE2 (only for healthy human organoids)	1 uM
Y-27632	10.5 mM
Wnt 3A conditioned Medium	50%

We grew organoids in 37°C incubator with 5% CO2.

Healthy pancreatic organoids were obtained from a suspension of exocrine cell aggregates obtained after human islet purification from collagenase-digested pancreas, gently provided by Prof. Piemonti, Diabetes Research Institute, San Raffaele Hospital.

To establish spheroids from murine pancreatic cancer, we used a primary KPC cell line isolated from the tumor bulk of KPC mice from Dr. Tuveson's Lab, kindly gifted by Dr. Piemonti. We resuspended 10.000 KPC (K848) cells in cold Matrigel and grew cells in murine organoids growth medium to obtain KPC spheroids.

Murine organoids growth medium	
B 27 w/o Vitamin A	1x
Nicotinamide	10 mM
N-AcetylCysteine	1.25 mM
rH R-Spondin 1	10 ng/ml
FGF 10	100 ng/ml
rh Noggin	100 ng/ml
A83 -01	500 nM
rh EGF	50 ng/ml
h Gastrin 1	10 nM
Y-27632 **	10.5 uM

To establish healthy murine organoids, we collected pancreases from wild type mice in a 50 mL sterile Falcon tube containing cold basal medium. We then transferred the pancreas in a sterile 10 mm Petri dish and mechanically digested the organ. The minced material was transferred to a 15 ml tube containing 10 ml of murine warmed Digestion solution (Basal medium, 0.125 mg/ml Collagenase type XI (Gibco), 0.125 mg/ml Dispase II (Sigma-Aldrich)). We incubated at 37°C for 5 minutes on a shaker. After enzymatic digestion, we performed mechanical digestion by vigorously pipetting with a P200 Gilson pipette. When the tissue was sufficiently disgregated, we filtered the cell suspension with a 40 µM cell strainer (Falcon) and transferred the digestion solution to a fresh 50 mL conical tube containing 10 mL cold Basal medium supplemented with 1% FBS. We pelleted the cells at 200 x g for 5 minutes at 8 °C, then we discarded the supernatant and washed twice with 10 mL of Basal Medium, repeating the pelleting method above described.

We resuspended the pellet in an appropriate volume of cold Matrigel (Corning) and plated the organoids following the same procedure used to establish human organoids.

2.1 Organoid splitting and freezing

We splitted human and murine organoids when they reached confluence, usually after 7 days of culture in growing medium. We removed medium and dissolved the matrix containing organoids with 500 µl of cold Basal medium per well. We collected organoids in a 15 ml tube and added Basal medium until a final volume of 10 ml; we then pelleted organoids at 300 x g for 5 minutes at 8°C. We removed the supernatant up to a remaining final volume of 2 ml and dissociated organoids by pipetting with a 21 Gauge needle syringe. After dissociation, we washed with cold Basal medium to remove matrix debris by pelleting procedure.. Finally, we removed the supernatant and resuspended organoids pellet in fresh cold Matrigel. Organoids were then plated as described above.

For cryopreservation, we resuspended one organoids dome in 50 ul freezing medium composed of 90% FBS and 10% Dimethylsulfoxide (DMSO) and we transferred suspension to cryovials (500 µL each) and stored them at −80 °C.

2.2 Organoid – DRGs coculture

Each confluent dome of spheroids was dissolved and resuspended in 500 ul of cold Basal medium and centrifuged for 5 min at 1200 rpm at 8°C. The pellet was then resuspended in 150 ul of cold Matrigel. In parallel, we dissected E13.5 DRGs from wild type mice as described above. We dissected DRGs from the same level of the spinal cord that were grown either with KPC spheroids or with healthy controls, so that DRGs growth could be reliably compared. To plate cells, we used a 15 micro-wells chambered glass coverslip (Ibidi). In details, we added 8 ul of organoids suspension in each micro-well and let the Matrigel drop solidify at 37° for 5 minutes; then, using a dissection microscope (Leica M80) we added a single DRG explant in the center of the well, and we layered the cell suspension with additional 7 ul of organoids. After 10 min in the incubator at 37°C, 5% CO2, we added 50 ul of organoids medium to each well. Medium was replaced every other day.

2.3 Whole mount immunofluorescence

We treated with the same immunofluorescence protocol both organoids alone or organoids-DRGs cocultures.

Basically, we fixed the Mtrigel domes in 2% paraformaldehyde-0.2% glutaraldehyde in PBS 1 x at room temperature for 30 minutes. We performed a quenching step with room temperature NH2Cl 100 mM in PBS for 20 minutes, followed by 3 washing steps of 10 minutes each with 500 µL 100 mM glycine in Tris pH 7.4 (IF wash medium).

We permeabilized the cultures with 0.5% Triton X-100 in PBS at room temperature for 5 minutes, performed three washing steps with IF wash medium and blocked them with blocking solution (IF wash medium + 10% donkey serum) for 3 h at room temperature. We then incubated the cultures overnight with the chosen primary antibody diluted in blocking solution. We washed 3 times for 20 minutes in IF wash solution and then incubated with Alexa Fluor secondary antibody diluted in IF wash solution for 1 h at room temperature. For nuclei staining we incubated with Hoechst for 5 minutes.

3. In vivo organoids transplantation

To perform orthotopic transplantation, we collected confluent Matrigel domes of KPC organoids by dissolving the Matrigel in cold Basal medium. The cells suspension was then centrifuged at 1200 rpm at 8°C for 5 minutes, obtaining a pellet of organoids. We injected 1x106 cells in each mice, corresponding to 4 organoids domes. In parallel, we prepared a single cell suspension from 4 confluent Matrigel domes by resuspending in 500 ul of trypsin 0.2% for 5 minutes each dome; single cells suspension was used to count the number of cells present in a single 4-well plate and to determine the appropriate resuspension volume . We then resuspended the organoids pellet in an appropriate volume of a solution of 25% Matrigel – 75% PBS, in order to obtain a final concentration of 1x106 cells/50ul Matrigel.

Mice were anesthetized with 5mg/Kg Ketoprofen. We performed a 1 cm-incision in the left abdominal flank, medial to the splenic silhouette to externalize the pancreas and the spleen. We injected 1x106 cells into the tail region of the pancreas using an insulin

syringe, with a tangential angle of insertion. Successful injections was verified by the appearance of a fluid bubble without signs of intraperitoneal leakage. After internalization of pancreas and spleen, abdominal muscle layer and skin was sutured. To thoroughly follow tumor growth, we performed ultrasound analyses at 10, 20, 30 40 and 50 and 75 days post tumor implantation. Mice were then sacrificed, and the following organs were collected in formalin: pancreas, to analyze the histological characteristics of the primary tumor; spleen, duodenum, stomach, liver, kidneys, lungs, peritoneum and diaphragm to assess the presence of metastases. The histological analyses were carried out by the

Mouse Pathology facility and reviewed by expert Pathologists (Prof. Doglioni and Dr. Sanvito). In addition, we included the whole abdominal cavity in OCT (Killik, Bio-Optica) to assess the presence of PNI in the posterior nerve trunks and ganglia. Transverse sections (12 μm thick) were cut at the cryostate (Leica), collected on Superfrost plus glass slides (Thermo Fisher Scientific) and subsequently processed for immunofluorescence.

3.1 Immunohistochemistry

12 um thick cryosections were permeabilized in cold acetone or methanol for 5 minutes and then blocked in 2% bovine serum albumin and 0.1% Triton in phosphate buffered saline (PBS) for 1 hour at room temperature. Primary antibody incubation was performed overnight, with appropriate antibodies diluted in blocking solution. Incubation with the appropriate secondary antibodies diluted in blocking solution for 1 hour at room temperature We performed nuclei staining with Hoechst (0.7 ng/ml) for 10 minutes before coverslip mounting with Vectashield (Vector Laboratories).

4. Microscopy and image analysis

Representative images were acquired with an epifluorescence microscope (Leica DFC 7000 T) and a Leica SP5 confocal microscope.

For myelin internodes quantification, 10 images/coverslip were acquired and myelin quantification was performed by counting the number of MBP positive segments through the use of ImageJ Software. This analysis was performed at least on three coverslips per embryo and on three embryos per experiment.

For Transwell assays, the number of migrated/invaded cells per area was counted using ImageJ software. Statistical analyses were performed using the Prism Software package (GraphPad).

To analyze the alterations induced by KPC cells seeded on top of non-myelinated versus myelinated cocultures, images were acquired with a Delta Vision Ultra microscope (GE LifeScience) and processed with Cell Profiler software by Dr. Valeria Berno (Alembic, OSR). For each object, the area, the major axis length and sphericity (form factor) were analyzed. Images of pHis3 positive cells were taken with a 20× (NA 0.5) objective on a DeltaVision Ultra microscope (GE LifeScience,) with a complete Z-series deconvolved and projected (Max Projection).

Whole mount immunofluorescences were acquired on an Upright Confocal microscope RS-G4 (MAVIG GmbH Research, Munich Germany) with a 10x (NA 0.3) objective. Images were reconstructed with Volocity software. Organoids objects were removed based on shape and intensity to avoid interference with the weaker signal of the neurofilament, then neurite length was analyzed as the distance between the two outermost axonal protrusions (calibration 783,8 pixel/mm).

5 Data collection, follow up and statistical analysis

Our monocentric retrospective study included only patients with histologically proven PDAC of the pancreas who underwent surgical resection between January 2015 and December 2019. Data were collected from a prospectively maintained database at San

Raffaele Scientific Institute, Milan, Italy. Only patients > 18 years with a definitive pathological diagnosis of PDAC were included. Patients with synchronous distant metastases at the time of resection and macroscopically positive surgical margins (R2 resection) were excluded. Patients who experienced post-operative mortality, defined as any in-hospital death or death occurred within 90 days of surgery, were excluded as well. At least 12 months of follow up were required unless patients developed recurrence and died before this period. Data regarding demographics, clinico-pathological variables, intraoperative and postoperative course including complications, neoadjuvant and adjuvant treatment, survival were analyzed.

Patient follow-up included the evaluation CA 19.9 levels and of computed tomography of the chest and abdomen every 4 months for the first 2 years, and then every 6 months for other three years, and yearly thereafter. Recurrence was considered as the first site of recurrence, and it was exemplified into local or systemic recurrence. Local recurrence was defined as recurrence in the pancreatic remnant or in the soft tissue along the hepatic, celiac, superior mesenteric artery, portal or superior mesenteric vein, or in the retroperitoneum. Systemic recurrence was defined as recurrence in the liver, lungs, peritoneum or in other distant locations.

Descriptive statistics were calculated to describe patients' demographic and prognostic factors. Comparison between categorical variables was performed using the Chi-square t test or Fisher's exact test, if appropriate. DFS was defined as the time (in months) from surgery to the first evidence of disease recurrence. DSS was defined as the time (months) from surgery to disease-related death. DFS and DSS by PNI score were estimated using the Kaplan-Meier method for cumulative probability. Multivariable Cox proportional hazard models were used to study the impact of various factors on DFS. A p value < 0.05 was considered statistically significant. All statistical analyses were performed using IBM SPSS Statistical Software, version 25 (IBM Corporation, Armonk, NY, USA).

6 List of antibodies

Antibody	Dilution	Company	RRID:AB

chicken anti-Neurofilament M	1:1000 (IF)	Covance	2564860
mouse Purified anti-Myelin Basic Protein	1:1000 (IF)	Biolegend	clone SMI 94 : 2616694 clone SMI 99: 2564742
Rabbit anti- c-Jun	1:1000 - 1:10000 (WB)	Cell Signaling	2130165
rat anti-MBP hybridoma supernatant	1:2 (IF)	gift from Virginia Lee	-
Rabbit anti-Cytokeratin 19	1:100 (IF)	Invitrogen	2809271
Rabbit Anti-Keratin 17/19	1:100 (IF)	Cell Signaling	2797912
Mouse anti-Sox 9	1:100 (IF)	Abcam	2715497
Mouse anti-Vinculin clone V284	1:1000 - 1:10000 (WB)	Millipore	11212640

References

Abiatari I, DeOliveira T, Kerkadze V, Schwager C, Esposito I, Giese NA, Huber P, Bergman F, Abdollahi A, Friess H, *et al* (2009) Consensus transcriptome signature of perineural invasion in pancreatic carcinoma. *Mol Cancer Ther* 8: 1494–1504

Adda G, Hannoun L & Loygue J (1984) Development of the human pancreas: variations and pathology. A tentative classification. *Anat Clin* 5: 275–283 doi:10.1007/BF01798752 [PREPRINT]

Adsay NV, Andea A, Basturk O, Kilinc N, Nassar H & Cheng JD (2004) Secondary tumors of the pancreas: An analysis of a surgical and autopsy database and review of the literature. *Virchows Arch* 444: 527–535 doi:10.1007/s00428-004-0987-3 [PREPRINT]

Aguirre AJ, Bardeesy N, Sinha M, Lopez L, Tuveson DA, Horner J, Redston MS & DePinho RA (2003) Activated Kras and Ink4a/Arf deficiency cooperate to produce metastatic pancreatic ductal adenocarcinoma. *Genes Dev* 17: 3112–3126

Aigner A, Ray PE, Czubayko F & Wellstein A (2002) Immunolocalization of an FGF-binding protein reveals a widespread expression pattern during different stages of mouse embryo development. *Histochem Cell Biol* 117: 1–11

Akinrodoye MA & Lui F (2020) Neuroanatomy, Somatic Nervous System StatPearls Publishing

Allen PJ, Kuk D, Castillo CF Del, Basturk O, Wolfgang CL, Cameron JL, Lillemoe KD, Ferrone CR, Morales-Oyarvide V, He J, *et al* (2017) Multi-institutional validation study of the American joint commission on cancer (8th edition) changes for Tand N staging in patients with pancreatic adenocarcinoma. *Ann Surg* 265: 185–191

Amit M, Na'ara S & Gil Z (2016) Mechanisms of cancer dissemination along nerves. *Nat Rev Cancer* 16: 399–408

Amit M, Takahashi H, Dragomir MP, Lindemann A, Gleber-netto FO, Pickering CR, Anfossi S, Osman AA, Cai Y, Wang R, *et al* (2020a) Loss of p53 drives neuron reprogramming in head and neck cancer. *Nature*

Amit M, Takahashi H, Dragomir MP, Lindemann A, Gleber-Netto FO, Pickering CR, Anfossi S, Osman AA, Cai Y, Wang R, *et al* (2020b) Loss of p53 drives neuron reprogramming in head and neck cancer. *Nature* 578: 449–454

Arrojo e Drigo R, Jacob S, García-Prieto CF, Zheng X, Fukuda M, Nhu HTT, Stelmashenko O, Peçanha FLM, Rodriguez-Diaz R, Bushong E, *et al* (2019) Structural basis for delta cell paracrine regulation in pancreatic islets. *Nat Commun* 10

Arthur-Farraj PJ, Latouche M, Wilton DK, Quintes S, Chabrol E, Banerjee A, Woodhoo A, Jenkins B, Rahman M, Turmaine M, *et al* (2012) c-Jun Reprograms Schwann Cells of Injured Nerves to Generate a Repair Cell Essential for Regeneration. *Neuron* 75: 633–647

Asakawa A, Inui A, Yuzuriha H, Ueno N, Katsuura G, Fujimiya M, Fujino MA, Niijima A, Meguid MM & Kasuga M (2003) Characterization of the effects of pancreatic polypeptide in the regulation of energy balance. *Gastroenterology* 124: 1325–1336

Atkinson MA, Campbell-Thompson M, Kusmartseva I & Kaestner KH (2020) Organisation of the human pancreas in health and in diabetes. *Diabetologia* 63: 1966–1973 doi:10.1007/s00125-020-05203-7 [PREPRINT]

Ayala GE, Dai H, Powell M, Li R, Ding Y, Wheeler TM, Shine D, Kadmon D, Thompson T, Miles BJ, *et al* (2008) Cancer-related axonogenesis and neurogenesis in prostate cancer. *Clin Cancer Res* 14: 7593–7603

Ayala GE, Wheeler TM, Shine HD, Schmelz M, Frolov A, Chakraborty S & Rowley D (2001) In vitro dorsal root ganglia and human prostate cell line interaction: redefining perineural invasion in prostate cancer. *Prostate* 49: 213–23

Babic T & Travagli RA (2016) Neural Control of the Pancreas 2 . Sensory innervation of the pancreas 3 . Sympathetic nervous system control of the pancreas.

Baker LA, Tiriac H, Clevers H & Tuveson DA (2016) Modeling Pancreatic Cancer with Organoids. *Trends in Cancer* 2: 176–190

Bakhti M, Aggarwal S & Simons M (2014) Myelin architecture: zippering membranes tightly together. *Cell Mol Life Sci* 71 doi:10.1007/s00018-013-1492-0 [PREPRINT]

Bakst RL, Glastonbury CM, Parvathaneni U, Katabi N, Hu KS & Yom SS (2019) Perineural Invasion and Perineural Tumor Spread in Head and Neck Cancer. *Int J Radiat Oncol* 103: 1109–1124

Banh RS, Biancur DE, Yamamoto K, Sohn ASW, Walters B, Kuljanin M, Gikandi A, Wang H, Mancias JD, Schneider RJ, *et al* (2020) Neurons Release Serine to Support mRNA Translation in Pancreatic Cancer. *Cell* 183: 1202-1218.e25

Bapat AA, Hostetter G, Von Hoff DD & Han H (2011) Perineural invasion and associated pain in pancreatic cancer. *Nat Rev Cancer* 11: 695–707

Bapat AA, Munoz RM, Von Hoff DD & Han H (2016) Blocking Nerve Growth Factor Signaling Reduces the Neural Invasion Potential of Pancreatic Cancer Cells. *PLoS One* 11: e0165586

Barnes CA, Chavez MI, Tsai S, Aldakkak M, George B, Ritch PS, Dua K, Clarke CN, Tolat P, Hagen C, *et al* (2019) Survival of patients with borderline resectable pancreatic cancer who received neoadjuvant therapy and surgery. *Surg (United States)* 166: 277–285

Beer H-D, Bittner M, Niklaus G, Munding C, Max N, Goppelt A & Werner S (2005) The fibroblast growth factor binding protein is a novel interaction partner of FGF-7, FGF-10 and FGF-22 and regulates FGF activity: implications for epithelial repair. *Oncogene* 24: 5269–5277

Beer RL, Parsons MJ & Rovira M (2016) Centroacinar cells: At the center of pancreas regeneration. *Dev Biol* 413: 8–15 doi:10.1016/j.ydbio.2016.02.027 [PREPRINT]

Belfiori G, Crippa S, Francesca A, Pagnanelli M, Tamburrino D, Gasparini G, Partelli S, Andreasi V, Rubini C, Zamboni G, *et al* (2021) Long-Term Survivors after Upfront Resection for Pancreatic Ductal Adenocarcinoma: An Actual 5-Year Analysis of Disease-Specific and Post-Recurrence Survival. *Ann Surg Oncol*

Belfiori G, Fiorentini G, Tamburrino D, Partelli S, Pagnanelli M, Gasparini G, Castoldi R, Balzano G, Rubini C, Zamboni G, *et al* (2020) Vascular resection during pancreatectomy for pancreatic head cancer: A technical issue or a prognostic sign? *Surgery*

Blomstrand H, Scheibling U, Bratthäll C, Green H & Elander NO (2019) Real world evidence on gemcitabine and nab-paclitaxel combination chemotherapy in advanced pancreatic cancer. *BMC Cancer* 19

Bockman DE (2007) Nerves in the pancreas: what are they for? *Am J Surg* 194: S61–S64

Bockman DE, Büchler M & Beger HG (1994) Interaction of pancreatic ductal carcinoma with nerves leads to nerve damage. *Gastroenterology* 107: 219–230

Boilly B, Faulkner S, Jobling P & Hondermarck H (2017) Nerve Dependence: From Regeneration to Cancer. *Cancer Cell* 31: 342–354 doi:10.1016/j.ccell.2017.02.005 [PREPRINT]

Boj SF, Hwang C Il, Baker LA, Chio IIC, Engle DD, Corbo V, Jager M, Ponz-Sarvise M, Tiriac H, Spector MS, *et al* (2015) Organoid models of human and mouse ductal pancreatic cancer. *Cell* 160: 324–338

Bolívar S, Navarro X & Udina E (2020) Schwann Cell Role in Selectivity of Nerve Regeneration. *Cells* 9 doi:10.3390/cells9092131 [PREPRINT]

Bosman FT, Carneiro F, Hruban RH & Theise ND WHO Classification of Tumours of the Digestive System

Bouwens L (1998) Cytokeratins and cell differentiation in the pancreas. *J Pathol* 184: 234–239

Braadland PR, Ramberg H, Grytli HH & TaskÃ©n KA (2015) Î²-Adrenergic Receptor Signaling in Prostate Cancer. *Front Oncol* 4

Bray SJ (2006) Notch signalling: A simple pathway becomes complex. *Nat Rev Mol Cell Biol* 7: 678–689 doi:10.1038/nrm2009 [PREPRINT]

Britsch S, Goerich DE, Riethmacher D, Peirano RI, Rossner M, Nave K-A, Birchmeier C & Wegner M (2001) The transcription factor Sox10 is a key regulator of peripheral glial development. *Genes Dev* 15: 66

Brosius Lutz A & Barres BA (2014) Contrasting the Glial Response to Axon Injury in the Central and Peripheral Nervous Systems. *Dev Cell* 28: 7–17

Butler SJ & Bronner ME (2015) From classical to current: Analyzing peripheral nervous system and spinal cord lineage and fate. *Dev Biol* 398: 135–146 doi:10.1016/j.ydbio.2014.09.033 [PREPRINT]

Cattin AL, Burden JJ, Van Emmenis L, MacKenzie FE, Hoving JJA, Garcia Calavia N, Guo Y, McLaughlin M, Rosenberg LH, Quereda V, *et al* (2015) Macrophage-Induced Blood Vessels Guide Schwann Cell-Mediated Regeneration of Peripheral Nerves. *Cell* 162: 1127–1139

Celesti G, Di Caro G, Bianchi P, Grizzi F, Marchesi F, Basso G, Rahal D, Delconte G, Catalano M, Cappello P, *et al* (2013) Early expression of the fractalkine receptor CX3CR1 in pancreatic carcinogenesis. *Br J Cancer* 109: 2424–2433

Cesmebasi A, Malefant J, Patel SD, Plessis M Du, Renna S, Tubbs RS & Loukas M (2015) The surgical anatomy of the lymphatic system of the pancreas. *Clin Anat* 28: 527–537 doi:10.1002/ca.22461 [PREPRINT]

Ceyhan GO, Bergmann F, Kadihasanoglu M, Altintas B, Demir IE, Hinz U, Müller MW, Giese T, Büchler MW, Giese NA, *et al* (2009a) Pancreatic Neuropathy and Neuropathic Pain-A Comprehensive Pathomorphological Study of 546 Cases. *YGAST* 136: 177-186.e1

Ceyhan GO, Bergmann F, Kadihasanoglu M, Altintas B, Demir IE, Hinz U, Müller MW, Giese T, Büchler MW, Giese NA, *et al* (2009b) Pancreatic Neuropathy and Neuropathic Pain—A Comprehensive Pathomorphological Study of 546 Cases. *Gastroenterology* 136: 177-186.e1

Ceyhan GO, Bergmann F, Kadihasanoglu M, Erkan M, Park W, Hinz U, Giese T, Muller MW, Buchler MW, Giese NA, *et al* (2007) The neurotrophic factor artemin influences the extent of neural damage and growth in chronic pancreatitis. *Gut* 56: 534–544

Ceyhan GO, Demir IE, Rauch U, Bergmann F, Müller MW, Büchler MW, Friess H & Schäfer KH (2009c) Pancreatic neuropathy results in neural remodeling and altered pancreatic innervation in chronic pancreatitis and pancreatic cancer. *Am J Gastroenterol* 104: 2555–2565

Chan MT, Lim GE, Skovsø S, Yang YHC, Albrecht T, Alejandro EU, Hoesli CA, Piret JM, Warnock GL & Johnson JD (2014) Effects of insulin on human pancreatic cancer progression modeled in vitro. *BMC Cancer* 14

Chédotal A, Kerjan G & Moreau-Fauvarque C (2005) The brain within the tumor: New roles for axon guidance molecules in cancers. *Cell Death Differ* 12: 1044–1056 doi:10.1038/sj.cdd.4401707 [PREPRINT]

Chen H, Qin S, Wang M, Zhang T & Zhang S (2015) Association between cholesterol intake and pancreatic cancer risk: Evidence from a meta-analysis. *Sci Rep* 5: 8243

Chen ZL & Strickland S (2003) Laminin γ1 is critical for Schwann cell differentiation, axon myelination, and regeneration in the peripheral nerve. *J Cell Biol* 163: 889–899

Cheng B, Zhang Y, Chen Q, Sun B, Deng Z, Shan H, Dou L, Wang J, Li Y, Yang X, *et al* (2018) Analysis of Fine-Needle Biopsy vs Fine-Needle Aspiration in Diagnosis of Pancreatic and Abdominal Masses: A Prospective, Multicenter, Randomized Controlled Trial. *Clin Gastroenterol Hepatol* 16: 1314–1321

Cheng P, Jin G, Hu X, Shi M, Zhang Y, Liu R, Zhou Y, Shao C, Zheng J & Zhu M (2012) Analysis of tumor-induced lymphangiogenesis and lymphatic vessel invasion of pancreatic carcinoma in the peripheral nerve plexus. *Cancer Sci* 103: 1756–1763

Chiu YC, Hua TE, Fu YY, Pasricha PJ & Tang SC (2012) 3-D imaging and illustration of the perfusive mouse islet sympathetic innervation and its remodelling in injury. *Diabetologia* 55: 3252–3261

Chuvin N, Vincent DF, Pommier RM, Alcaraz LB, Gout J, Caligaris C, Yacoub K, Cardot V, Roger E, Kaniewski B, *et al* (2017) Acinar-to-Ductal Metaplasia Induced by Transforming Growth Factor Beta Facilitates KRASG12D-driven Pancreatic Tumorigenesis. *CMGH* 4: 263–282

Cienfuegos JA, Martínez P, Baixauli J, Beorlegui C, Rosenstone S, Sola JJ, Rodríguez J & Hernández-Lizoáin JL (2017) Perineural Invasion is a Major Prognostic and Predictive Factor of Response to Adjuvant Chemotherapy in Stage I–II Colon Cancer. *Ann Surg Oncol* 24: 1077–1084

Citri A, Skaria KB & Yarden Y (2003) The deaf and the dumb: The biology of ErbB-2 and ErbB-3. *Exp Cell Res* 284: 54–65 doi:10.1016/S0014-4827(02)00101-5 [PREPRINT]

Cleveland MH, Sawyer JM, Afelik S, Jensen J & Leach SD (2012) Exocrine ontogenies: On the development of pancreatic acinar, ductal and centroacinar cells. *Semin Cell Dev Biol* 23: 711–719

Conceição F, Sousa DM, Paredes J & Lamghari M (2021) Sympathetic activity in breast cancer and metastasis: partners in crime. *Bone Res* 9: 1–11 doi:10.1038/s41413-021-00137-1 [PREPRINT]

Conroy T, Desseigne F, Ychou M, Bouché O, Guimbaud R, Bécouarn Y, Adenis A, Raoul J-L, Gourgou-Bourgade S, de la Fouchardière C, *et al* (2011) FOLFIRINOX versus Gemcitabine for Metastatic Pancreatic Cancer. *N Engl J Med* 364: 1817–1825

Conroy T & Ducreux M (2019) Adjuvant treatment of pancreatic cancer. *Curr Opin Oncol* 31: 346–353 doi:10.1097/CCO.0000000000000546 [PREPRINT]

Crippa S, Partelli S, Belfiori G, Palucci M, Muffatti F, Adamenko O, Cardinali L, Doglioni C, Zamboni G & Falconi M (2016) Management of neuroendocrine carcinomas of the pancreas (WHO G3): A tailored approach between proliferation and morphology. *World J Gastroenterol* 22: 9944–9953 doi:10.3748/wjg.v22.i45.9944 [PREPRINT]

Crippa S, Pergolini I, Javed AA, Honselmann KC, Weiss MJ, Di Salvo F, Burkhart R, Zamboni G, Belfiori G, Ferrone CR, *et al* (2020) Implications of Perineural Invasion on Disease Recurrence and Survival After Pancreatectomy for Pancreatic Head Ductal Adenocarcinoma. *Ann Surg* Publish Ah

Czubayko F, Liaudet-Coopman EDE, Aigner A, Tuveson AT, Berchem GJ & Wellstein A (1997) A secreted FGF-binding protein can serve as the angiogenic switch in human cancer. *Nat Med* 3: 1137–1140

D'Agosto S, Lupo F & Corbo V (2020a) Generation of Pancreatic Organoid-Derived Isografts. *STAR Protoc* 1: 100047

D'Agosto S, Lupo F & Corbo V (2020b) Generation of Pancreatic Organoid-Derived Isografts. *STAR Protoc* 1: 100047

D'Haese JG, Hartel M, Demir IE, Hinz U, Bergmann F, Büchler MW, Friess H & Ceyhan GO (2014) Pain sensation in pancreatic diseases is not uniform: The different facets of pancreatic pain. *World J Gastroenterol* 20: 9154–9161

Dang C, Zhang Y, Ma Q & Shimahara Y (2006) Expression of nerve growth factor receptors is correlated with progression and prognosis of human pancreatic cancer. *J Gastroenterol Hepatol* 21: 850–858

De S, Trigueros MA, Kalyvas A & David S (2003) Phospholipase A2 plays an important role in myelin breakdown and phagocytosis during wallerian degeneration. *Mol Cell Neurosci* 24: 753–765

Deborde S, Omelchenko T, Lyubchik A, Zhou Y, He S, McNamara WF, Chernichenko N, Lee SY, Barajas F, Chen CH, *et al* (2016) Schwann cells induce cancer cell dispersion and invasion. *J Clin Invest* 126: 1538–1554

Deborde S, Yu Y, Marcadis A, Chen C-H, Fan N, Bakst RL & Wong RJ (2018) An In Vivo Murine Sciatic Nerve Model of Perineural Invasion. *J Vis Exp*

Delaspre F, Beer RL, Rovira M, Huang W, Wang G, Gee S, Del Carmen Vitery M, Wheelan SJ & Parsons MJ (2015) Centroacinar cells are progenitors that contribute to endocrine pancreas regeneration. *Diabetes* 64: 3499–3509

Demir IE, Friess H & Ceyhan GO (2015a) Neural plasticity in pancreatitis and pancreatic cancer. *Nat Rev Gastroenterol Hepatol* 12: 649–659 doi:10.1038/nrgastro.2015.166 [PREPRINT]

Demir IE, Friess H & Ceyhan GO (2015b) Neural plasticity in pancreatitis and pancreatic cancer. *Nat Rev Gastroenterol Hepatol* 12: 649–659

Dibble EH, Karantanis D, Mercier G, Peller PJ, Kachnic LA & Subramaniam RM (2012) PET/CT of Cancer Patients: Part 1, Pancreatic Neoplasms. *Am J Roentgenol* 199: 952–967

Ding Y, He D, Florentin D, Frolov A, Hilsenbeck S, Ittmann M, Kadmon D, Miles B, Rowley D & Ayala G (2013) Semaphorin 4F as a critical regulator of neuroepithelial interactions and a biomarker of aggressive prostate cancer. *Clin Cancer Res* 19: 6101–6111

Distler M, Aust D, Weitz J, Pilarsky C & Grützmann R (2014) Precursor lesions for sporadic pancreatic cancer: PanIN, IPMN, and MCN. *Biomed Res Int* 2014: 474905

Dolenšek J, Rupnik MS & Stožer A (2015) Structural similarities and differences between the human and the mouse pancreas. *Islets* 7 doi:10.1080/19382014.2015.1024405 [PREPRINT]

Domènech-Estévez E, Baloui H, Meng X, Zhang Y, Deinhardt K, Dupree JL, Einheber S, Chrast R & Salzer JL (2016) Akt regulates axon wrapping and myelin sheath thickness in the PNS. *J Neurosci* 36: 4506–4521

Dominiak A, Chełstowska B, Olejarz W & Nowicka G (2020) Communication in the Cancer Microenvironment as a Target for Therapeutic Interventions. *Cancers (Basel)* 12: 1232

Dowsing BJ, Morrison WA, Nicola NA, Starkey GP, Bucci T & Kilpatrick TJ (1999) Leukemia inhibitory factor is an autocrine survival factor for Schwann cells. *J Neurochem* 73: 96–104

Drapiewski JF (1944) Carcinoma of the Pancreas: A Study of Neoplastic Invasion of Nerves and its Possible Clinical Significance. *Am J Clin Pathol* 14: 549–556

Dreesmann L, Mittnacht U, Lietz M & Schlosshauer B (2009) Nerve fibroblast impact on Schwann cell behavior. *Eur J Cell Biol* 88: 285–300

Du L & Wang-Gillam A (2017) Trends in neoadjuvant approaches in pancreatic cancer. *JNCCN J Natl Compr Cancer Netw* 15: 1070–1077 doi:10.6004/jnccn.2017.0134 [PREPRINT]

Dun X-P, Carr L, Woodley PK, Barry RW, Drake LK, Mindos T, Roberts SL, Lloyd AC & Parkinson DB (2019) Macrophage-Derived Slit3 Controls Cell Migration and Axon Pathfinding in the Peripheral Nerve Bridge. *Cell Rep* 26: 1458-1472.e4

Eldridge CF, Bunge MB, Bunge RP & Wood PM (1987) Differentiation of axon-related Schwann cells in vitro. I. Ascorbic acid regulates basal lamina assembly and myelin formation. *J Cell Biol* 105: 1023–1034

Ernsberger U & Rohrer H (2018) Sympathetic tales: subdivisons of the autonomic nervous system and the impact of developmental studies. *Neural Dev* 13: 20

Expression of FGFBP1 in pancreatic cancer - The Human Protein Atlas (2016) (https://www.proteinatlas.org/ENSG00000137440-FGFBP1/pathology/pancreatic+cancer) [PREPRINT]

Fearon K, Strasser F, Anker SD, Bosaeus I, Bruera E, Fainsinger RL, Jatoi A, Loprinzi C, MacDonald N, Mantovani G, *et al* (2011) Definition and classification of cancer cachexia: An international consensus. *Lancet Oncol* 12: 489–495 doi:10.1016/S1470-2045(10)70218-7 [PREPRINT]

Ferrone CR, Finkelstein DM, Thayer SP, Muzikansky A, Fernandez-Del Castillo C & Warshaw AL (2006) Perioperative CA19-9 levels can predict stage and survival in patients with

resectable pancreatic adenocarcinoma. *J Clin Oncol* 24: 2897–2902

Ferrone CR, Marchegiani G, Hong TS, Ryan DP, Deshpande V, McDonnell EI, Sabbatino F, Santos DD, Allen JN, Blaszkowsky LS, *et al* (2015a) Radiological and surgical implications of neoadjuvant treatment with FOLFIRINOX for locally advanced and borderline resectable pancreatic cancer. In *Annals of Surgery* pp 12–17. Lippincott Williams and Wilkins

Ferrone CR, Marchegiani G, Hong TS, Ryan DP, Deshpande V, McDonnell EI, Sabbatino F, Santos DD, Allen JN, Blaszkowsky LS, *et al* (2015b) Radiological and surgical implications of neoadjuvant treatment with FOLFIRINOX for locally advanced and borderline resectable pancreatic cancer. *Ann Surg* 261: 12–7

Filbin MT (2003) Myelin-associated inhibitors of axonal regeneration in the adult mammalian CNS. *Nat Rev Neurosci* 4: 703–713

Filippini D, Agosto SD, Delfino P, Simbolo M, Piro G, Rusev B, Veghini L, Cantù C, Lupo F, Ugel S, *et al* (2019) Immunoevolution of mouse pancreatic organoid isografts from preinvasive to metastatic disease. *Sci Rep* 9

Finzsch M, Schreiner S, Kichko T, Reeh P, Tamm ER, Bösl MR, Meijer D & Wegner M (2010) Sox10 is required for Schwann cell identity and progression beyond the immature Schwann cell stage. *J Cell Biol* 189: 701–712

Fogel EL, Shahda S, Sandrasegaran K, Dewitt J, Easler JJ, Agarwal DM, Eagleson M, Zyromski NJ, House MG, Ellsworth S, *et al* (2017) A Multidisciplinary Approach to Pancreas Cancer in 2016: A Review. *Am J Gastroenterol* 112: 537–554 doi:10.1038/ajg.2016.610 [PREPRINT]

Fontaine AK, Ramirez DG, Littich SF, Piscopio RA, Kravets V, Schleicher WE, Mizoguchi N, Caldwell JH, Weir RF f. & Benninger RKP (2021) Optogenetic stimulation of cholinergic fibers for the modulation of insulin and glycemia. *Sci Rep* 11: 3670

Forese MG, Pellegatta M, Canevazzi P, Gullotta GS, Podini P, Rivellini C, Previtali SC, Bacigaluppi M, Quattrini A & Taveggia C (2020) Prostaglandin D2 synthase modulates macrophage activity and accumulation in injured peripheral nerves. *Glia* 68: 95–110

De Franco L, Marrelli D, Voglino C, Vindigni C, Ferrara F, Di Mare G, Iudici L, Marini M & Roviello F (2018) Prognostic Value of Perineural Invasion in Resected Gastric Cancer Patients According to Lauren Histotype. *Pathol Oncol Res* 24: 393–400

Frappart P-O & Hofmann TG (2020) Pancreatic Ductal Adenocarcinoma (PDAC) Organoids: The Shining Light at the End of the Tunnel for Drug Response Prediction and Personalized Medicine. *Cancers (Basel)* 12: 2750

Fricker FR, Antunes-Martins A, Galino J, Paramsothy R, La Russa F, Perkins J, Goldberg R, Brelstaff J, Zhu N, McMahon SB, *et al* (2013) Axonal neuregulin 1 is a rate limiting but not essential factor for nerve remyelination. *Brain* 136: 2279–2297

Furse S & De Kroon AIPM (2015) Phosphatidylcholines functions beyond that of a membrane brick. *Mol Membr Biol* 32 doi:10.3109/09687688.2015.1066894 [PREPRINT]

Furusho M, Dupree JL, Bryant M & Bansal R (2009) Disruption of Fibroblast Growth Factor Receptor Signaling in Nonmyelinating Schwann Cells Causes Sensory Axonal Neuropathy and Impairment of Thermal Pain Sensitivity. *J Neurosci* 29: 1608–1614

Gao L, Bo H, Wang Y, Zhang J & Zhu M (2015) Neurotrophic Factor Artemin Promotes Invasiveness and Neurotrophic Function of Pancreatic Adenocarcinoma In Vivo and In Vitro. *Pancreas* 44: 134–143

García-González D, Khodosevich K, Watanabe Y, Rollenhagen A, Lübke JHR & Monyer H (2017) Serotonergic Projections Govern Postnatal Neuroblast Migration. *Neuron* 94: 534-549.e9

Garratt AN, Britsch S & Birchmeier C (2000a) Neuregulin, a factor with many functions in the life of a Schwann cell. *BioEssays* 22: 987–996

Garratt AN, Voiculescu O, Topilko P, Charnay P & Birchmeier C (2000b) A dual role of erbB2 in myelination and in expansion of the Schwann cell precursor pool. *J Cell Biol* 148: 1035–1046

Gil Z, Cavel O, Kelly K, Brader P, Rein A, Gao SP, Carlson DL, Shah JP, Fong Y & Wong RJ (2010) Paracrine regulation of pancreatic cancer cell invasion by peripheral nerves. *J Natl Cancer Inst* 102: 107–118

Girouard MP, Bueno M, Julian V, Drake S, Byrne AB & Fournier AE (2018) The Molecular Interplay between Axon Degeneration and Regeneration. *Dev Neurobiol* 78: 978–990 doi:10.1002/dneu.22627 [PREPRINT]

Gohrig A, Detjen KM, Hilfenhaus G, Korner JL, Welzel M, Arsenic R, Schmuck R, Bahra M, Wu JY, Wiedenmann B, *et al* (2014) Axon Guidance Factor SLIT2 Inhibits Neural Invasion and Metastasis in Pancreatic Cancer. *Cancer Res* 74: 1529–1540

Gomez-Sanchez JA, Carty L, Iruarrizaga-Lejarreta M, Palomo-Irigoyen M, Varela-Rey M, Griffith M, Hantke J, Macias-Camara N, Azkargorta M, Aurrekoetxea I, *et al* (2015) Schwann cell autophagy, myelinophagy, initiates myelin clearance from injured nerves. *J Cell Biol* 210: 153–168

Gomez-Sanchez JA, Pilch KS, Van Der Lans M, Fazal S V., Benito C, Wagstaff LJ, Mirsky R & Jessen KR (2017) After nerve injury, lineage tracing shows that myelin and Remak Schwann cells elongate extensively and branch to form repair Schwann cells, which shorten radically on remyelination. *J Neurosci* 37: 9086–9099

Goonetilleke KS & Siriwardena AK (2007) Systematic review of carbohydrate antigen (CA 19-9) as a biochemical marker in the diagnosis of pancreatic cancer. *Eur J Surg Oncol* 33: 266–270 doi:10.1016/j.ejso.2006.10.004 [PREPRINT]

Grapin-Botton A (2005) Ductal cells of the pancreas. *Int J Biochem Cell Biol* 37: 504–510 doi:10.1016/j.biocel.2004.07.010 [PREPRINT]

Griffin JW, George R, Lobato C, Tyor WR, Li CY & Glass JD (1992) Macrophage responses and myelin clearance during Wallerian degeneration: relevance to immune-mediated demyelination. *J Neuroimmunol* 40: 153–165

Groot VP, Rezaee N, Wu W, Cameron JL, Fishman EK, Hruban RH, Weiss MJ, Zheng L, Wolfgang CL & He J (2018) Patterns, Timing, and Predictors of Recurrence Following Pancreatectomy for Pancreatic Ductal Adenocarcinoma. *Ann Surg* 267: 936–945

Grossberg AJ, Chu LC, Deig CR, Fishman EK, Hwang WL, Maitra A, Marks DL, Mehta A, Nabavizadeh N, Simeone DM, *et al* (2020) Multidisciplinary standards of care and recent progress in pancreatic ductal adenocarcinoma. *CA Cancer J Clin* 70: 375–403

Gu G, Brown JR & Melton DA (2003) Direct lineage tracing reveals the ontogeny of pancreatic cell fates during mouse embryogenesis. *Mech Dev* 120: 35–43 doi:10.1016/S0925-4773(02)00330-1 [PREPRINT]

Guertin AD, Zhang DP, Mak KS, Alberta JA & Kim HA (2005) Microanatomy of axon/glial signaling during Wallerian degeneration. *J Neurosci* 25: 3478–3487

Guillaumond F, Bidaut G, Ouaissi M, Servais S, Gouirand V, Olivares O, Lac S, Borge L, Roques J, Gayet O, *et al* (2015) Cholesterol uptake disruption, in association with chemotherapy, is a promising combined metabolic therapy for pancreatic adenocarcinoma. *Proc Natl Acad Sci* 112: 2473–2478

Häcker U, Nybakken K & Perrimon N (2005) Heparan sulphate proteoglycans: the sweet side of development. *Nat Rev Mol Cell Biol 2005 67* 6: 530–541

Haeberle L & Esposito I (2019) Pathology of pancreatic cancer. *Transl Gastroenterol Hepatol* 4: 50–50

Harrisingh MC, Perez-Nadales E, Parkinson DB, Malcolm DS, Mudge AW & Lloyd AC (2004) The Ras/Raf/ERK signalling pathway drives Schwann cell dedifferentiation. *EMBO J* 23: 3061–3071

He S, Chen C-H, Chernichenko N, He S, Bakst RL, Barajas F, Deborde S, Allen PJ, Vakiani E, Yu Z, *et al* (2014) GFRα1 released by nerves enhances cancer cell perineural invasion through GDNF-RET signaling. *Proc Natl Acad Sci U S A* 111: E2008-17

Heller BA, Ghidinelli M, Voelkl J, Einheber S, Smith R, Grund E, Morahan G, Chandler D, Kalaydjieva L, Giancotti F, *et al* (2014) Functionally distinct PI 3-kinase pathways regulate myelination in the peripheral nervous system. *J Cell Biol* 204: 1219–1236

Hendifar AE, Chang JI, Huang BZ, Tuli R & Wu BU (2018) Cachexia, and not obesity, prior to pancreatic cancer diagnosis worsens survival and is negated by chemotherapy. *J Gastrointest Oncol* 9: 17–23

Hendifar AE, Petzel MQB, Zimmers TA, Denlinger CS, Matrisian LM, Picozzi VJ, Rahib L, Hendifar A, Tuli R, Wolpin B, *et al* (2019) Pancreas Cancer-Associated Weight Loss. *Oncologist* 24: 691–701

Hewitt MJ, McPhail MJW, Possamai L, Dhar A, Vlavianos P & Monahan KJ (2012) EUS-guided FNA for diagnosis of solid pancreatic neoplasms: A meta-analysis. *Gastrointest Endosc* 75: 319–331

Hibsher D, Epshtein A, Oren N & Landsman L (2016) Pancreatic Mesenchyme Regulates Islet Cellular Composition in a Patched/Hedgehog-Dependent Manner. *Sci Rep* 6

Hidalgo M (2011) Pancreatic Cancer : Pancreatic Cancer : Overview. *Lancet* 378: 1605–1617

Higashiyama H, Sumitomo H, Ozawa A, Igarashi H, Tsunekawa N, Kurohmaru M & Kanai Y (2016) Anatomy of the Murine Hepatobiliary System: A Whole-Organ-Level Analysis Using a Transparency Method. *Anat Rec* 299: 161–172

Hingorani SR, Wang L, Multani AS, Combs C, Deramaudt TB, Hruban RH, Rustgi AK, Chang S & Tuveson DA (2005) Trp53R172H and KrasG12D cooperate to promote chromosomal instability and widely metastatic pancreatic ductal adenocarcinoma in mice. *Cancer Cell* 7: 469–483

Horiguchi SI & Kamisawa T (2010) Major duodenal papilla and its normal anatomy. *Dig Surg* 27: 90–93

Horih SI (1989) Basic Neurochemistry: Molecular, Cellular, and Medical Aspects, 4th Ed. *Neurology* 39: 460–460

Hruban RH, Maitra A & Goggins M (2008) Update on Pancreatic Intraepithelial Neoplasia

Huang W, Chen Z, Shang X, Tian D, Wang D, Wu K, Fan D & Xia L (2015) Sox12, a direct target of FoxQ1, promotes hepatocellular carcinoma metastasis through up-regulating Twist1 and FGFBP1. *Hepatology* 61: 1920–1933

Husain S & Thrower E (2009) Molecular and cellular regulation of pancreatic acinar cell function. *Curr Opin Gastroenterol* 25: 466–471 doi:10.1097/MOG.0b013e32832ebfac [PREPRINT]

Huyett P, Gilbert M, Liu L, Ferris RL & Kim S (2017) A model for perineural invasion in head and neck squamous cell carcinoma. *J Vis Exp* 2017

Ibukuro K (2001) Vascular anatomy of the pancreas and clinical applications. *Int J Gastrointest Cancer* 30 doi:10.1385/ijgc:30:1-2:087 [PREPRINT]

Ijichi H, Chytil A, Gorska AE, Aakre ME, Fujitani Y, Fujitani S, Wright CVE & Moses HL (2006) Aggressive pancreatic ductal adenocarcinoma in mice caused by pancreas-specific blockade of transforming growth factor-β signaling in cooperation with active Kras expression. *Genes Dev* 20: 3147–3160

Isaji S, Mizuno S, Windsor JA, Bassi C, Fernández-del Castillo C, Hackert T, Hayasaki A, Katz MHG, Kim SW, Kishiwada M, *et al* (2018) International consensus on definition and criteria of borderline resectable pancreatic ductal adenocarcinoma 2017. *Pancreatology* 18: 2–11

Ishii A, Furusho M & Bansal R (2013) Sustained activation of ERK1/2 MAPK in oligodendrocytes and schwann cells enhances myelin growth and stimulates oligodendrocyte progenitor expansion. *J Neurosci* 33: 175–186

Ito Y, Okada Y, Sato M, Sawai H, Funahashi H, Murase T, Hayakawa T & Manabe T (2005) Expression of glial cell line–derived neurotrophic factor family members and their receptors in pancreatic cancers. *Surgery* 138: 788–794

Jessen KR (2004) Glial cells. *Int J Biochem Cell Biol* 36: 1861–1867 doi:10.1016/j.biocel.2004.02.023 [PREPRINT]

Jessen KR & Mirsky R (2005) The origin and development of glial cells in peripheral nerves. *Nat Rev Neurosci* 6: 671–682 doi:10.1038/nrn1746 [PREPRINT]

Jessen KR & Mirsky R (2008) Negative regulation of myelination: Relevance for development, injury, and demyelinating disease. *Glia* 56: 1552–1565

Jessen KR & Mirsky R (2016) The repair Schwann cell and its function in regenerating nerves. *J Physiol* 594: 3521–3531

Jessen KR, Mirsky R & Lloyd AC (2015) Schwann cells: Development and role in nerve repair. *Cold Spring Harb Perspect Biol* 7: 1–15

Jørgensen MC, Ahnfelt-Rønne J, Hald J, Madsen OD, Serup P & Hecksher-Sørensen J (2007) An

Illustrated Review of Early Pancreas Development in the Mouse. *Endocr Rev* 28: 685–705

Jurcak NR, Rucki AA, Muth S, Thompson E, Sharma R, Ding D, Zhu Q, Eshleman JR, Anders RA, Jaffee EM, *et al* (2019) Axon Guidance Molecules Promote Perineural Invasion and Metastasis of Orthotopic Pancreatic Tumors in Mice. *Gastroenterology* 157: 838-850.e6

Kamisawa T, Wood LD, Itoi T & Takaori K (2016) Pancreatic cancer. *Lancet* 388: 73–85 doi:10.1016/S0140-6736(16)00141-0 [PREPRINT]

Kang X, Lin Z, Xu M, Pan J & Wang Z (2019) Deciphering role of FGFR signalling pathway in pancreatic cancer. *Cell Prolif* 52: e12605

Kim J, Koo BK & Knoblich JA (2020) Human organoids: model systems for human biology and medicine. *Nat Rev Mol Cell Biol* 21: 571–584 doi:10.1038/s41580-020-0259-3 [PREPRINT]

Klimstra DS, Modlin IR, Coppola D, Lloyd R V. & Suster S (2010) The pathologic classification of neuroendocrine tumors: A review of nomenclature, grading, and staging systems. *Pancreas* 39: 707–712 doi:10.1097/MPA.0b013e3181ec124e [PREPRINT]

Knijn N, Mogk SC, Teerenstra S, Simmer F & Nagtegaal ID (2016) Perineural invasion is a strong prognostic factor in colorectal cancer. *Am J Surg Pathol* 40: 103–112 doi:10.1097/PAS.0000000000000518 [PREPRINT]

Koorstra JBM, Feldmann G, Habbe N & Maitra A (2008) Morphogenesis of pancreatic cancer: Role of pancreatic intraepithelial neoplasia (PanINs). *Langenbeck's Arch Surg* 393: 561–570

Kopp JL, von Figura G, Mayes E, Liu FF, Dubois CL, Morris JP, Pan FC, Akiyama H, Wright CVE, Jensen K, *et al* (2012) Identification of Sox9-Dependent Acinar-to-Ductal Reprogramming as the Principal Mechanism for Initiation of Pancreatic Ductal Adenocarcinoma. *Cancer Cell* 22: 737–750

Kumar KH, Garg S, Yadav TD, Sahni D, Singh H & Singh R (2021) Anatomy of peripancreatic arteries and pancreaticoduodenal arterial arcades in the human pancreas: a cadaveric study. *Surg Radiol Anat* 43

Kurata Y, Shiraki T, Ichinose M, Kubota K & Imai Y (2021) Effect and limitation of neoadjuvant chemotherapy for pancreatic ductal adenocarcinoma: consideration from a new perspective. *World J Surg Oncol* 19: 1–11

Landsman L, Nijagal A, Whitchurch TJ, VanderLaan RL, Zimmer WE, MacKenzie TC & Hebrok M (2011) Pancreatic mesenchyme regulates epithelial organogenesis throughout development. *PLoS Biol* 9

Lau HCH, Kranenburg O, Xiao H & Yu J (2020) Organoid models of gastrointestinal cancers in basic and translational research. *Nat Rev Gastroenterol Hepatol* 17: 203–222 doi:10.1038/s41575-019-0255-2 [PREPRINT]

Lazzarini R & Nave K (2004) Myelin biology and disorders.

Lazzarini RA, Griffin JW, Lassman H, Nave KA, Miller R & Trapp BD (2004) Myelin Biology and Disorders

LeBouef T & Whited L (2019) Physiology, Autonomic Nervous System StatPearls Publishing

Lee ES & Lee JM (2014) Imaging diagnosis of pancreatic cancer: A state-of-the-art review.

World J Gastroenterol 20: 7864–7877

Lee JW, Komar CA, Bengsch F, Graham K & Beatty GL (2016) Genetically engineered mouse models of pancreatic cancer: The KPC model (LSL-KrasG12D/+;LSL-Trp53R172H/+;Pdx-1-Cre), its variants, and their application in immuno-oncology drug discovery. *Curr Protoc Pharmacol* 2016: 14.39.1-14.39.20

Lee MJ, Brennan A, Blanchard A, Zoidl G, Dong Z, Tabernero A, Zoidl C, Dent MAR, Jessen KR & Mirsky R (1997) P0 is constitutively expressed in the rat neural crest and embryonic nerves and is negatively and positively regulated by axons to generate non- myelin-forming and myelin-forming Schwann cells, respectively. *Mol Cell Neurosci* 8: 336–350

Lee T, Teng TZJ & Shelat VG (2020) Carbohydrate antigen 19-9 — tumor marker: Past, present, and future. *World J Gastrointest Surg* 12: 468–490

Lemery S, Keegan P & Pazdur R (2017) First FDA Approval Agnostic of Cancer Site — When a Biomarker Defines the Indication. *N Engl J Med* 377: 1409–1412

Lemke G & Axel R (1985) Isolation and sequence of a cDNA encoding the major structural protein of peripheral myelin. *Cell* 40: 501–508

De Leon-Casasola OA (2000) Critical evaluation of chemical neurolysis of the sympathetic axis for cancer pain. *Cancer Control* 7: 142–148

Lewis MPN, Reber HA & Ashley SW (1998) Pancreatic blood flow and its role in the pathophysiology of pancreatitis. *J Surg Res* 75: 81–89 doi:10.1006/jsre.1998.5268 [PREPRINT]

Li D (2012) Diabetes and pancreatic cancer. *Mol Carcinog* 51: 64–74

Li W, Yu G, Liu Y & Sha L (2019) Intrapancreatic Ganglia and Neural Regulation of Pancreatic Endocrine Secretion. *Front Neurosci* 13: 21

Liebig C, Ayala G, Wilks JA, Berger DH & Albo D (2009) Perineural invasion in cancer: A review of the literature. *Cancer* 115: 3379–3391

Liebl F, Demir IE, Mayer K, Schuster T, D'Haese JG, Becker K, Langer R, Bergmann F, Wang K, Rosenberg R, *et al* (2014) The impact of neural invasion severity in gastrointestinal malignancies: A Clinicopathological Study. In *Annals of Surgery* pp 900–908.

Lindsay TH, Jonas BM, Sevcik MA, Kubota K, Halvorson KG, Ghilardi JR, Kuskowski MA, Stelow EB, Mukherjee P, Gendler SJ, *et al* (2005) Pancreatic cancer pain and its correlation with changes in tumor vasculature, macrophage infiltration, neuronal innervation, body weight and disease progression. *Pain* 119: 233–246

Ling Q, Xu X, Zheng S-S & Kalthoff H (2013) The diversity between pancreatic head and body/tail cancers: clinical parameters and in vitro models. *Hepatobiliary Pancreat Dis Int* 12: 480–487

Lohse I & Brothers SP (2020) Pathogenesis and treatment of pancreatic cancer related pain. *Anticancer Res* 40: 1789–1796 doi:10.21873/anticanres.14133 [PREPRINT]

Longnecker DS (2021) Anatomy and Histology of the Pancreas. *Pancreapedia Exocrine Pancreas Knowl Base*

Love JA, Yi E & Smith TG (2007) Autonomic pathways regulating pancreatic exocrine secretion.

Auton Neurosci Basic Clin 133: 19–34 doi:10.1016/j.autneu.2006.10.001 [PREPRINT]

Lynn FC, Smith SB, Wilson ME, Yang KY, Nekrep N & German MS (2007) Sox9 coordinates a transcriptional network in pancreatic progenitor cells. *Proc Natl Acad Sci U S A* 104: 10500–5

M Jobert (1840) NEW TREATMENT OF CANCER. *Lancet* 34: 112 doi:10.1016/S0140-6736(02)98476-X [PREPRINT]

Ma J, Jiang Y, Jiang Y, Sun Y & Zhao X (2008) Expression of nerve growth factor and tyrosine kinase receptor A and correlation with perineural invasion in pancreatic cancer. *J Gastroenterol Hepatol* 23: 1852–1859

Mackay TM, van Erning FN, van der Geest LGM, de Groot JWB, Haj Mohammad N, Lemmens VE, van Laarhoven HW, Besselink MG & Wilmink JW (2019) Association between primary origin (head, body and tail) of metastasised pancreatic ductal adenocarcinoma and oncologic outcome: A population-based analysis. *Eur J Cancer* 106: 99–105

Maddaluno L, Urwyler C & Werner S (2017) Fibroblast growth factors: key players in regeneration and tissue repair. *Development* 144: 4047–4060

Magnon C, Hall SJ, Lin J, Xue X, Gerber L, Freedland SJ & Frenette PS (2013) Autonomic Nerve Development Contributes to Prostate Cancer Progression. *Science (80-)* 341: 1236361–1236361

Mahadevan V (2019) Anatomy of the pancreas and spleen. *Surg (United Kingdom)* 37: 297–301 doi:10.1016/j.mpsur.2019.04.008 [PREPRINT]

Makhmutova M & Caicedo A (2021) Optical Imaging of Pancreatic Innervation. *Front Endocrinol (Lausanne)* 12

Makhmutova M, Weitz J, Tamayo A, Pereira E, Boulina M, Almaça J, Rodriguez-Diaz R & Caicedo A (2021) Pancreatic β-Cells Communicate With Vagal Sensory Neurons. *Gastroenterology* 160: 875-888.e11

Malin SA, Molliver DC, Koerber HR, Cornuet P, Frye R, Albers KM & Davis BM (2006) Glial Cell Line-Derived Neurotrophic Factor Family Members Sensitize Nociceptors In Vitro and Produce Thermal Hyperalgesia In Vivo. *J Neurosci* 26: 8588–8599

Marchetti P, Bugliani M, De Tata VD, Suleiman M & Marselli L (2017) Pancreatic beta cell identity in humans and the role of type 2 diabetes. *Front Cell Dev Biol* 5: 55 doi:10.3389/fcell.2017.00055 [PREPRINT]

Masamune A & Shimosegawa T (2013) Pancreatic stellate cells e multi-functional cells in the pancreas. In *Pancreatology* pp 102–105. Elsevier B.V.

Mauffrey P, Tchitchek N, Barroca V, Bemelmans A, Firlej V, Allory Y, Roméo PH & Magnon C (2019) Progenitors from the central nervous system drive neurogenesis in cancer. *Nature* 569: 672–678

McKerracher L & Rosen KM (2015) MAG, myelin and overcoming growth inhibition in the CNS. *Front Mol Neurosci* 8: 51 doi:10.3389/fnmol.2015.00051 [PREPRINT]

Megibow AJ (2012) Unusual Solid Pancreatic Tumors. *Radiol Clin North Am* 50: 499–513 doi:10.1016/j.rcl.2012.03.009 [PREPRINT]

Meier C, Parmantier E, Brennan A, Mirsky R & Jessen KR (1999) Developing schwann cells acquire the ability to survive without axons by establishing an autocrine circuit involving insulin-like growth factor, neurotrophin-3, and platelet-derived growth factor-BB. *J Neurosci* 19: 3847–3859

Meijer TG, Naipal KA, Jager A & van Gent DC (2017) Ex vivo tumor culture systems for functional drug testing and therapy response prediction. *Futur Sci OA* 3: FSO190

Mezza T, Cefalo CMA, Cinti F, Quero G, Pontecorvi A, Alfieri S, Holst JJ & Giaccari A (2020) Endocrine and Metabolic Insights from Pancreatic Surgery. *Trends Endocrinol Metab* 31: 760–772 doi:10.1016/j.tem.2020.07.003 [PREPRINT]

Michailov G V., Sereda MW, Brinkmann BG, Fischer TH, Haug B, Birchmeier C, Role L, Lai C, Schwab MH & Nave KA (2004) Axonal Neuregulin-1 Regulates Myelin Sheath Thickness. *Science (80-)* 304: 700–703

Miura F, Takada T, Amano H, Yoshida M, Furui S & Takeshita K (2006) Diagnosis of pancreatic cancer. *HPB* 8: 337–342 doi:10.1080/13651820500540949 [PREPRINT]

Molnár R, Madácsy T, Varga Á, Németh M, Katona X, Görög M, Molnár B, Fanczal J, Rakonczay Z, Hegyi P, *et al* (2019) Mouse pancreatic ductal organoid culture as a relevant model to study exocrine pancreatic ion secretion. *Lab Investig 2019 1001* 100: 84–97

Monk KR, Feltri ML & Taveggia C (2015) New insights on schwann cell development. *Glia* 63: 1376–1393

Morell P & Quarles RH (1959) The Myelin Sheath. *Lancet* 273: 665–667 doi:10.1016/S0140-6736(59)92409-2 [PREPRINT]

Müller MW, Giese NA, Swiercz JM, Ceyhan GO, Esposito I, Hinz U, Büchler P, Giese T, Büchler MW, Offermanns S, *et al* (2007) Association of axon guidance factor Semaphorin 3A with poor outcome in pancreatic cancer. *Int J Cancer* 121: 2421–2433

Mundinger TO, Mei Q, Foulis AK, Fligner CL, Hull RL & Taborsky GJ (2016) Human type 1 diabetes is characterized by an early, marked, sustained, and islet-selective loss of sympathetic nerves. *Diabetes* 65: 2322–2330

Muranaka T, Kuwatani M, Komatsu Y, Sawada K, Nakatsumi H, Kawamoto Y, Yuki S, Kubota Y, Kubo K, Kawahata S, *et al* (2017) Comparison of efficacy and toxicity of FOLFIRINOX and gemcitabine with nab-paclitaxel in unresectable pancreatic cancer. *J Gastrointest Oncol* 8: 566–571

Mutgan AC, Besikcioglu HE, Wang S, Friess H, Ceyhan GO & Demir IE (2018) Insulin/IGF-driven cancer cell-stroma crosstalk as a novel therapeutic target in pancreatic cancer. *Mol Cancer* 17 doi:10.1186/s12943-018-0806-0 [PREPRINT]

Na'ara S, Gil Z & Amit M (2016) In Vitro modeling of cancerous neural invasion: The dorsal root ganglion model. *J Vis Exp* 2016

Napoli I, Noon LA, Ribeiro S, Kerai AP, Parrinello S, Rosenberg LH, Collins MJ, Harrisingh MC, White IJ, Woodhoo A, *et al* (2012) A Central Role for the ERK-Signaling Pathway in Controlling Schwann Cell Plasticity and Peripheral Nerve Regeneration In Vivo. *Neuron* 73: 729–742

Ndlovu R, Deng L-C, Wu J, Li X-K & Zhang J-S (2018) Fibroblast Growth Factor 10 in Pancreas

Development and Pancreatic Cancer. *Front Genet* 9

Neuhuber WL (1989) Vagal afferent fibers almost exclusively innervate islets in the rat pancreas as demonstrated by anterograde tracing. *J Auton Nerv Syst* 29: 13–18

Newbern J & Birchmeier C (2010) Nrg1/ErbB signaling networks in Schwann cell development and myelination. *Semin Cell Dev Biol* 21: 922–928 doi:10.1016/j.semcdb.2010.08.008 [PREPRINT]

Newbern JM, Li X, Shoemaker SE, Zhou J, Zhong J, Wu Y, Bonder D, Hollenback S, Coppola G, Geschwind DH, *et al* (2011) Specific Functions for ERK/MAPK Signaling during PNS Development. *Neuron* 69: 91–105

Nocera G & Jacob C (2020) Mechanisms of Schwann cell plasticity involved in peripheral nerve repair after injury. *Cell Mol Life Sci* 77: 3977–3989 doi:10.1007/s00018-020-03516-9 [PREPRINT]

Oba A, Ho F, Bao QR, Al-Musawi MH, Schulick RD & Chiaro M Del (2020) Neoadjuvant Treatment in Pancreatic Cancer. *Front Oncol* 10: 245 doi:10.3389/fonc.2020.00245 [PREPRINT]

Oettle H, Neuhaus P, Hochhaus A, Hartmann JT, Gellert K, Ridwelski K, Niedergethmann M, Zülke C, Fahlke J, Arning MB, *et al* (2013) Adjuvant chemotherapy with gemcitabine and long-term outcomes among patients with resected pancreatic cancer: The CONKO-001 randomized trial. *JAMA - J Am Med Assoc* 310: 1473–1481

Orth M, Metzger P, Gerum S, Mayerle J, Schneider G, Belka C, Schnurr M & Lauber K (2019) Pancreatic ductal adenocarcinoma: Biological hallmarks, current status, and future perspectives of combined modality treatment approaches. *Radiat Oncol* 14: 1–20 doi:10.1186/s13014-019-1345-6 [PREPRINT]

Van Paassen BW, Van Der Kooi AJ, Van Spaendonck-Zwarts KY, Verhamme C, Baas F & De Visser M (2014) PMP22 related neuropathies: Charcot-Marie-Tooth disease type 1A and Hereditary Neuropathy with liability to Pressure Palsies. *Orphanet J Rare Dis* 9: 1–15 doi:10.1186/1750-1172-9-38 [PREPRINT]

Pan FC, Bankaitis ED, Boyer D, Xu X, Van de Casteele M, Magnuson MA, Heimberg H & Wright CVE (2013) Spatiotemporal patterns of multipotentiality in Ptf1aexpressing cells during pancreas organogenesis and injuryinduced facultative restoration. *Dev* 140: 751–764

Pancreatic Cancer: Statistics | Cancer.Net

Pandol SJ (2010) Anatomy.

Pannala R, Basu A, Petersen GM & Chari ST (2009) New-onset diabetes: a potential clue to the early diagnosis of pancreatic cancer. *Lancet Oncol* 10: 88–95

Parkinson DB, Bhaskaran A, Arthur-Farraj P, Noon LA, Woodhoo A, Lloyd AC, Feltri ML, Wrabetz L, Behrens A, Mirsky R, *et al* (2008a) c-Jun is a negative regulator of myelination. *J Cell Biol* 181: 625–637

Parkinson DB, Bhaskaran A, Arthur-Farraj P, Noon LA, Woodhoo A, Lloyd AC, Feltri ML, Wrabetz L, Behrens A, Mirsky R, *et al* (2008b) c-Jun is a negative regulator of myelination. *J Cell Biol* 181: 625

Partecke LI, Käding A, Trung DN, Diedrich S, Sendler M, Weiss F, Kühn J-P, Mayerle J, Beyer K,

von Bernstorff W, *et al* (2017) Subdiaphragmatic vagotomy promotes tumor growth and reduces survival via TNFα in a murine pancreatic cancer model. *Oncotarget* 8: 22501–22512

Pascual-Goñi E, Martín-Aguilar L, Lleixà C, Martínez-Martínez L, Simón-Talero MJ, Díaz-Manera J, Cortés-Vicente E, Rojas-García R, Moga E, Juárez C, *et al* (2019) Clinical and laboratory features of anti-MAG neuropathy without monoclonal gammopathy. *Sci Rep* 9: 1–5

Peltonen S, Alanne M & Peltonen J (2013) Barriers of the peripheral nerve. *Tissue Barriers* 1: e24956

Poitelon Y, Kopec AM & Belin S (2020) Myelin Fat Facts: An Overview of Lipids and Fatty Acid Metabolism. *Cells* 9 doi:10.3390/cells9040812 [PREPRINT]

Ponz-Sarvise M, Tuveson DA & Yu KH (2015) Mouse Models of Pancreatic Ductal Adenocarcinoma. *Hematol Oncol Clin North Am* 29: 609–617 doi:10.1016/j.hoc.2015.04.010 [PREPRINT]

Power ML & Schulkin J (2008) Anticipatory physiological regulation in feeding biology: Cephalic phase responses. *Appetite* 50: 194–206 doi:10.1016/j.appet.2007.10.006 [PREPRINT]

Puli SR, Bechtold ML, Buxbaum JL & Eloubeidi MA (2013) How good is endoscopic ultrasound-guided fine-needle aspiration in diagnosing the correct etiology for a solid pancreatic mass?: A meta-analysis and systematic review. *Pancreas* 42: 20–26

Puri S & Hebrok M (2007) Dynamics of embryonic pancreas development using real-time imaging. *Dev Biol* 306: 82–93

Qiu W & Su GH (2013) Development of orthotopic pancreatic tumor mouse models. *Methods Mol Biol* 980: 215–223

Quarles RH (2007) Myelin-associated glycoprotein (MAG): Past, present and beyond. *J Neurochem* 100: 1431–1448 doi:10.1111/j.1471-4159.2006.04319.x [PREPRINT]

Raman SP, Salaria SN, Hruban RH & Fishman EK (2013) Groove pancreatitis: Spectrum of imaging findings and radiology-pathology correlation. *Am J Roentgenol* 201 doi:10.2214/AJR.12.9956 [PREPRINT]

Rasband MN & Peles E (2016) The nodes of Ranvier: Molecular assembly and maintenance. *Cold Spring Harb Perspect Biol* 8

Raut CP, Grau AM, Staerkel GA, Kaw M, Tamm EP, Wolff RA, Vauthey JN, Lee JE, Pisters PWT, Evans DB, *et al* (2003) Diagnostic accuracy of endoscopic ultrasound-guided fine-needle aspiration in patients with presumed pancreatic cancer. *J Gastrointest Surg* 7: 118–128

Reichert M & Rustgi AK (2011) Pancreatic ductal cells in development, regeneration, and neoplasia. *J Clin Invest* 121 doi:10.1172/JCI57131 [PREPRINT]

Reichert M, Takano S, Heeg S, Bakir B, Botta GP & Rustgi AK (2013) Isolation, culture and genetic manipulation of mouse pancreatic ductal cells. *Nat Protoc* 8: 1354–1365

Ren K, Yi SQ, Dai Y, Kurosawa K, Miwa Y & Sato I (2020) Clinical anatomy of the anterior and posterior hepatic plexuses, including relations with the pancreatic plexus: A cadaver study. *Clin Anat* 33: 630–636

Renz BW, Takahashi R, Tanaka T, Macchini M, Hayakawa Y, Dantes Z, Maurer HC, Chen X, Jiang

Z, Westphalen CB, *et al* (2018a) β2 Adrenergic-Neurotrophin Feedforward Loop Promotes Pancreatic Cancer. *Cancer Cell* 33: 75-90.e7

Renz BW, Tanaka T, Sunagawa M, Takahashi R, Jiang Z, Macchini M, Dantes Z, Valenti G, White RA, Middelhoff MA, *et al* (2018b) Cholinergic Signaling via Muscarinic Receptors Directly and Indirectly Suppresses Pancreatic Tumorigenesis and Cancer Stemness. *Cancer Discov* 8: 1458–1473

Rickels MR, Norris AW & Hull RL (2020) A tale of two pancreases: exocrine pathology and endocrine dysfunction. *Diabetol 2020 6310* 63: 2030–2039

Riethmacher D, Sonnenberg-Riethmacher E, Brinkmann V, Yamaai T, Lewin GR & Birchmeier C (1997) Severe neuropathies in mice with targeted mutations in the ErbB3 receptor. *Nature* 389: 725–730

Robertis R De (2015) Diffusion-weighted imaging of pancreatic cancer. *World J Radiol* 7: 319

Roberts SL, Dun XP, Doddrell RDS, Mindos T, Drake LK, Onaitis MW, Florio F, Quattrini A, Lloyd AC, D'Antonio M, *et al* (2017) Sox2 expression in schwann cells inhibits myelination in vivo and induces influx of macrophages to the nerve. *Dev* 144: 3114–3125

Rodarte-Shade M & Kahaleh M (2015) Stent placement as a bridge to surgery in malignant biliary obstruction (pancreatic cancer, distal bile duct cancer, and hilar tumors). *Gastrointest Interv* 4: 21–26

Roger E, Martel S, Bertrand-Chapel A, Depollier A, Chuvin N, Pommier RM, Yacoub K, Caligaris C, Cardot-Ruffino V, Chauvet V, *et al* (2019) Schwann cells support oncogenic potential of pancreatic cancer cells through TGFβ signaling. *Cell Death Dis* 10: 1–19

Roland CL, Yang AD, Katz MHG, Chatterjee D, Wang H, Lin H, Vauthey JN, Pisters PW, Varadhachary GR, Wolff RA, *et al* (2015) Neoadjuvant therapy is associated with a reduced lymph node ratio in patients with potentially resectable pancreatic cancer. *Ann Surg Oncol* 22: 1168–75

Rosenberg AF, Isaacman-Beck J, Franzini-Armstrong C & Granato M (2014) Schwann cells and deleted in colorectal carcinoma direct regenerating motor axons towards their original path. *J Neurosci* 34: 14668–14681

Rosenbluth J (2009) Multiple functions of the paranodal junction of myelinated nerve fibers. *J Neurosci Res* 87: 3250–3258 doi:10.1002/jnr.22013 [PREPRINT]

Rotshenker S (2011) Wallerian degeneration: The innate-immune response to traumatic nerve injury. *J Neuroinflammation* 8: 109

Rozeveld CN, Johnson KM, Zhang L & Razidlo GL (2020) KRAS Controls Pancreatic Cancer Cell Lipid Metabolism and Invasive Potential through the Lipase HSL. *Cancer Res* 80: 4932–4945

Saher G, Brügger B, Lappe-Siefke C, Möbius W, Tozawa RI, Wehr MC, Wieland F, Ishibashi S & Nave KA (2005) High cholesterol level is essential for myelin membrane growth. *Nat Neurosci* 8: 468–475

Saher G, Quintes S & Nave KA (2011) Cholesterol: A novel regulatory role in myelin formation. *Neuroscientist* 17: 79–93 doi:10.1177/1073858410373835 [PREPRINT]

Saiki Y & Horii A (2014) Molecular pathology of pancreatic cancer. *Pathol Int* 64: 10–19

doi:10.1111/pin.12114 [PREPRINT]

Sakorafas GH & Tsiotou AG (1999) Multi-step pancreatic carcinogenesis and its clinical implications. *Eur J Surg Oncol* 25 doi:10.1053/ejso.1999.0706 [PREPRINT]

Salleh S, Thyagarajan A & Sahu RP (2020) Exploiting the relevance of CA 19-9 in pancreatic cancer. *J Cancer Metastasis Treat* 2020

Saloman JL, Albers KM, Li D, Hartman DJ, Crawford HC, Muha EA, Rhim AD & Davis BM (2016) Ablation of sensory neurons in a genetic model of pancreatic ductal adenocarcinoma slows initiation and progression of cancer. *Proc Natl Acad Sci* 113: 3078–3083

Saloman JL, Singhi AD, Hartman DJ, Normolle DP, Albers KM & Davis BM (2018) Systemic Depletion of Nerve Growth Factor Inhibits Disease Progression in a Genetically Engineered Model of Pancreatic Ductal Adenocarcinoma. *Pancreas* 47: 856–863

Saporta MA & Shy ME (2015) Peripheral Neuropathies. In *Neurobiology of Brain Disorders: Biological Basis of Neurological and Psychiatric Disorders* pp 167–188. Academic Press

Saricaoglu ÖC, Teller S, Wang X, Wang S, Stupakov P, Heinrich T, Istvanffy R, Friess H, Ceyhan GO & Demir IE (2020) Localisation analysis of nerves in the mouse pancreas reveals the sites of highest nerve density and nociceptive innervation. *Neurogastroenterol Motil* 32: 13880

Sarrazin S, Lamanna WC & Esko JD (2011) Heparan sulfate proteoglycans. *Cold Spring Harb Perspect Biol* 3: 1–33

Schlitter AM, Jesinghaus M, Jäger C, Konukiewitz B, Muckenhuber A, Demir IE, Bahra M, Denkert C, Friess H, Kloeppel G, *et al* (2017) pT but not pN stage of the 8th TNM classification significantly improves prognostication in pancreatic ductal adenocarcinoma. *Eur J Cancer* 84: 121–129

Schnipper J, Dhennin-Duthille I, Ahidouch A & Ouadid-Ahidouch H (2020) Ion Channel Signature in Healthy Pancreas and Pancreatic Ductal Adenocarcinoma. *Front Pharmacol* 11

Schnittert J, Bansal R & Prakash J (2019) Targeting Pancreatic Stellate Cells in Cancer. *Trends in Cancer* 5: 128–142 doi:10.1016/j.trecan.2019.01.001 [PREPRINT]

Schorn S, Demir IE, Haller B, Scheufele F, Reyes CM, Tieftrunk E, Sargut M, Goess R, Friess H & Ceyhan GO (2017) The influence of neural invasion on survival and tumor recurrence in pancreatic ductal adenocarcinoma – A systematic review and meta-analysis. *Surg Oncol* 26: 105–115

Seymour PA, Freude KK, Tran MN, Mayes EE, Jensen J, Kist R, Scherer G & Sander M (2007) SOX9 is required for maintenance of the pancreatic progenitor cell pool. *Proc Natl Acad Sci U S A* 104: 1865–70

Sherman DL & Brophy PJ (2005) Mechanisms of axon ensheathment and myelin growth. *Nat Rev Neurosci* 6: 683–690 doi:10.1038/nrn1743 [PREPRINT]

Shimizu F, Sano Y, Abe M, Maeda T, Ohtsuki S, Terasaki T & Kanda T (2011) Peripheral nerve pericytes modify the blood-nerve barrier function and tight junctional molecules through the secretion of various soluble factors. *J Cell Physiol* 226: 255–266

Shiratori K & Shimizu K (2018) Insulo-Acinar Relationship. In *The Pancreas* pp 123–131. John

Wiley & Sons, Ltd

Shroff S, Rashid A, Wang H, Katz MH, Abbruzzese JL, Fleming JB & Wang H (2014) SOX9: a useful marker for pancreatic ductal lineage of pancreatic neoplasms. *Hum Pathol* 45: 456–463

Siegel RL, Miller KD & Jemal A (2020) Cancer statistics, 2020. *CA Cancer J Clin* 70: 7–30

Da Silva Xavier G (2018) The Cells of the Islets of Langerhans. *J Clin Med* 7: 54

Simons M, Krämer EM, Thiele C, Stoffel W & Trotter J (2000) Assembly of myelin by association of proteolipid protein with cholesterol- and galactosylceramide-rich membrane domains. *J Cell Biol* 151: 143–153

Siolas D & Hannon GJ (2013) Patient-derived tumor xenografts: Transforming clinical samples into mouse models. *Cancer Res* 73: 5315–5319 doi:10.1158/0008-5472.CAN-13-1069 [PREPRINT]

Smith-Slatas C & Barbarese E (2000) Myelin basic protein gene dosage effects in the PNS. *Mol Cell Neurosci* 15: 343–354

Smithy JW & O'Reilly EM (2021) Pancreas cancer: Therapeutic trials in metastatic disease. *J Surg Oncol* 123: 1475–1488

De Souza A, Irfan K, Masud F & Saif MW (2016) Diabetes Type 2 and Pancreatic Cancer: A History Unfolding. *JOP* 17: 144–148

Stahl N, Harry J & Popko B (1990) Quantitative analysis of myelin protein gene expression during development in the rat sciatic nerve. *Mol Brain Res* 8: 209–212

Stassart RM, Fledrich R, Velanac V, Brinkmann BG, Schwab MH, Meijer D, Sereda MW & Nave KA (2013) A role for Schwann cell-derived neuregulin-1 in remyelination. *Nat Neurosci* 16: 48–54

Stopczynski RE, Normolle DP, Hartman DJ, Ying H, DeBerry JJ, Bielefeldt K, Rhim AD, DePinho RA, Albers KM & Davis BM (2014) Neuroplastic changes occur early in the development of pancreatic ductal adenocarcinoma. *Cancer Res* 74: 1718–1727

Stratton JA & Shah PT (2016) Macrophage polarization in nerve injury: Do Schwann cells play a role? *Neural Regen Res* 11: 53–57

Strijker M, Chen JW, Mungroop TH, Jamieson NB, van Eijck CH, Steyerberg EW, Wilmink JW, Groot Koerkamp B, van Laarhoven HW & Besselink MG (2019) Systematic review of clinical prediction models for survival after surgery for resectable pancreatic cancer. *Br J Surg* 106: 342–354 doi:10.1002/bjs.11111 [PREPRINT]

Sundaram VK, El Jalkh T, Barakat R, Fernandez CJI, Massaad C & Grenier J (2021) Retracing Schwann Cell Developmental Transitions in Embryonic Dissociated DRG/Schwann Cell Cocultures in Mice. *Front Cell Neurosci* 15

Sung H, Ferlay J, Siegel RL, Laversanne M, Soerjomataram I, Jemal A & Bray F (2021) Global cancer statistics 2020: GLOBOCAN estimates of incidence and mortality worldwide for 36 cancers in 185 countries. *CA Cancer J Clin*: caac.21660

Susuki K (2010) Myelin: a specialized membrane for cell communication. *Nat Educ* 3: 59

Taetzsch T, Brayman VL & Valdez G (2018) FGF binding proteins (FGFBPs): Modulators of FGF signaling in the developing, adult, and stressed nervous system. *Biochim Biophys Acta - Mol Basis Dis* 1864: 2983–2991

Taetzsch T, Tenga MJ & Valdez G (2017a) Muscle fibers secrete FGFBP1 to slow degeneration of neuromuscular synapses during aging and progression of ALS. *J Neurosci* 37

Taetzsch T, Tenga MJ & Valdez G (2017b) Muscle Fibers Secrete FGFBP1 to Slow Degeneration of Neuromuscular Synapses during Aging and Progression of ALS. *J Neurosci* 37: 70–82

Takakura K, Sumiyama K, Munakata K, Ashida H, Arihiro S, Kakutani H & Tajiri H (2011) Clinical usefulness of diffusion-weighted MR imaging for detection of pancreatic cancer: Comparison with enhanced multidetector-row CT. *Abdom Imaging* 36: 457–462

Takuma K, Kamisawa T, Gopalakrishna R, Hara S, Tabata T, Inaba Y, Egawa N & Igarashi Y (2012) Strategy to differentiate autoimmune pancreatitis from pancreas cancer. *World J Gastroenterol* 18: 1015–1020

Tan X, Sivakumar S, Bednarsch J, Wiltberger G, Kather JN, Niehues J, de Vos-Geelen J, Valkenburg-van Iersel L, Kintsler S, Roeth A, *et al* (2021) Nerve fibers in the tumor microenvironment in neurotropic cancer—pancreatic cancer and cholangiocarcinoma. *Oncogene* 40: 899–908

Tassi E, Al-Attar A, Aigner A, Swift MR, McDonnell K, Karavanov A & Wellstein A (2001) Enhancement of Fibroblast Growth Factor (FGF) Activity by an FGF-binding Protein. *J Biol Chem* 276: 40247–40253

Tassi E, Henke RT, Bowden ET, Swift MR, Kodack DP, Kuo AH, Maitra A & Wellstein A (2006) Expression of a fibroblast growth factor-binding protein during the development of adenocarcinoma of the pancreas and colon. *Cancer Res* 66: 1191–1198

Tassi E, McDonnell K, Gibby KA, Tilan JU, Kim SE, Kodack DP, Schmidt MO, Sharif GM, Wilcox CS, Welch WJ, *et al* (2011) Impact of fibroblast growth factor-binding protein1 expression on angiogenesis and wound healing. *Am J Pathol* 179: 2220–2232

Taveggia C & Bolino A (2018) DRG neuron/schwann cells myelinating cocultures. In *Methods in Molecular Biology* pp 115–129.

Taveggia C, Zanazzi G, Petrylak A, Yano H, Rosenbluth J, Einheber S, Xu X, Esper RM, Loeb JA, Shrager P, *et al* (2005) Neuregulin-1 type III determines the ensheathment fate of axons. *Neuron* 47: 681–694

Tempero MA, Malafa MP, Al-Hawary M, Behrman SW, Benson AB, Cardin DB, Chiorean EG, Chung V, Czito B, Del Chiaro M, *et al* (2021) Pancreatic Adenocarcinoma, Version 2.2021, NCCN Clinical Practice Guidelines in Oncology. *J Natl Compr Canc Netw* 19: 439–457

Terada N, Saitoh Y, Kamijo A, Yamauchi J, Ohno N & Sakamoto T (2019) Structures and Molecular Composition of Schmidt–Lanterman Incisures. In *Advances in Experimental Medicine and Biology* pp 181–198. Springer

Tiriac H, Belleau P, Engle DD, Plenker D, Deschênes A, Somerville TDD, Froeling FEM, Burkhart RA, Denroche RE, Jang GH, *et al* (2018) Organoid profiling identifies common responders to chemotherapy in pancreatic cancer. *Cancer Discov* 8: 1112–1129

Tomasello G, Ghidini M, Costanzo A, Ghidini A, Russo A, Barni S, Passalacqua R & Petrelli F

(2019) Outcome of head compared to body and tail pancreatic cancer: A systematic review and meta-analysis of 93 studies. *J Gastrointest Oncol* 10: 259–269

Topilko P, Schneider-Maunoury S, Levi G, Baron-Van Evercooren A, Chennoufi ABY, Seitanidou T, Babinet C & Charnay P (1994) Krox-20 controls myelination in the peripheral nervous system. *Nature* 371: 796–799

Travagli RA & Anselmi L (2016) Vagal neurocircuitry and its influence on gastric motility. *Nat Rev Gastroenterol Hepatol* 13: 389–401 doi:10.1038/nrgastro.2016.76 [PREPRINT]

Triantopoulou C, Kolliakou E, Karoumpalis I, Yarmenitis S & Dervenis C (2012) Metastatic disease to the pancreas: An imaging challenge. *Insights Imaging* 3: 165–172 doi:10.1007/s13244-011-0144-x [PREPRINT]

Tsai S, McOlash L, Palen K, Johnson B, Duris C, Yang Q, Dwinell MB, Hunt B, Evans DB, Gershan J, *et al* (2018) Development of primary human pancreatic cancer organoids, matched stromal and immune cells and 3D tumor microenvironment models. *BMC Cancer* 18: 1–13

Tuveson Lab Protocols and Requests for Reagents.

Venglovecz V, Hegyi P & Gray MA (2021) Ion Channels in Pancreatic Duct Epithelial Cells in Health and Disease I . Physiology of Pancreatic Ductal Cells II . Pathophysiology of Pancreatic Duct Cells. *Pancreapedia Exocrine Pancreas Knowl Base*: 1–10

Verheijen MHG, Camargo N, Verdier V, Nadra K, De Preux Charles AS, Médard JJ, Luoma A, Crowther M, Inouye H, Shimano H, *et al* (2009) SCAP is required for timely and proper myelin membrane synthesis. *Proc Natl Acad Sci U S A* 106: 21383–21388

Villasenor A & Cleaver O (2012) Crosstalk between the developing pancreas and its blood vessels: An evolving dialog. *Semin Cell Dev Biol* 23 doi:10.1016/j.semcdb.2012.06.003 [PREPRINT]

Waise TMZ, Dranse HJ & Lam TKT (2018) The metabolic role of vagal afferent innervation. *Nat Rev Gastroenterol Hepatol* 15: 625–636 doi:10.1038/s41575-018-0062-1 [PREPRINT]

Wang J, Wang H, Cai J, Du S, Xin B, Wei W, Zhang T & Shen X (2018) Artemin regulates CXCR4 expression to induce migration and invasion in pancreatic cancer cells through activation of NF-κB signaling. *Exp Cell Res* 365: 12–23

Wang K, Demir IE, D'Haese JG, Tieftrunk E, Kujundzic K, Schorn S, Xing B, Kehl T, Friess H & Ceyhan GO (2014) The neurotrophic factor neurturin contributes toward an aggressive cancer cell phenotype, neuropathic pain and neuronal plasticity in pancreatic cancer. *Carcinogenesis* 35: 103–113

Wang L, Xie D & Wei D (2019) Pancreatic acinar-to-ductal metaplasia and pancreatic cancer. In *Methods in Molecular Biology* pp 299–308. Humana Press Inc.

Wang W, Li L, Chen N, Niu C, Li Z, Hu J & Cui J (2020) Nerves in the Tumor Microenvironment: Origin and Effects. *Front Cell Dev Biol* 0: 1630

Wang X, Misawa R, Zielinski MC, Cowen P, Jo J, Periwal V, Ricordi C, Khan A, Szust J, Shen J, *et al* (2013) Regional Differences in Islet Distribution in the Human Pancreas - Preferential Beta-Cell Loss in the Head Region in Patients with Type 2 Diabetes. *PLoS One* 8: 67454

Watila MM & Balarabe SA (2015) Molecular and clinical features of inherited neuropathies due

to PMP22 duplication. *J Neurol Sci* 355: 18–24 doi:10.1016/j.jns.2015.05.037 [PREPRINT]

Webster H de F, Martin JR & O'Connell MF (1973) The relationships between interphase Schwann cells and axons before myelination: A quantitative electron microscopic study. *Dev Biol* 32: 401–416

Wegner M & Stolt CC (2005) From stem cells to neurons and glia: a Soxist's view of neural development. *Trends Neurosci* 28: 583–588

Wendt A & Eliasson L (2020) Pancreatic α-cells – The unsung heroes in islet function. *Semin Cell Dev Biol* 103: 41–50 doi:10.1016/j.semcdb.2020.01.006 [PREPRINT]

Westphalen CB & Olive KP (2012) Genetically engineered mouse models of pancreatic cancer. *Cancer J (United States)* 18: 502–510 doi:10.1097/PPO.0b013e31827ab4c4 [PREPRINT]

Wierup N, Sundler F & Scott Heller R (2013) The islet ghrelin cell. *J Mol Endocrinol* 52: 35–49 doi:10.1530/JME-13-0122 [PREPRINT]

Williams AH, Valdez G, Moresi V, Qi X, McAnally J, Elliott JL, Bassel-Duby R, Sanes JR & Olson EN (2009) MicroRNA-206 Delays ALS Progression and Promotes Regeneration of Neuromuscular Synapses in Mice. *Science (80-)* 326: 1549–1554

Williams JA (2010) Regulation of acinar cell function in the pancreas. *Curr Opin Gastroenterol* 26: 478–483 doi:10.1097/MOG.0b013e32833d11c6 [PREPRINT]

Woldeyesus MT, Britsch S, Riethmacher D, Xu L, Sonnenberg-Riethmacher E, Abou-Rebyeh F, Harvey R, Caroni P & Birchmeier C (1999) Peripheral nervous system defects in erbB2 mutants following genetic rescue of heart development. *Genes Dev* 13: 2538–2548

Wolpowitz D, Mason TBA, Dietrich P, Mendelsohn M, Talmage DA & Role LW (2000) Cysteine-rich domain isoforms of the Neuregulin-1 gene are required for maintenance of peripheral synapses. *Neuron* 25: 79–91

Woodhoo A, Alonso MBD, Droggiti A, Turmaine M, D'Antonio M, Parkinson DB, Wilton DK, Al-Shawi R, Simons P, Shen J, *et al* (2009) Notch controls embryonic Schwann cell differentiation, postnatal myelination and adult plasticity. *Nat Neurosci* 12: 839–847

Wu DQ, Kan MK, Sato GH, Okamoto T & Sato JD (1991) Characterization and molecular cloning of a putative binding protein for heparin-binding growth factors. *J Biol Chem* 266: 16778–16785

Xu M, Jung X, Hines OJ, Eibl G & Chen Y (2018) Obesity and Pancreatic Cancer. *Pancreas* 47: 158–162

Yi SQ, Miwa K, Ohta T, Kayahara M, Kitagawa H, Tanaka A, Shimokawa T, Akita K & Tanaka S (2003) Innervation of the pancreas from the perspective of perineural invasion of pancreatic cancer. *Pancreas* 27: 225–229

You MS, Lee SH, Choi YH, Shin BS, Paik WH, Ryu JK, Kim YT, Jang DK, Lee JK, Kwon W, *et al* (2019) Lymph node ratio as valuable predictor in pancreatic cancer treated with R0 resection and adjuvant treatment. *BMC Cancer* 19: 1–8

Zahalka AH, Arnal-Estapé A, Maryanovich M, Nakahara F, Cruz CD, Finley LWS & Frenette PS (2017) Adrenergic nerves activate an angio-metabolic switch in prostate cancer. *Science (80-)* 358: 321–326

Zahalka AH & Frenette PS (2020) Nerves in cancer. *Nat Rev Cancer* 20

Zamboni GA, Ambrosetti MC, D'Onofrio M & Pozzi Mucelli R (2012) Ultrasonography of the Pancreas. *Radiol Clin North Am* 50: 395–406 doi:10.1016/j.rcl.2012.03.010 [PREPRINT]

Zareba P, Flavin R, Isikbay M, Rider JR, Gerke TA, Finn S, Pettersson A, Giunchi F, Unger RH, Tinianow AM, *et al* (2017) Perineural invasion and risk of lethal prostate cancer. *Cancer Epidemiol Biomarkers Prev* 26: 719–726

Zhang L, Sanagapalli S & Stoita A (2018a) Challenges in diagnosis of pancreatic cancer. *World J Gastroenterol* 24: 2047–2060 doi:10.3748/wjg.v24.i19.2047 [PREPRINT]

Zhang M, Zhu ZL, Gao XL, Wu JS, Liang XH & Tang YL (2018b) Functions of chemokines in the perineural invasion of tumors (Review). *Int J Oncol* 52: 1369–1379 doi:10.3892/ijo.2018.4311 [PREPRINT]

Zhang Z, Liu M, Hu Q, Xu W, Liu W, Sun Q, Ye Z, Fan G, Xu X, Yu X, *et al* (2019) FGFBP1, a downstream target of the FBW7/c-Myc axis, promotes cell proliferation and migration in pancreatic cancer. *Am J Cancer Res* 9: 2650

Zhang Z, Zhou Y, Hu K, Wang D, Wang Z & Huang Y (2020) Perineural invasion as a prognostic factor for intrahepatic cholangiocarcinoma after curative resection and a potential indication for postoperative chemotherapy: A retrospective cohort study. *BMC Cancer* 20: 1–11

Zhao C-M, Hayakawa Y, Kodama Y, Muthupalani S, Westphalen CB, Andersen GT, Flatberg A, Johannessen H, Friedman RA, Renz BW, *et al* (2014a) Denervation suppresses gastric tumorigenesis. *Sci Transl Med* 6: 250ra115-250ra115

Zhao Q, Yang Y, Liang X, Du G, Liu L, Lu L, Dong J, Han H & Zhang G (2014b) The clinicopathological significance of neurogenesis in breast cancer. *BMC Cancer* 14: 1–6

Zhou Y, Sun B, Li W, Zhou J, Gao F, Wang X, Cai M & Sun Z (2019) Pancreatic Stellate Cells: A Rising Translational Physiology Star as a Potential Stem Cell Type for Beta Cell Neogenesis. *Front Physiol* 10

Zhu Y, Colak T, Shenoy M, Liu L, Pai R, Li C, Mehta K & Pasricha PJ (2011) Nerve Growth Factor Modulates TRPV1 Expression and Function and Mediates Pain in Chronic Pancreatitis. *Gastroenterology* 141: 370–377